Escola de Camins
Escola Tècnica Superior d'Enginyeria de Camins, Canals i Ports
UPC BARCELONATECH

TRABAJO FINAL DE MÁSTER

Modelling the effect of in-soil temperature and relative humidity on the performance of PET strap soil reinforcement products

Trabajo realizado por:
Aníbal Andrés Moncada Ramírez

Dirigido por:
Ivan Puig Damians
Sebastià Olivella Pastellé

Máster en:
Ingeniería del Terreno

Barcelona, 31 de Enero del 2022

Departamento de Ingeniería Civil y Ambiental

ABSTRACT

Polyester (PET) strap reinforcement materials are now used routinely as soil reinforcement for mechanically stabilized earth (MSE) walls. The important role of temperature and relative humidity on the chemical degradation of PET fibres due to hydrolysis is well documented in the literature. Strength and stiffness of the polyester fibres can be expected to decrease with increasing temperature and in the presence of moisture. This has practical implications for the selection of the partial factor for chemical degradation and long-term deformation that is used in internal stability limit state design in MSE walls. The PET multi-filament core of the straps is protected against installation damage and moisture by a polyethylene sheath.

This study presents the results of analyses using numerical simulations that were carried out to estimate, first, the temperature and relative humidity changes in-soil regarding different ground properties and atmospheric boundary conditions, and second, the temporal strength and stiffness changes in simulated buried PET straps placed in different soil environments while subjected to different tensile loads and temperatures. Though no in site measurements are available, modelled results are compared and found consistent with similar previous research regarding in-soil temperature distributions. Finally, a first approach at a fully coupled thermo-hydro-mechanical (THM) is presented. Creep behaviour is adequately modeled withing single simulated PET straps but not on the full MSE wall model.

RESUMEN

Los materiales de refuerzo de fibras de poliéster (PET) se utilizan actualmente de forma rutinaria como refuerzo del suelo para los muros de tierra mecánicamente estabilizada (MSE por sus siglas en ingles). El rol de la temperatura y la humedad relativa en la degradación química de las fibras PET debido a la hidrólisis está bien documentado en la literatura. Es de esperar que la rigidez y resistencia de las fibras de poliéster disminuyan con el aumento de la temperatura y en presencia de humedad. Esto tiene implicaciones prácticas para la selección de los factores parciales de degradación química y deformación a largo plazo que se utiliza en el diseño del estado límite de estabilidad interna en los muros MSE. El núcleo de multifilamentos de PET de las correas está protegido contra los daños de la instalación y la humedad por una funda de polietileno.

El presente estudio detalla los resultados de los análisis realizados mediante simulaciones numéricas para estimar, en primer lugar, los cambios de temperatura y humedad relativa en el suelo en relación con diferentes propiedades del terreno y condiciones atmosféricas impuestas, y, en segundo lugar, los cambios a lo largo del tiempo en resistencia y rigidez en refuerzos tipo PET simulando diferentes entornos de suelo mientras se someten a variados estados de cargas y temperaturas. Aun cuando no se dispone de mediciones de campo, los resultados modelados son comparados y se encuentran concordantes con investigaciones anteriores con respecto a la distribución de temperaturas en el terreno. Por último, se presenta una primera aproximación a un sistema termo-hidro-mecánico (THM) totalmente acoplado. El comportamiento de fluencia a largo plazo de refuerzos PET es modelado de forma adecuada para elementos individuales, no así dentro del modelo completo del muro MSE

ACKNOWLEDGEMENTS

I would like to thank Ivan Puig Damians for giving me the opportunity to develop this project alongside him. He was always available and willing to help and proved to be an invaluable guide.

To Sebastià Olivella for the guidance and patience, especially for the help provided during the elaboration of the numerical model

Special thanks are in hand to Aaron Kim from GECO Industrial (Korea, Rep.) for providing data for polymeric straps (FASTEN products) from reliability assessment testing records. The provided data has allowed to carry out various calibration processes for the implemented numerical model for PET strap reinforcements and will be crucial in the continuous development of future lines of investigations and continuous improvement of reinforcements testing procedures and behaviour understanding.

Finally, I would like to thank my family for the constant support at a distance as well as those friends who I have met along the way that have helped me keep my mind in the right place. Your support has been irreplaceable.

CONTENTS

LIST OF FIGURES

LIST OF TABLES

1. **INTRODUCTION**

Polymeric reinforcement materials are used routinely in civil engineering works for soil reinforcement and stabilization. Geosynthetic materials have proven to be a sustainable solution for mechanically stabilized earth (MSE) wall applications. (Dixon et al. 2017, Damians et al. 2018).

In mechanically stabilized earth structures, the crucial role of temperature and relative humidity on the mechanical and chemical degradation of polyester (PET) fibres due to hydrolysis is well documented in the literature (Jailloux et al. 2008, Greenwood et al. 2012). Strength and stiffness of the polyester fibres can be expected to decrease with increasing temperature and in the presence of moisture. These reductions modify the partial factor for creep and chemical degradation that is used in internal stability limit state design for PET strap MSE walls. Hence, realistic local ambient and in soil conditions should be accounted for at the design phase. The PET multi-filament core of the straps is protected by a polyethylene sheath to mitigate installation damage and moisture deterioration. Nevertheless, this sheath still permits the exposure of the polyester filaments to moisture over the life of reinforcement. For instance, high density polyethylene (HDPE) coatings are permeable to water vapor over the long term and thus moisture can accumulate in the air voids between the PET fibres. The rate of degradation due to hydrolysis leading to creep deformation will change with temperature, which can vary widely depending on the environment in which the straps are placed, and temporally with time of day and season.

In order to analyze the long-term behaviour of PET straps, the present study proposes a coupled finite element model based on the software CODE_BRIGHT (Olivella et al. 1996), in which the in-soil distribution of temperature and relative humidity for different atmospheric conditions are evaluated. The effect of atmospheric conditions is first evaluated using a simplified soil model, followed by the implementation of a 2D thermo-hydraulic (TH) MSE wall model. Atmospheric conditions include temperature, relative humidity and precipitation daily records. Next, linear elastic, bi linear elastic, visco-elastic and visco-plastic constitutive models are implemented to simulate PET strap long-term response calibrated using the laboratory results of You-Kyum et al. (2018) for GECO's FASTEN FS products (GECO 2021). The proposed models incorporate variations in temperature and saturation on the constitutive laws. Finally, a linear coupled thermo-hydro-mechanical (THM) MSE wall 2D model is proposed as a preliminary approach.

2. THEORICAL BACKGROUND

2.1 MSE wall design considerations

MSE walls are soil retaining structures base on the incorporation of in-soil horizontal reinforcement, parallel to the principal strain direction, which provide tensile strength and thus increase soil resisting properties. Being tolerant to a greater level of deformation and differential settlements than gravity walls or reinforced concrete structures, these types of structures are commonly used in bridge abutments and earth retaining among other solutions, as detailed in Figure 2-1.

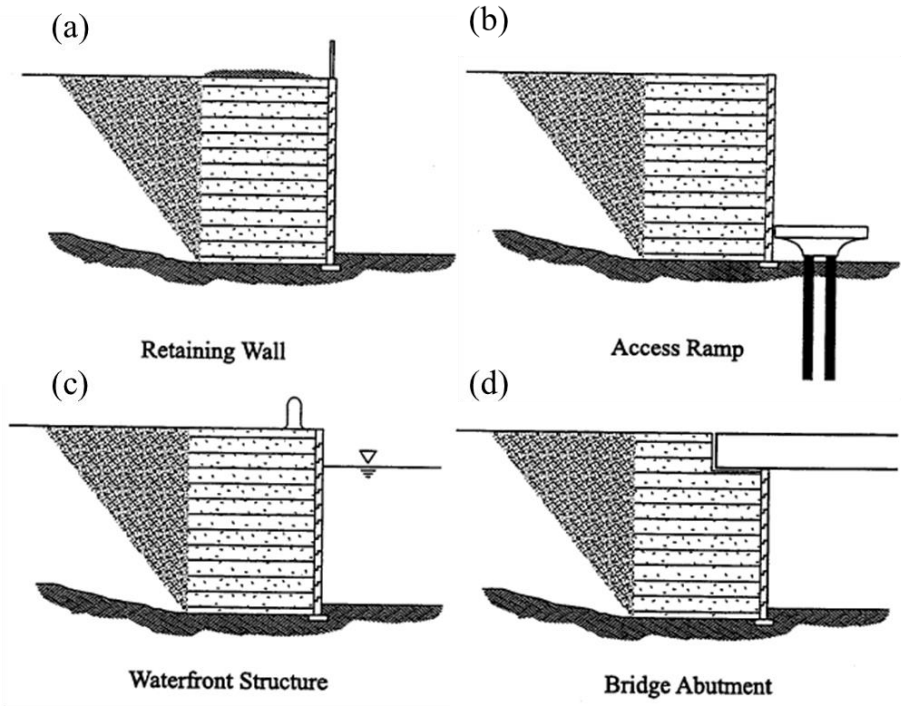

Figure 2-1. Representation of MSE wall applications as (a) retaining wall, (b) access ramp, (c) waterfront structure and (d) bridge abutment. (Berg et al. 2009)

The main components conforming a typical MSE wall include:

- *Facing panels* are the exposed visual elements which are responsible for the proper confinement and tension balance of the soil backfill mass. Panels provide protection against erosion and, when mounted, can include horizontal or vertical gaps, held together by bearing pads, which provide MSE walls with greater draining capabilities. Typically, facing panels are composed of precast concrete with square or hexagonal geometry with areas of 2 to 5 m^2. Otherwise, facing elements can be composed of welded wire mesh, dry cast modular blocks or geosynthetics facings, among other types. As to provide a proper footing and toe confinement, base facing panels must me embedded approximately 10 to 15% of the total MSE wall heigh.

- *In-soil reinforcements* can be categorized by various descriptions. Regarding geometry, three types can be identified. Those being linear unidirectional, which include both metallic and geosynthetic strip, composite unidirectional, composed of grids or mats with spacings greater than 150 mm, and planar bi-directional, which include geosynthetic sheets and welded or woven wire meshes. Another description of reinforcements is that by material type, being categorized in metallic (steel) and non-metallic (polymeric materials). Finally, if extensibility relative to the soil´s extensibility is considered, reinforcement can be classified as inextensible, as in the elongation at failure of the reinforcement is considerably less than the soil, and extensible, in which the deformation at failure is equal or greater than the soil deformability. Depending on the selected type of reinforcement, durability and corrosion resistance must be ensured for the design life of the structure. Reinforcements are usually attached to the inside face of panels by means of metallic connection elements

- *Backfill* material must be carefully curated and comply with draining, granulometric and mechanical criteria. In order to obtain the desired friction within the reinforcement and reinforced soil, backfill material with high frictional characteristic is required, generally granular soils with low fine content. Depending on the type of reinforcement used (mainly metallic or polymeric), considerations must be taken into account in order to avoid chemical degradation and installation damage. Backfill material shall be carefully placed and compacted, attaining the desired maximum density and optimal water content for every layer placed.

- *Bearing pads* serve the purpose of avoiding concrete to concrete contact, provide a gap between panels for draining purposes, transfer the load between facing elements and accommodate possible settlements that occur during the construction process. These elements are usually made from polymeric materials.

- *Leveling pads* usually consist in a mortar of low-grade cement at the base of the structure to function as a footing for the first row of facing elements. These elements do not intend to act as a foundation which supports the structure, but as an aligning element in which to properly position and align the soon to be built structure. With this criterion in mind, leveling pad dimension must be limited to the facing element dimension.

Figure 2-2 details a MSE wall under construction for and overpass with precast concrete panels (a) as well as an under construction MSE wall with its main components labeled, including facing panels, backfill material, polymeric strips reinforcement and connection elements (b). Depending on the use and application of the structure, permanent MSE walls can require design life period of up to 120 years.

MSE wall design criteria must verify both external and internal stability. Failure mechanisms must be verified via ultimate limit state. Deformation conditions must be verified via service limit state (AASTHO 2020). External stability verifications include toppling, foundation bearing resistance, base plane sliding and global stability as depicted in Figure 2-3.

(a)

(b)

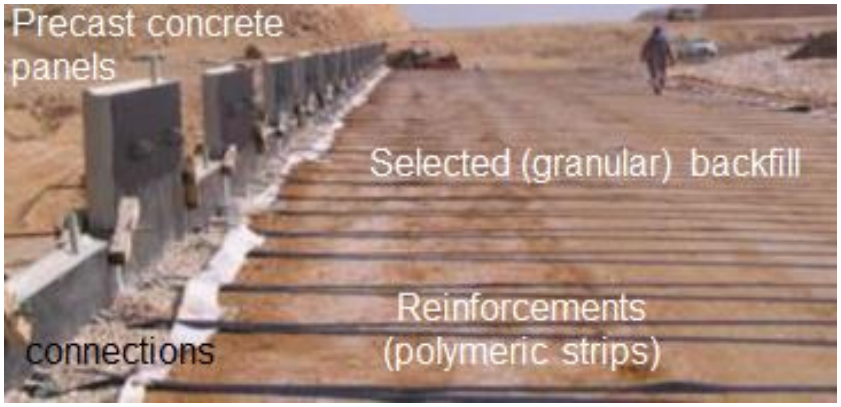

Figure 2-2. (a) Construction of a MSE wall for an overpass and (b) MSE wall under construction with all its main components.

Regarding internal stability, reinforcement rupture, unwarranted reinforcement elongation, or failure at the ground-reinforcement interface (pullout failure) must be verified. For this, the location of the theorical maximum tensile load acting over the reinforcements is crucial. This boundary separates the active and resistance zones, those being the active earth pressure zone acting against the retaining wall and the zone in which the reinforcements provide added strength to the soil. Inextensible materials present lower deformations at failure when compared to the soil, on the other hand, extensible materials present higher strain rates at failure points, thus, maximum tensile loads will should have different distributions through the reinforced backfill. Figure 2-4 details the theorical delimitation of active and passive zones present in a MSE wall with inextensible, for instance steel strips, and extensible reinforcements, such as PET straps. The potential failure zone indicates the zone of maximum stress that the reinforcement must endure and, as such, proves a relevant zone when analyzing the effect of ambient conditions.

When analyzing structures with extensible reinforcements, the maximum stress zone will be a bilinear function based on face batter, wall height and the inclination of any fills at

above the structure. In the case of extensible reinforcements, particularly for near vertical, the potential failure surface is traced from the foot of the structure and upwards with an angle of $\varphi = 45 + \frac{\phi_r}{2}$, with ϕ_r being the reinforced soil friction angle.

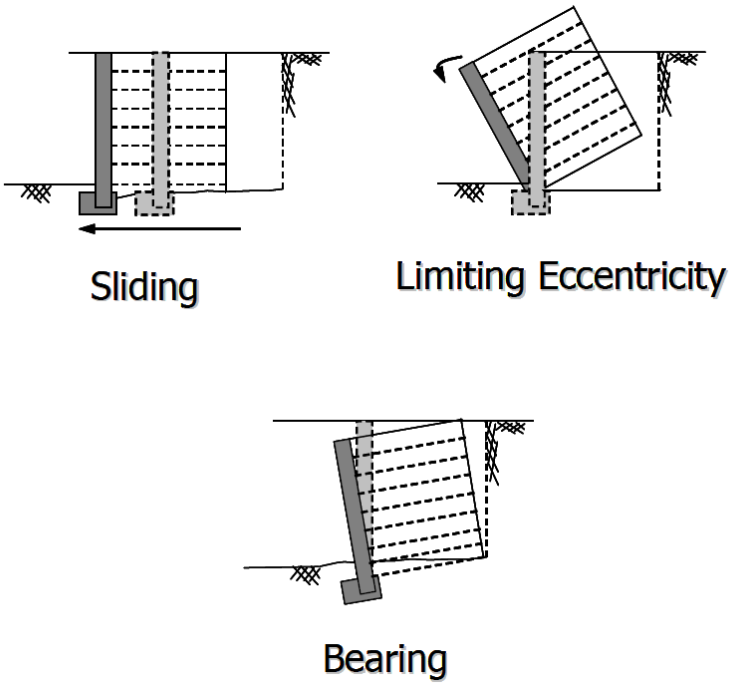

Figure 2-3. Potential external failure mechanism of MSE walls (Berg et at. 2009)

Depending on the desired type of wall, mainly the facing element and reinforcement type selection, the construction process will vary. For stiff facing elements with strip-like reinforcements the construction sequence is detailed below.

- Installation of a small foundation at the foot of the wall to serve not as a structural element but as a leveling pad.
- Placement of the first facing element is placed in a vertical manner.
- Spread and compaction of reinforced soil material up to the first panel-reinforcement connection.
- Placement of the first reinforcement element perpendicular to the facing panel direction. Reinforcements can be attached to the facing panels in various ways depending on the chosen connection.
- Continue to fill and compact material up to the next panel-reinforcement connection and repeat the reinforcement installation.
- Fill and compact with selected granular backfill until the full panel height is reached
- Place a new panel above the already installed panel. In order to prevent concrete to concrete contact, bearing pads must be placed between panels.
- Repeat the fill and compact process until the desired height is reached.

(a) Inextensible reinforcementes

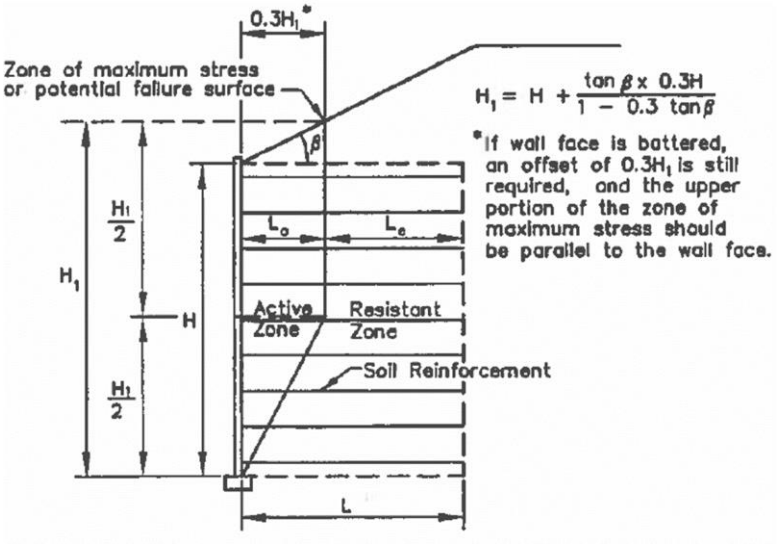

(b) Extensible reinforcements

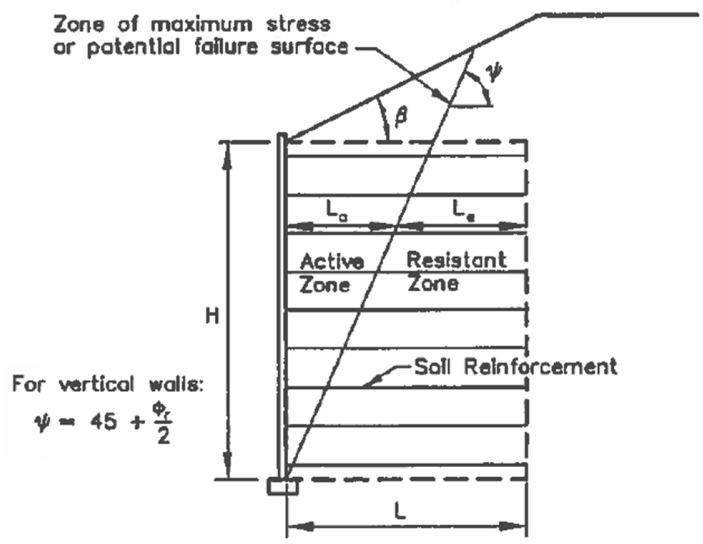

Figure 2-4. Location of theorical potential failure surface for internal stability design of MSE wall using (a) inextensible and (b) extensible reinforcements (AASHTO 2020)

Figure 2-5 details the stress-strain behaviour of a dense sandy soil under different confining pressures. When in shear loading, a significant increase in volumetric strains can be observed for high density, low confined cohesionless soils, which is reflected in an increase in strength ($\phi_{peak} > \phi_{constant\ volume}$) when compared to a high confined state at constant volume. The described phenomenon is commonly name as soil dilatancy.

When horizontal reinforcements are embedded within the compacted soil backfill, if the aforementioned dilatancy effect is considered, when vertical loading is applied, lateral pressures are developed and in consequence stresses are developed along the reinforcements. If no reinforcements are included, the effect of dilatancy results in a different stress distribution, as detailed in Figure 2-6, where lateral earth pressures differ (Damians 2016).

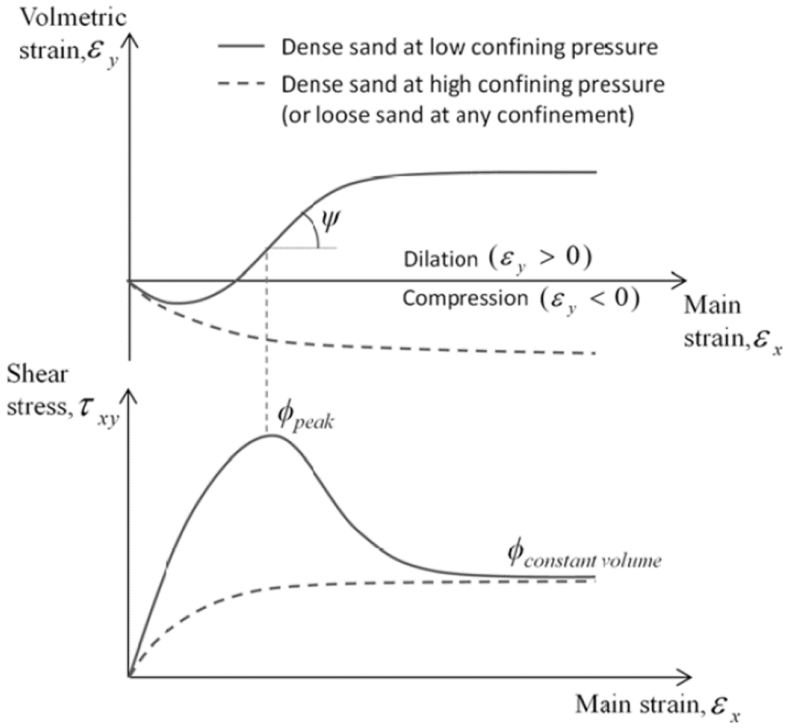

Figure 2-5. Stress-strain behaviour over different confining pressures for sandy soils (Damians 2016).

Due to the effect of dilatancy, an increase in volume increases the vertical stresses within the placed reinforcements. As a consequence, an apparent cohesion is developed, increasing the soil strength as an apparent cohesion. Another explanation relies on the absorption of part of the horizontal stresses by the reinforcement elements, which results in a reduces horizontal stress for the reinforced soil and, under low confining pressures, results in an increased friction angle. Figure 2-7 depicts Mohr´s circle with the previously described phenomenon.

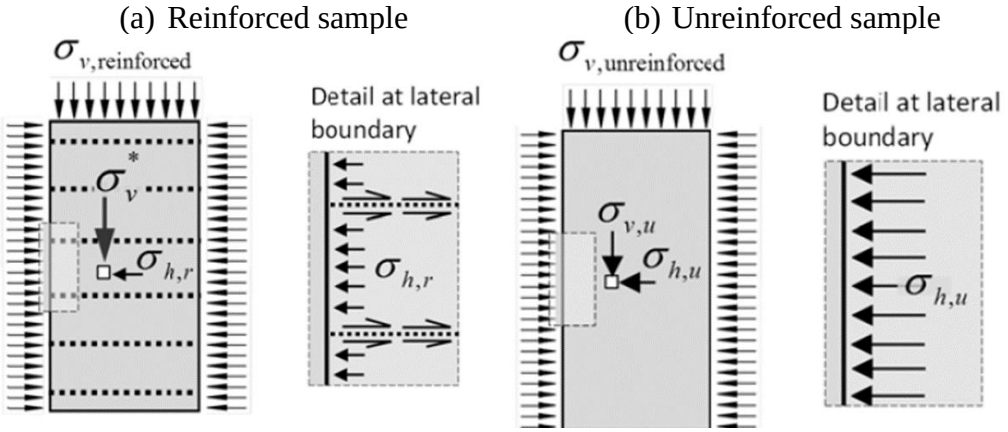

Figure 2-6. Example of (a) reinforced and (b) unreinforced soil samples under load (Damians 2016).

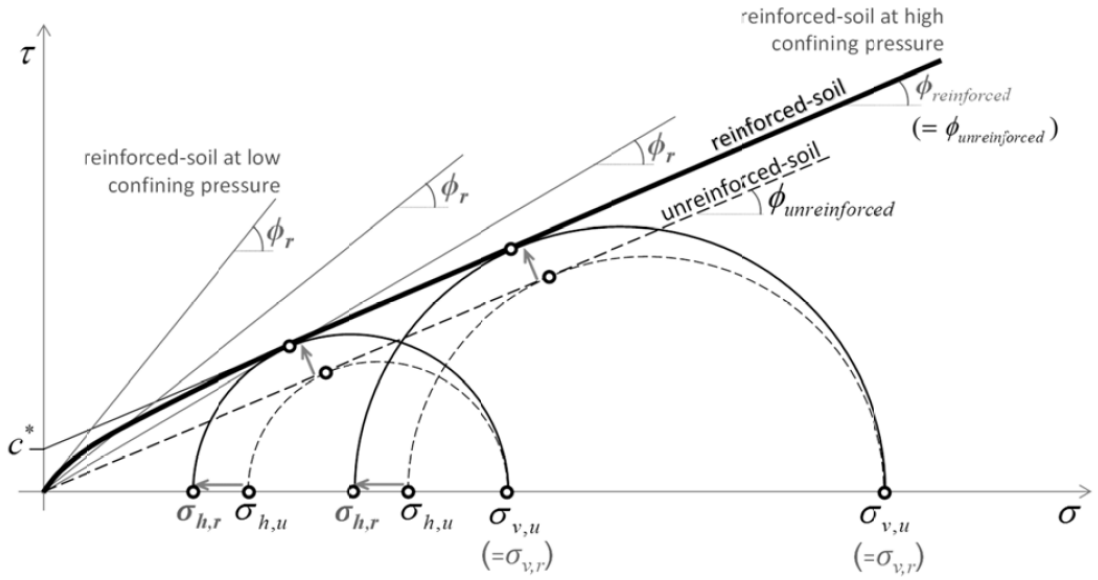

Figure 2-7. Mohr-Coulomb failure criteria for reinforced soil (Damians 2016)

2.2 MSE wall sustainability considerations

Polymeric reinforcement materials are now used routinely as soil reinforcement and stabilization, as well as barrier systems, roads and hydraulics, within the framework of Civil Engineering projects. Geosynthetic materials can play a role in meeting the global challenges facing society in terms of United Nations sustainability goals, approaches for counting carbon in both mitigating, and adapting to the impacts of climate change (Dixon et al. 2017).

Besides an economic and social assessment of a project, it has become more common or even required the inclusion of an environmental sustainability assessment, defined mainly by the generation of greenhouse gas (GHG) emissions. GHG emissions must consider all generations sources, being direct or indirect during a clearly defined period of time.

In order to analyze and compare the environmental impact of a project, emissions over its complete construction, use and disposal period must be considered. One possible method of doing so is the Life Cycle Assessment (LCA), in which the impact, beginning from the extraction of raw materials, up until site delivery (cradle-to-gate) or to end-of -life (cradle-to-grave), is evaluated. (ISO 2006a, ISO 2006b).

Damians et al. (2016) studied the environmental impact of various earth retaining structures, mainly gravity, cantilever and MSE walls with steel and polymeric reinforcements for various heights. Said study considered a cradle-to-operation time frame in which material production, transportation and construction stages are considered. Figure 2-8 details a flow chart showing the stages and components included in the mentioned LCA study, detailing included and excluded stages. Figure 2-9 shows the obtained results regarding equivalent carbon dioxide (CO_2) emissions as a function of wall height for various structure types. Results showed that MSE wall prove to be a better solution for every case study as the environmental impact is lower than that of cantilever and gravity wall solutions when comparing global warming potential (as in GHG emissions), cumulative energy demand and various midpoint and endpoint categories. The main reasons being the materials and components used, that being concrete for

gravity walls and a larger use of steel in cantilever walls. Polymeric reinforced MSE walls showed slightly but not significant better results regarding environmental impact when compared to steel reinforced MSE walls.

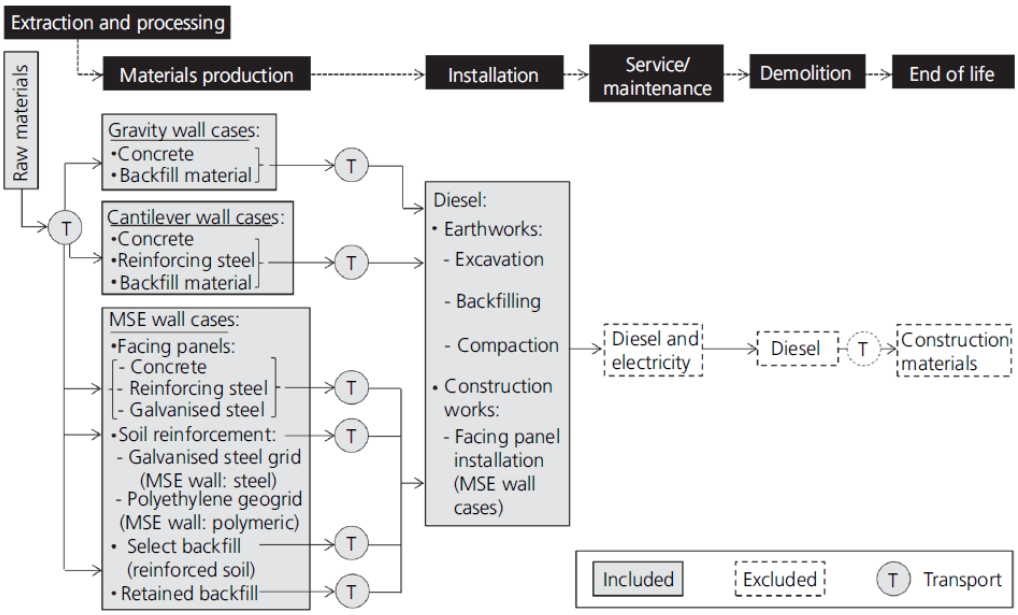

Figure 2-8. Flow chart of the included stages and components of an LCA cradle-to-grave system (Damians et al 2016)

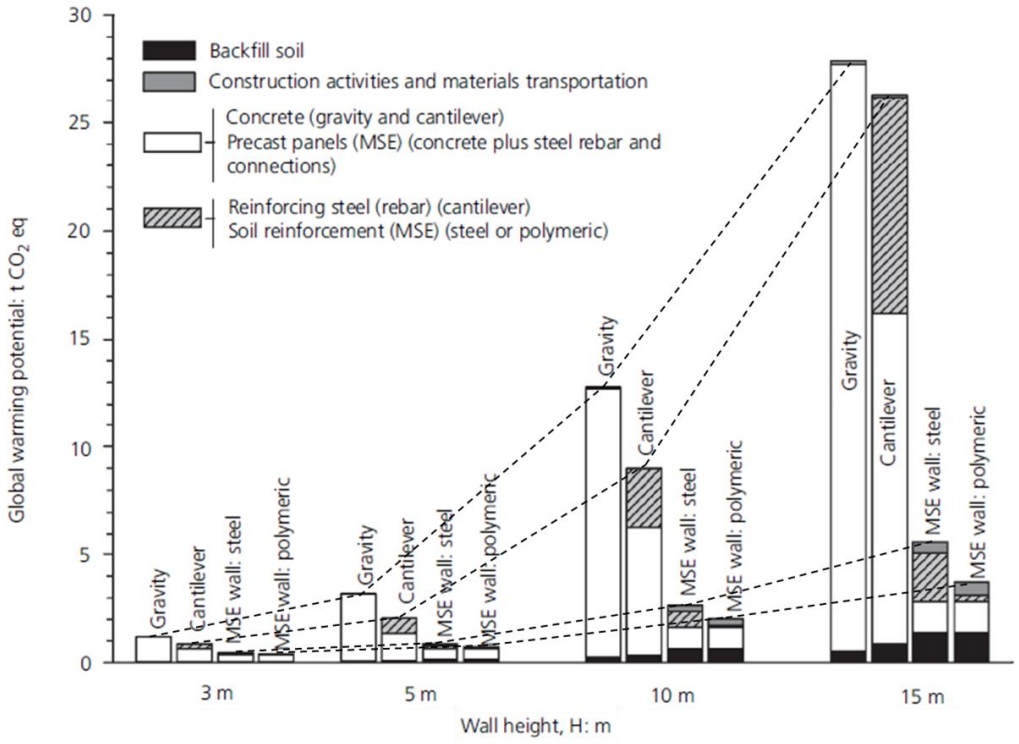

Figure 2-9. Total global warming potential (as equivalent CO_2) for earth retaining structures for various wall heights including material categories, transportation and construction (Damians et al. 2016)

As describe by Damians et al. (2018), in order to develop a full sustainability assessment, economic and social factors must also be incorporated. Regarding economic consideration, manufacture, transport and loss of materials, as well as on site fabrication and labor must be included. Additionally, depending on the used time frame, operation maintenance, dismantling and disposal of material must be included. Social factors vary widely between project and can be listed but not limited to safety and aesthetic considerations as well as design and constructability criteria.

Figure 2-10 presents the calculated total economic costs for various wall types in which MSE walls, for polymeric or steel reinforcements, prove to be the most cost-effective solution as wall height increases when compared to gravity or cantilever wall solutions. For smaller wall heights (3 to 5 meters) cost discrepancy between solutions is negligible

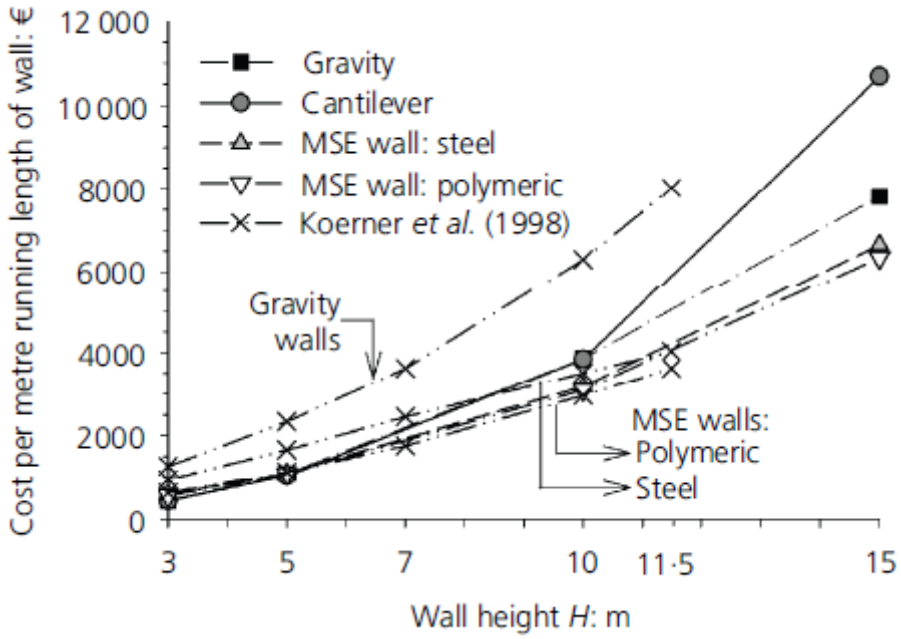

Figure 2-10. Total cost for various wall types as a function of wall height (Damians et al. 2018).

2.3 Atmospheric effects

Previous studies have shown that ambient boundary temperatures can have considerable effect on in-soil temperatures distributions in MSE wall backfills, especially near the surface (Segrestin and Jailloux 1988, Kazosi et al. 2015, Bathurst 1992). Furthermore, backfill temperatures have been shown to follow an annual cyclic pattern (Murray and Farrar 1988), oscillating within a certain degree of the annual mean temperature. As the depth increases, in-soil temperature tends to a constant value that can be approximated by the annual mean ambient temperature. As such, the average backfill temperature for MSE walls, depending on the geographic location, can be higher than the values presented in design standards (Kazosi et al. 2015).

Thermal models for MSE walls found in the literature (Murray and Farrar 1988, Segrestin and Jailloux 1988, Kazosi et al. 2015) have modelled temperature series data by sinusoidal curves.

In this study, daily reported in-situ measurements for various locations were used directly from weather databases (WeatherOnline Ltd) in order to evaluate the effect of four different climates on in-soil temperature and relative humidity propagation with depth. The locations corresponded to continental (Toronto), Mediterranean (Barcelona), desert (Abu Dhabi) and tropical (Singapore) climates. Annual registries from 2016 to 2020 were obtained in order to be used as input data within the model. Figure 2-11 show the annual data registry for temperature and relative humidity for Abu Dhabi, Barcelona, Singapore and Toronto over the year 2020. It can be observed that the chosen climates have varied temperature ranges and different relative humidity variations throughout the year which will allow to evaluate a wide range of scenarios when modelling. Temperature values range from 4 to 48°C, -1 to 37°C, 21 to 35°C and -24 to 35°C for Abu Dhabi, Barcelona, Singapore and Toronto, respectively. Relative humidity values range from 16 to 94%, 26 to 99%, 57 to 100% and 28 to 100% for Abu Dhabi, Barcelona, Singapore and Toronto, respectively. Complete 5-year ambient registries for all four locations are presented in the annexes.

Previous studies have shown the importance of soil suction and the impact of precipitation on soil saturation (e.g., Vahedifard et al. 2017), particularly on the mechanical analysis of MSE walls. Hence, two global scenarios are analyzed, those being study cases with and without considering rainfall events in the boundary conditions.

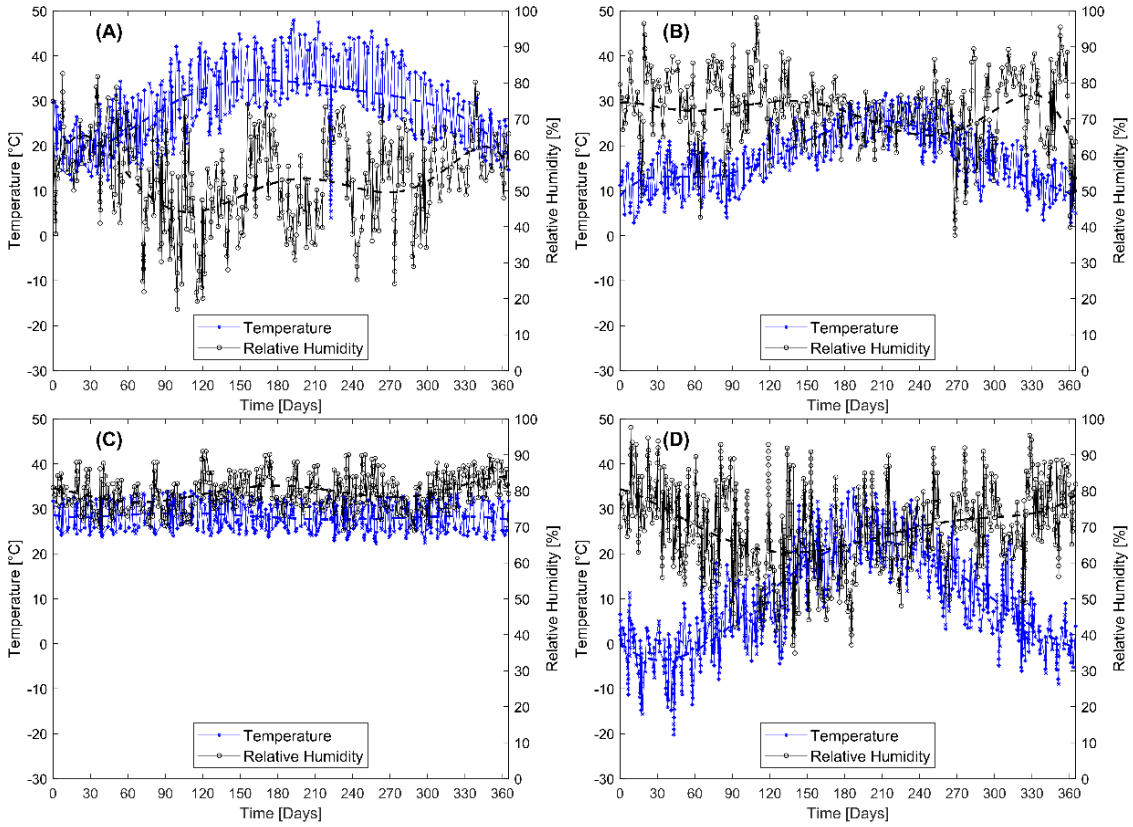

Figure 2-11. Temperature and relative humidity data from (a) Abu Dhabi, (b) Barcelona, (c) Singapore and (d) Toronto 2020 registry (WeatherOnline Ltd).

2.4 PET strap reinforcement behavior

The design process for MSE walls including PET strap walls require the use of partial factors to account for product-specific reduction in mechanical strength due to installation damage, chemical weathering (mainly due to UV light exposure), environmental degradation (primarily due to hydrolysis), and creep (ISO 20432:2007). The general reduction factor can be calculated as Eq. 2.

$$PF = PF_{CR} * PF_{ID} * PF_{w} * PF_{CH} * f_{s} \quad (1)$$

Where PF_{CR}, PF_{ID}, PF_{w} and PF_{CH} refer to creep, installation damage, weathering and chemical degradation partial factors, respectively and f_s is an uncertainty factor.

The determination of partial factors must be based on laboratory testing. In most cases, the degradation caused by UV light can be avoided with proper protection of the material prior to installation, nevertheless, based on on-site exposure time, reduction factor could require values of up to 1.25 (Greenwood et al. 2012). Installation damage must be accounted for by considering the project-specific backfill material and the type of sheath protecting the polyester fibres, with typical partial factor values ranging from 1.05 to 1.10. Figure 2-12 (a) shows a sample polyester yarn enclosed within a polyethylene sheathing.

On a short-term basis, the tensile behaviour of PET straps is measured using constant rate of deformation laboratory tests (e.g., ASTM D4595-17, EN ISO 10319:2015). Manufacturers usually offer product lines with a range of tensile resistance (grades), ranging from 30 kN to 100 kN per strap. Figure 2-12 (b) show a typical short-term load-extension curve for a PET strap product. Like other reinforcement geosynthetics, the strength and stiffness of PET straps is load-, time- and temperature-dependent (Bathurst and Naftchali 2021).

(a) (b)

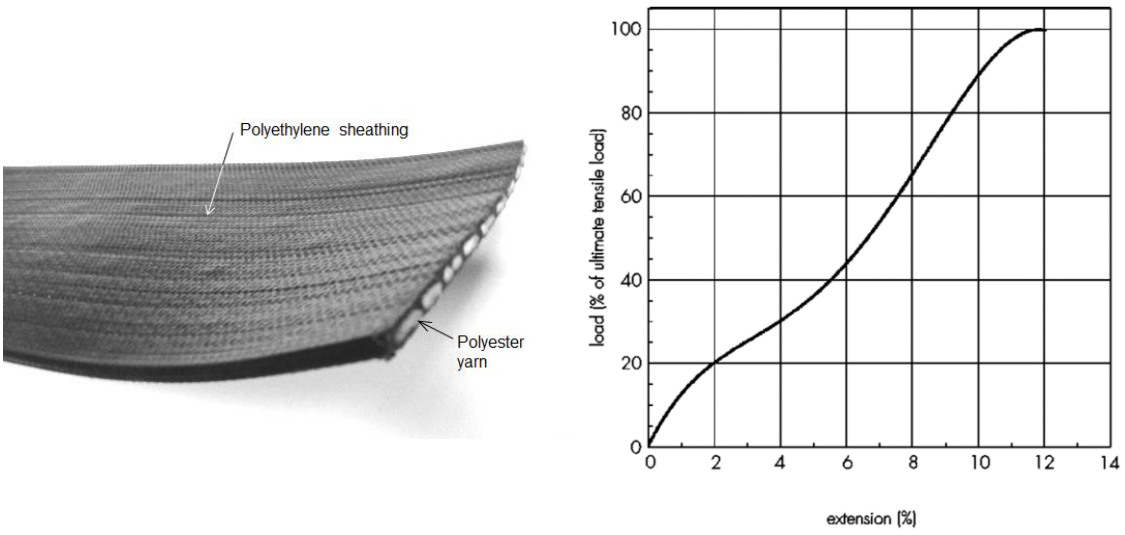

Figure 2-12. (a) Sample PET strap reinforcement and (b) typical polyester reinforcement short term tensile behaviour (Chamberlain & Cooper 2009)

Long-term deformation (creep) can be measured under constant tensile load for a given time, typically 1000 or 10000 hours, constant standard temperature of 20°C and relative humidity of 65% (ASTM D5262-97). Polyester reinforcements have presented a particular sensitivity to the initial loading sequence. In order to dimmish uncertainties in long term creep tests, it is common practice to perform short term creep ramp and hold tests, at the same load for durations of no longer than an hour. The obtained results are then averaged with the long-term creep results in order to better accommodate the creep data, particularly in initial strains (Greenwood et al. 2012). Depending on the available data and design life requirements, creep curves are generally extrapolated by a power law such as in Eq.2, in which ε is the strain, *A*, *B* and *n* are constants to be found for the best fit scenario and *t* is time.

$$\varepsilon = A + Bt^n \tag{2}$$

It is recommended though to not extrapolate by more than a factor of 10, as in if 1 year data is available, do not exceed 10 years when extrapolating results. For extended period of time, accelerated test by time-temperature shifting are required, such as the stepped isothermal method (ASTM D6992-03). The stepped isothermal methos (SIM) consist of performing various temperature steps on a conventional creep test over the course of equal time periods up until the glass transition temperature of the essayed material. By plotting the obtained results, a creep modulus can be calculated for each step and, subsequently, a strain-time plot representing the creep master curve for the desired load condition at a standard 20°C temperature. Figure 2-13 details graphically the process from (a) strain-time curves at various temperature into (b) creep modulus-shifted time and (c) creep master curve.

When implementing the shifted time plots, a thermal shift factor must be obtained in order to correct curves at each temperature step and generate a continuous curve. Thermal shift factors are also useful to predict creep strain for various design temperatures in combination with the obtained creep master curve via the SIM results.

According to laboratory results for PET strap reinforcements (You-Kyum et al. 2018), creep partial factor values range from 1.4 to 1.5, depending on design life time and applied load.

Creep under constant tensile load can be divided into three stages characterized by (1) a decreasing rate of elongation, followed by (2) a constant rate of strain over time, concluding with (3) an increasing rate of strain over time until rupture. PET strap reinforcement typically exhibits primary and tertiary creep stages, though in most applications, only primary creep is observed (Greenwood et al. 2012). Figure 2-14 shows constant load creep curves for a FASTEN PET strap product presented as strain versus log time obtained using the SIM. Creep master curves for various strap grades and UTS load conditions are presented in the annexes.

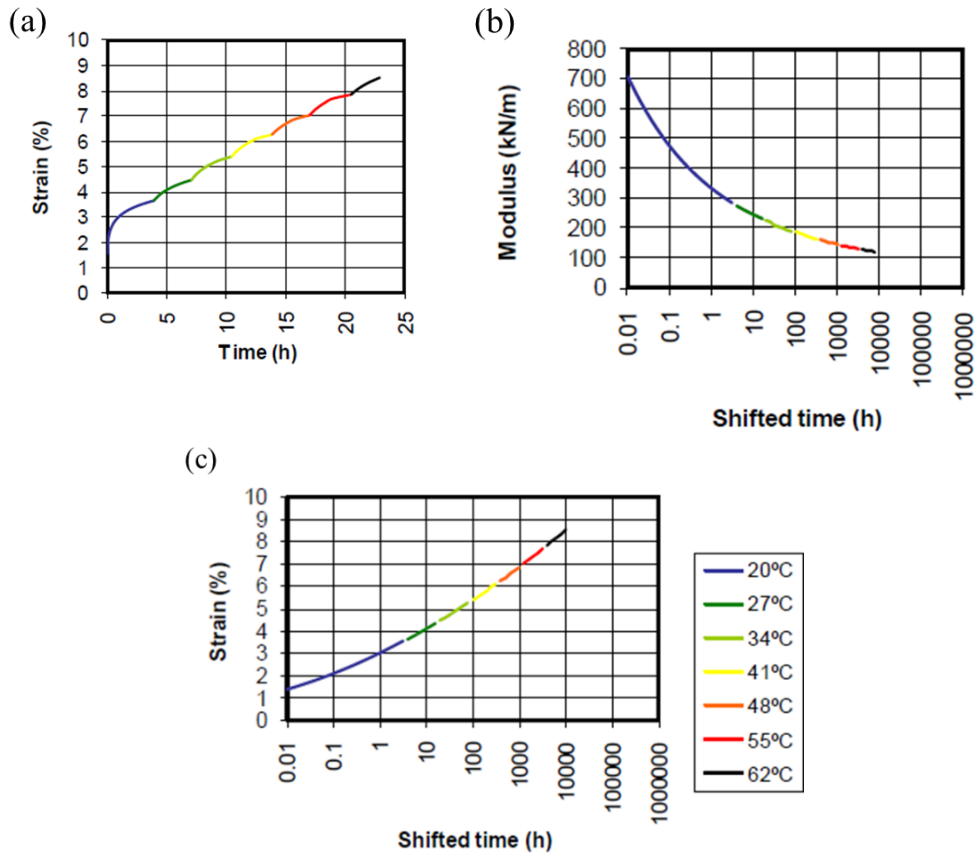

Figure 2-13. Graphic representation of the (a) SIM test results, (b) creep modulus estimation and (c) predicted creep master curve from a single constant load (Greenwood et al. 2012).

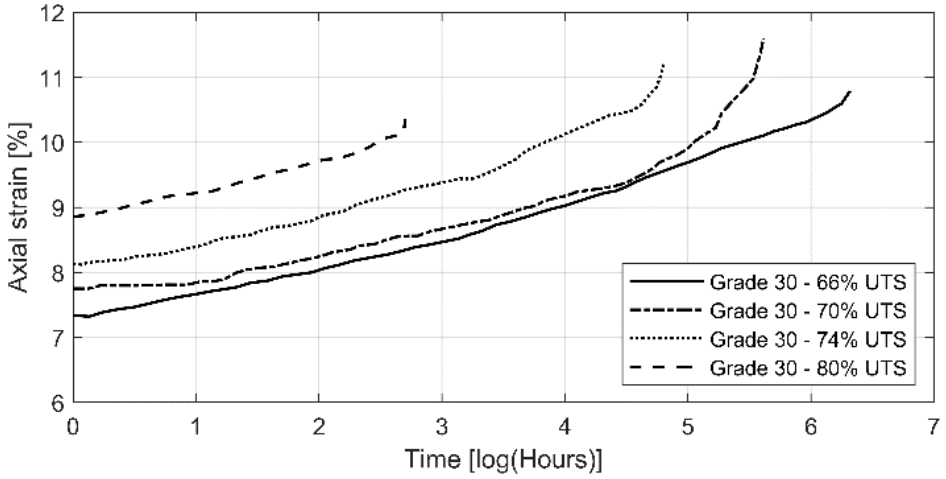

Figure 2-14. Axial strain versus log time under constant load for grade 30 PET strap reinforcement specimens (You Kyum et al. 2018). Note: UTS = ultimate tensile strength.

Figure 2-15 shows the reaction in which a diacid (terephthalic acid) and dialchol (ethylene glycol) go through a polycondensation process in order to manufacture PET yarns. This is a reversible process and thus, when water molecules come in contact with polyester, a progressive rupture of the polymer chains results in loss of strength of the material, which is known as degradation by hydrolysis (Jailloux et al. 2008, Greenwood et al. 2012).

The reaction is related to the number of carboxyl end groups present at the end of the polymer chains. a higher molecular weight refers to a lower number of carboxyl end group, which in turn results in a lower tendency to hydrolysis. Hydrolysis can be defined as internal or external depending on the location at which it occurs. Shows the produced degradation by hydrolysis on a PET sample after a 4-year immersion in saturated lime solution at 50°C.

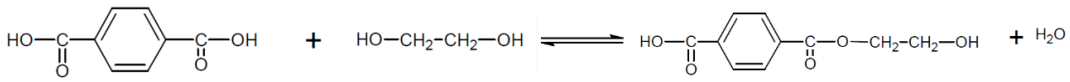

Figure 2-15. Degradation of PET by hydrolysis (Jailloux et al. 2008)

Both phenomena are activated by temperature, reacting faster as temperature increases following Arrhenius´ formulation (Eq.3).

$$A = A_0 \exp(-\frac{E}{R\theta}) \quad (3)$$

Where *A* is the rate of degradation, A_0 a pre-exponential factor, *E* is activation energy of the process in J/mol, *R* the universal gas constant in J/mol K and θ the absolute temperature in K. Values of activation energy within polymers can be approximated within 30 to 110 kJ/mol

Laboratory tests to determine the level of degradation due to hydrolysis are carried out by completely submerging samples at high water temperature (98°C), accounting for a fully saturated medium for a period of 28 days (EN 12447-02:2001). As the rate of hydrolysis is sensitive to temperature and relative humidity, the in-soil conditions of MSE walls seem crucial for the determination of a safety factor regarding the expected degradation of the reinforcement caused by hydrolysis. Typical values for chemical degradation partial factors range from 1.0 to 1.4 (ISO 20432:2007).

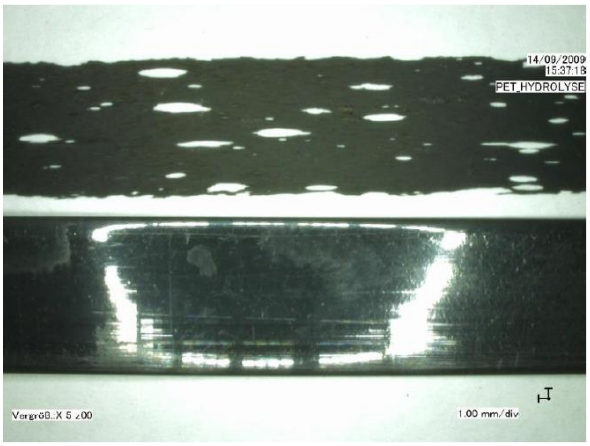

Figure 2-16. PET sample before (below) and after (above) a 4-year immersion in saturated lime solution at 50°C (Greenwood et al. 2012)

3. NUMERICAL MODEL

3.1 Overview

The numerical simulations in this study considering environmental effects and PET strap mechanical response were carried out using the software CODE_BRIGHT (Olivella et al. 1996, CODE_BRIGHT 2021). This code is used to solve coupled thermal, hydraulic and mechanical problems.

Two main model were developed. The first consist in a 2D simplified domain in order to evaluate parameter influences, boundary condition effects and generate an overall view as to what needs to be prioritized when generating a more detailed model. The second model consist of a 2D MSE wall structure, including all its components, such as concrete facing panels, in-soil reinforcements, HDPE leveling pads and soil interfaces.

3.2 Simplified soil model

In order to study the effect of ambient temperature (T), relative humidity (RH) and precipitation (PR) variations on the numerical model, a simplified domain was developed as a first approach. (See Figure 3-1). Points M, N and O, located at 2, 4 and 6 meters of depth, are chosen as to analyze and compare in-soil results. The generated mesh consists of 450 structural triangular elements with 256 nodes. Material properties used correspond to a sandy soil, with the values depicted in Table 3-1. No water table was assumed. The bottom base temperature was constant at +1°C higher than the mean annual temperature reported from the temperature registry used for each analysis.

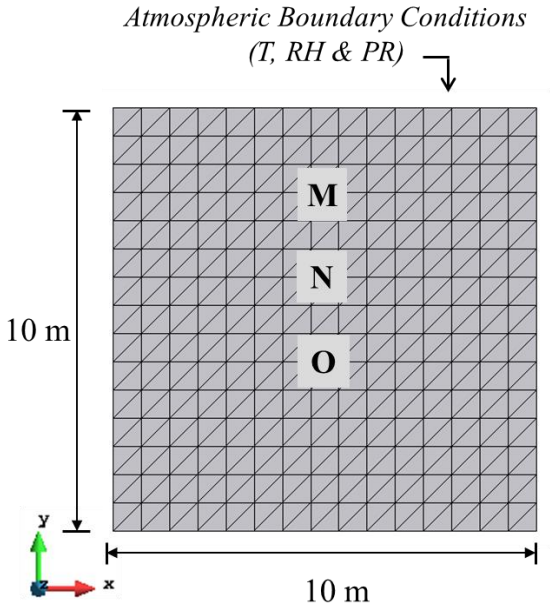

Figure 3-1. 2D numerical model domain and finite element mesh for the simplified soil model

Regarding the implementation of precipitations in the numerical model, a flow boundary conditions is used in which the prescribed rain mass is included in a boundary condition file with discrete real time series of various geographical locations. Rain must be incorporated in mass over time and surface units [kg/s/m]. Initial conditions include temperature values equal to the mean annual temperature obtained from the ambient temperature registry used for each analysis.

3.3 MSE wall model

The geometry of the TH coupled model is presented in Figure 3-2. In order to model the in-soil behaviour due to temperature and relative humidity from the ambient in-air data, a 15 m-high reinforced soil wall was assumed (tall enough to identify in-soil propagation of temperature and relative humidity). The upper boundaries are in direct contact with the atmosphere (i.e., no surface material such as vegetation or pavement is considered). The generated 2D mesh consists of 5536 structural quadrilateral elements with 5714 nodes. Mesh construction included all mechanical elements such as the 1.5 m-high concrete facing panels, the 20 mm-thick bearing pads and the 3 mm-thick PET reinforcement layers with 0.7H length. Mesh sensitivity analyses were first carried out to optimize element size, especially at the boundary surfaces where the ambient in-air boundary conditions are applied. As a consequence, smaller size elements are used at the superior boundaries. The used software does not count with interface or zero-length elements to represent interfaces between materials. As such, a soil-facing equivalent width is considered with reduced resistant parameters to account for the soil-structure interaction as proposed by Damians et al. (2015) for the first 10 cm of soil. Following this, a transition material within the equivalent interface and the reinforced backfill is included.

The water table in this study was located at 10 m depth below the ground surface at the wall toe (i.e., at 10 m-height from model bottom). The bottom base temperature was constant at +2°C higher than the mean annual temperature reported from the temperature registry used for each analysis. Initial model temperature was considered to be equal to the annual mean in-air ambient temperature for each registry. Staged construction was not used in this study to simplify the model.

Actual real time series input data were used for temperature, relative humidity and precipitations for each control location, rather than smoothed or simulated sinusoidal temperature, relative humidity and simulated precipitation distributions. Boundary conditions consist of ambient in-air data from daily records including T (daily minimum and maximum), RH that included flux at all surface boundaries in contact with the air and rain mass prescribed flow (see Figure 3-2). T and RH conditions are imposed on all superior boundaries, while precipitation is imposed in all but the vertical retaining wall (i.e., only the horizontal boundaries).

Points A, B and C, located 2 m from facing and at 1, 7 and 14 m-depth, respectively, were used as measuring points to compare results.

As previously stated, T and RH environmental data were obtained at four different geographic locations in order to analyze a range of worldwide conditions. Analyses for each model were for 1-, 3- and 5-year periods using daily records from years 2016 through 2020.

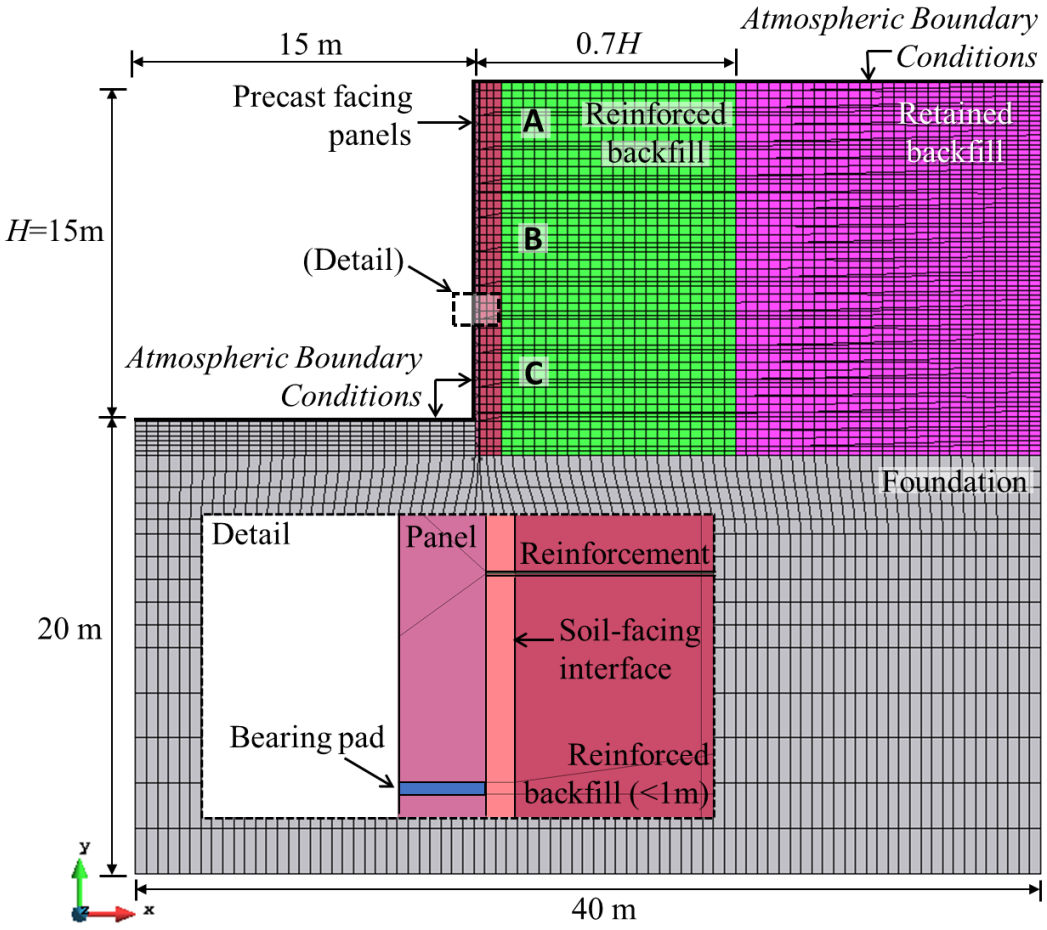

Figure 3-2. 2D model domain and finite element mesh used for the MSE wall analyses. Note: BC = boundary conditions.

Regarding the mechanical analysis, a linear model with an elastic modulus E = 32 GPa and Poisson´s ratio ν= 0.2 was used to model the precast concrete facing panels. Initial conditions consider equilibrium of soils self-weight with a resting coefficient K_0=0.5. All boundaries have a 0.1 MPa imposed stress as to account for atmospheric pressure. Lateral boundaries are fixed on the x-axis.

3.4 Hydraulic and thermal properties

A granular soil was considered in this study. The hydraulic and thermal model formulations and matching soil material parameters are presented in Table 3-1. Soil thermal dispersion is modeled by Fick´s law with a horizontal and vertical dispersivity of d_l = 5 m and d_t = 0.5 m, respectively. Thermal conductivity was modelled using Fourier´s law, with dry and saturated conductivity values of γ_{dry} = 0.5 W/mK and γ_{sat} = 1 W/mK. Default values for solid phase specific heat (c_s = 1000 Jkg-1K-1) and density (ρ_s = 2700 kgm-3) were also used. The same soil was used for the simplified soil model as well as the MSE wall model.

Table 3-1. Thermal and hydraulic properties for soil used in the numerical model.

Constitutive law	Formulation	Parameter	Value
Water retention curve (Van Genuchten)	$S_e = \frac{S_l - S_{rl}}{S_{ls} - S_{rl}} = \left(1 + \left(\frac{P_g - P_l}{P}\right)^{\frac{1}{1-\lambda}}\right)^{-\lambda}$	Residual saturation, S_{rl} [-]	0
		Maximum saturation, S_{ls} [-]	1
		Reference pressure, P_o [MPa]	0.005
		Shape parameter, λ [-]	0.8
Relative liquid phase permeability	$k_{rl} = S_e^n$	Shape Parameter, n [-]	3

Regarding the MSE wall model, the water retention curve (Van Genuchten model) for the concrete facing panels was modelled with a reference pressure P_0 = 0.001 MPa and shape parameter λ = 0.4. Table 3-2 shows porosity and intrinsic permeability values used in the model. Values for the PET strap reinforcement layers, precast facing panels and HDPE bearing pads correspond have been adjusted to equivalent values for a 2D plane strain 1-m slice.

Table 3-2. Porosity and permeability values for used materials.

Material	Initial porosity [-]	Intrinsic permeability [m^2]
Soil (Backfills and Foundation)	0.3	1×10^{-12}
Precast facing panels	0.15	1×10^{-12}
PET strap reinforcements	0.01	1×10^{-16}
HDPE bearing pads	0.4	1×10^{-10}

3.5 PET strap mechanical properties and modelling

As shown in Figure 2-12 (b), short-term behaviour of PET straps presents variations on its elastic moduli, but can be approximated using linear stress-strain relationships. The present study considers two cases, a linear model with a single elastic modulus, using a Young´s modulus (E) and Poisson´s ratio (ν), and secondly, a bi-linear model with two elastic moduli (E_1 and E_2) and Poisson´s ratio, as shown schematically in Figure 3-3.

In order to simulate in-soil conditions acting over the PET strap reinforcement, a temperature- and saturation-dependent visco-elastic (VE) constitutive model was used to account for creep, with rate of deformation ($d\varepsilon/dt$) and viscosity (η) formulated as (Eq.3) and (Eq.4), respectively:

$$\frac{d\varepsilon}{dt} = \frac{1}{2\eta^{VE}}(\sigma' - p'I) \quad (4)$$

$$\frac{1}{\eta^{VE}} = B(T)\sqrt{S_l} \quad (5)$$

Here, σ' is effective stress, p' is mean stress, I is the identity matrix, S_l is degree of saturation and $B(T)$ is a function of temperature (T), the universal gas constant (R), and activation energy (Q).

Additionally, a visco-plasticity (VP) model was implemented to account for strain softening over long-term constant load. (Eq.5-7):

$$\frac{\mathrm{d}\varepsilon^{VP}}{\mathrm{d}t} = \Gamma\langle\Phi(F)\rangle\frac{\partial G}{\partial\sigma} \tag{6}$$

$$\Phi(F) = F^m \tag{7}$$

$$\Gamma = \Gamma_0 \exp\left(\frac{-Q}{RT}\right) \tag{8}$$

Here, F and G are functions of mean stress (p), a frictional parameter (δ) and adhesion (a), and m is a power stress parameter. Parameter Γ is fluidity which is a function of temperature, reference fluidity (Γ_o), universal gas constant (R), and activation energy Q. Parameters δ and a are controlled by a softening parameter (η^*) which provides a transition between peak and residual stages.

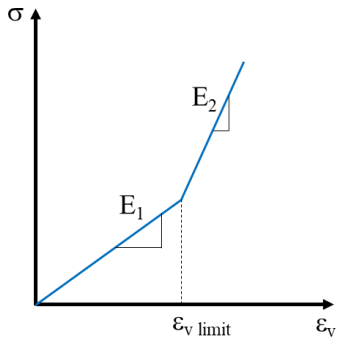

Figure 3-3. Bi-linear elastic model representation

To determine the model parameters to represent the mechanical behaviour of the PET strap reinforcements, a 2D model consisting of 134 structural triangular elements with 136 nodes was generated, as shown in Figure 3-4. A manual calibration process was carried out to determine model parameters which permitted a best fit when compared to laboratory results obtained for GECO's FASTEN FS products (GECO 2021)

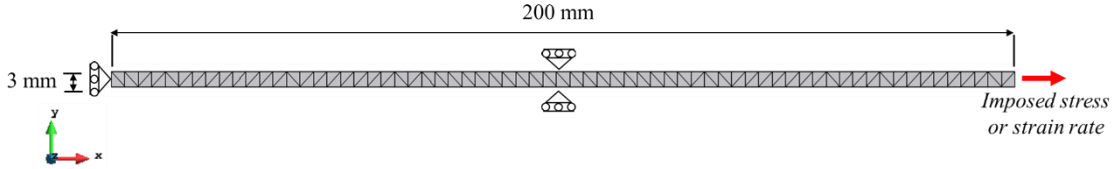

Figure 3-4. 2D finite element model domain and mesh used to calibrate PET strap reinforcement model

The mechanical parameters used to model the PET straps are presented in Table 3-3. Since the implemented model is 2D (i.e., 1 m-plane strain slice), an equivalent plane strain stiffness was calculating considering an average width of 89 mm per strap and two connections every 2.5 m in the wall face direction (i.e., single panel width) (see Damians et al. 2021).

Table 3-3. Model parameters range for PET strap reinforcement.

Constitutive model	Parameter	Value
Linear elasticity	Elastic modulus, E [MPa]	2.2 to 4.8
	Poisson's ratio, ν [-]	0.30 to 0.34
Bi-Linear elasticity	1st elastic modulus, E_1 [MPa]	1.7 to 3.9
	2nd elastic modulus, E_2 [MPa]	45 to 100
	Poisson ratio, ν [-]	0.20 to 0.33
	Volumetric strain limit for E_i change, $e_{v\text{-}limit}$ [-]	0.0078 to 0.086
Visco-elasticity	Fluidity, B [$s^{-1}MPa^{-1}$]	5.3×10^{-14} to 2.1×10^{-10}
Visco-plasticity	Power of stress function, m [-]	2.6 to 3.8
	Fluidity, Γ [$s^{-1}MPa^{-m}$]	3.6×10^{-4} to 1.4×10^{-3}
	Softening parameter, η^*, [-]	1×10^{-3} to 8×10^{-2}
	Peak & residual parameters for adhesion, a_{peak} & $a_{res.}$ [MPa]	0.05 to 0.12 and 0.03 to 0.12
	Peak & residual parameters for friction, δ_{peak} & $\delta_{res.}$ [°]	10^{-4} and 10^{-5}

Two scenarios were analyzed. First, elements with bi-linear elastic moduli and VE properties were subjected to an initial tension, followed by a ramp increase up to the desired load representing a selected fraction of the ultimate tensile strength (UTS). Second, elements with linear elastic modulus, VE and VP properties were subjected to a constant initial load.

4. RESULTS

4.1 Simplified soil model

Figure 4-1 shows T and RH distributions over a 5-year analysis period using Abu Dhabi climate data for years 2016 to 2020 for points M, N and O (see Figure 3-1). Results show cyclic oscillations on temperature values with yearly cycles The impact of ambient conditions over in-soil temperature values is more meaningful at surface level, with variations of ±3C, ±1C and ±0.3°C on points M, N and O respectively with a mean value of 29.5°C. Results suggest that mean in-soil temperature can be approximated by the mean annual temperature. Similar results were obtained with all four climate registries. In-soil relative humidity values also reflect the reduced influence of in-air conditions as depth increases, with mean values of 66%, 76% and 85% for points M, N and O, respectively.

Figure 4-2 shows the temperature and relative humidity evolution for the base case and rain case over a 5-year analysis using the Toronto registry. It can be observed that, as rain is included as a boundary condition, temperature decreases throughout the whole model. The mean temperature of the model, considering points M, N and O, decreases from 9.5 °C to 5.3 °C through the 5-year analysis period. Nevertheless, temperature distributions do not appear to change, as boundary conditions have more influence over near-surface values (point M), while in-depth values present less oscillations (points N and O). When observing relative humidity results, a clear increase at all depth can be appreciated near the first rainfall event (day 6), which increases in-soil values to over 90% within a shorter period of time as compared to the base case. For the remainder of the analysis, relative humidity values appear unaffected when comparing base and rain cases, reaching almost constant values within 99%.

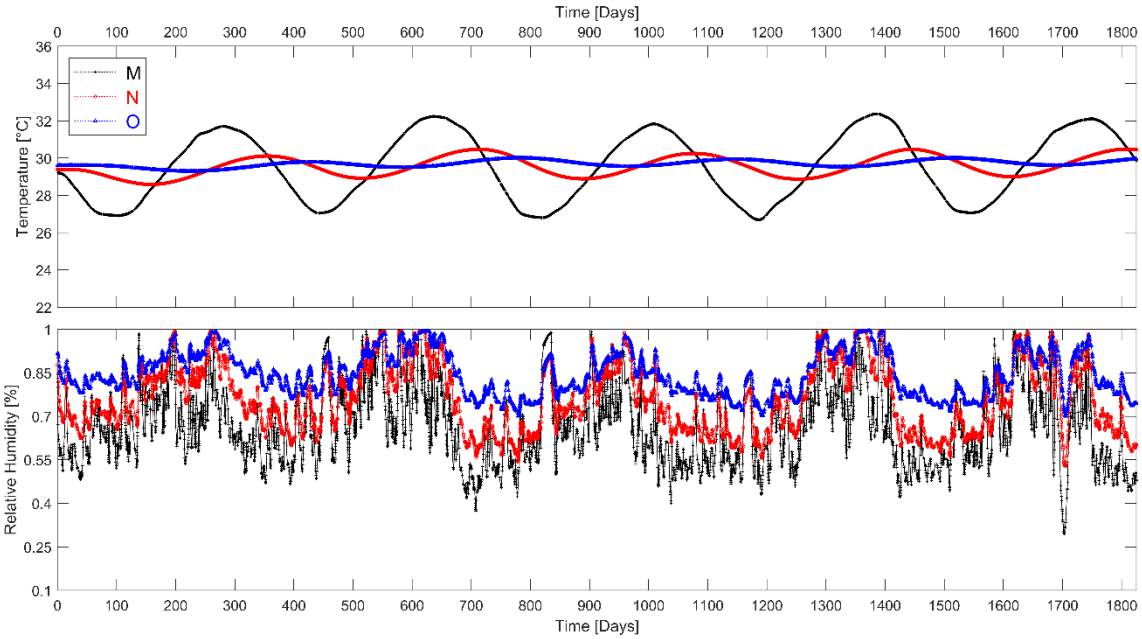

Figure 4-1. Temperature and relative humidity distributions over a 5-year analysis period using Abu Dhabi climate registry in the simplified soil model.

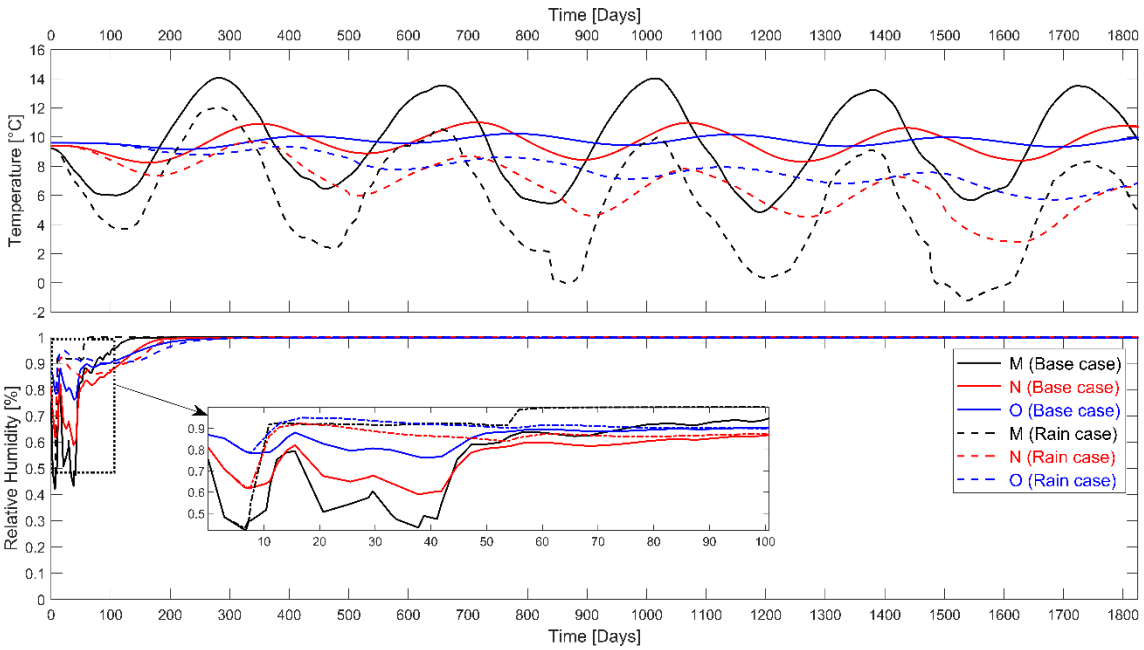

Figure 4-2. Temperature and relative humidity result comparisons after a 5-year analysis for base case and rainfall case using the Toronto in-air conditions with the simplified soil model.

Table 4-1 details mean soil temperatures and relative humidity values for cases with and without incorporating rain as a boundary condition for points M, N and O for all climate registries. When in absence of rainfall, the mean soil temperature can be approximated by the yearly mean annual temperature. Nonetheless, it has been observed that when rainfall is incorporated as a boundary condition, mean in-soil temperatures throughout decreases between 2°C and 4°C for all ambient conditions, save for Abu Dhabi, which has the lowest rain frequency and intensity of the four boundary conditions. When in the presence of rain, in-soil relative humidity average values for Barcelona and Toronto cases present small variations, between 0.3% and 3%, while Abu Dhabi and Singapore cases presents increments from 6% up to 20%.

Table 4-1. Mean temperature and relative humidity values for all climate conditions with and without the incorporation of rainfall for points M, N and O after a 5-year analysis.

Location	Observation point	Base case		Rainfall case	
		T [°C]	RH [%]	T [°C]	RH [%]
Abu Dhabi	M	29.4	66.7	29	87.6
	N	29.5	76.5	29.2	87.6
	O	29.7	84.9	29.5	94.4
Barcelona	M	17.6	96	15.2	99.3
	N	17.7	97.2	15.6	98.3
	O	17.8	98.2	16.3	98.5
Singapore	M	28.6	86	25.6	99.8
	N	28.7	90	26.3	99.8
	O	28.8	93.8	26.3	99.8
Toronto	M	9.3	98.3	5.2	99.3
	N	9.5	98	6.5	98.3
	O	9.7	98.5	7.7	98.5

4.2 PET strap modelling

Figure 4-3 depicts the adjustment of the proposed models with creep laboratory measurements obtained by You-Kyum et al. (2018) for grade 30, 50 and 70 kN straps under loads of 66% and 70% of UTS. The obtained adjustment is adequate for both the bi-linear elastic and VE models, and VE and VP models. Figure 4-4 illustrates the influence of temperature on creep behaviour for a grade 30 reinforcement material under 70% UTS load at constant temperature. The range of temperatures used (10°C and 29°C) are the maximum and minimum mean values obtained using the thermo-hydraulic models with different ambient in-air conditions (Base case). When subjected to temperature variations, both the VE and VP models update their equivalent fluidity, thus, long-term deformation varies within a range of 1-1.5% for a 19°C variation over a 50-year period. By including a linear expansive model, an initial change in temperature (from 20°C to 10°C or 20°C to 29°C), followed by a constant temperature modelling, shifts the creep curve to higher or lower deformation for increasing or decreasing temperatures, respectively.

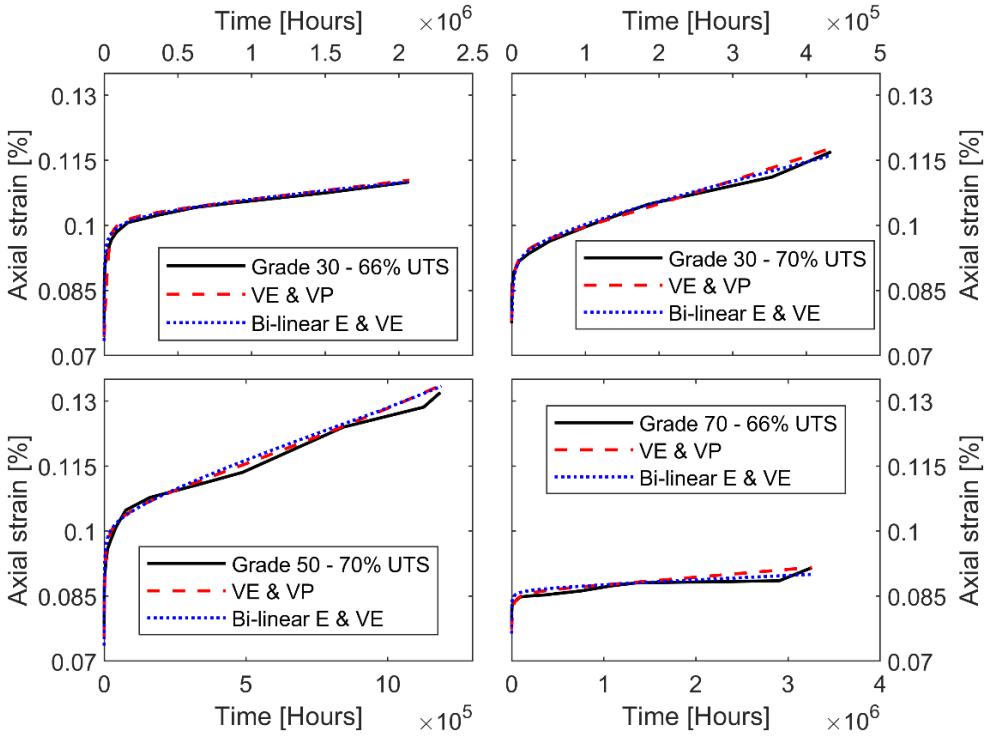

Figure 4-3. Long-term deformation model results for grades 30, 50 and 70 kN at 66 or 70% of UTS load compared to accelerated laboratory creep tests.

Using a grade 30 strap under 70% of UTS load condition, a mesh sensitivity analysis was carried out considering a VE and VP model. 8 cases corresponding to various number of elements (from 4 to 134) were analyzed, resulting in no significant differences. Figure 4-5 shows three of the used meshes. Figure 4-6 details the obtained axial strain over time curves for these three cases. Studying the effect of different meshes when modelling PET straps is crucial, as the geometry of the mesh can vary considerably when implementing a full MSE wall model compared to the single reinforcement element used to calibrate the mechanical behaviour.

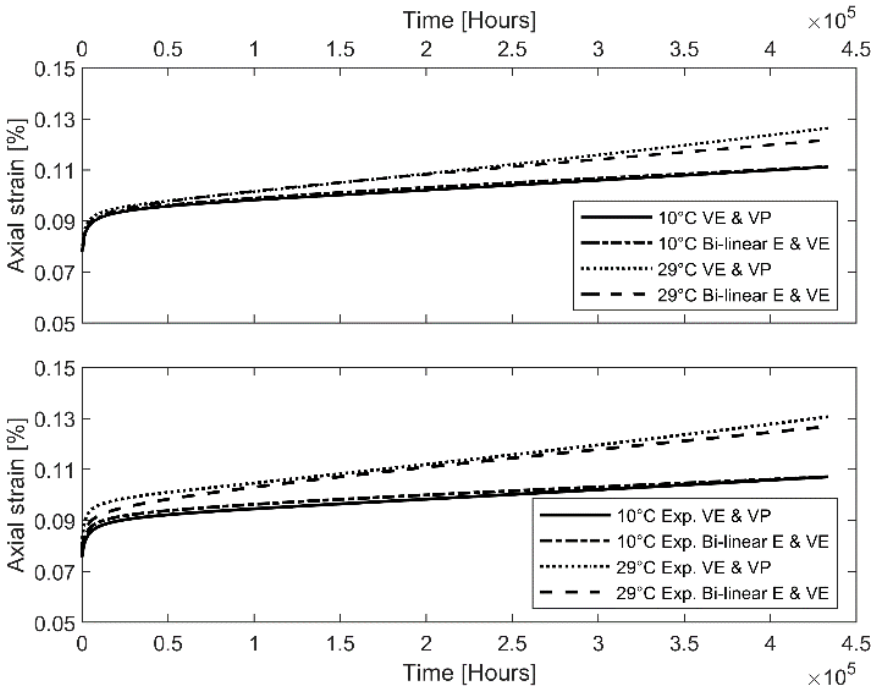

Figure 4-4. Creep behavior changes due to temperature variations from 20°C to 10°C or 29°C for a grade 30 strap at 70% UTS load.

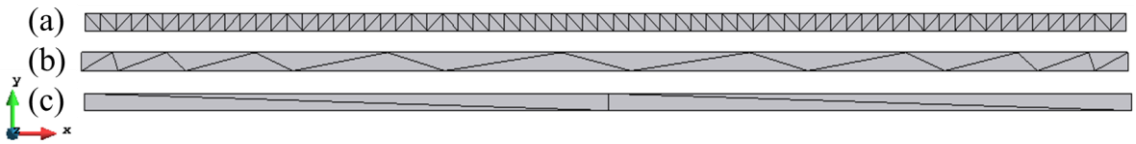

Figure 4-5. Used meshes for sensitivity analysis with (a) 134, (b) 20 and (c) 4 elements

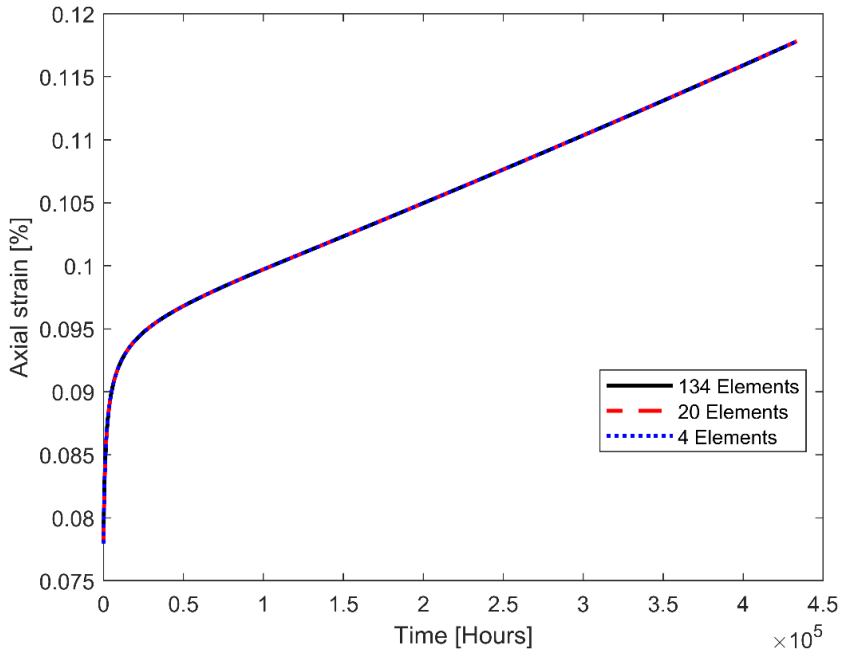

Figure 4-6. Obtained axial deformation under 70% of UTS load for a grade 30 PET strap reinforcement using various mesh geometries (134, 20 and 4 elements).

4.3 MSE wall model

4.3.1 TH MSE wall base model

The following results consider the base MSE wall model, which does not include rainfall as a boundary condition.

Figure 4-7 and Figure 4-8 present T and RH distributions over a 5-year analysis period for Abu Dhabi atmospheric conditions using the 2016 to 2020 registries. Steep T variations are observed within the first meter from the atmospheric conditions ($\Delta T \approx 15°C$), followed by a 3 to 4 meters wide area in which T oscillations become less pronounced ($\Delta T \approx 7°C$), but still relevant. After 5 meters from the boundary, T variations fall to almost constant values ($\Delta T \approx 1°C$) within the reinforced soil. RH values show a considerable increase after 18 months within the reinforced soil. For the 35- and 60-months periods, RH values present a gradual variation in depth up to the imposed water table, ranging from approximately 25% up to 100%. During the main course of the analysis, the maximum tension zone is exposed to RH values of 60% or less, save for its near surface points.

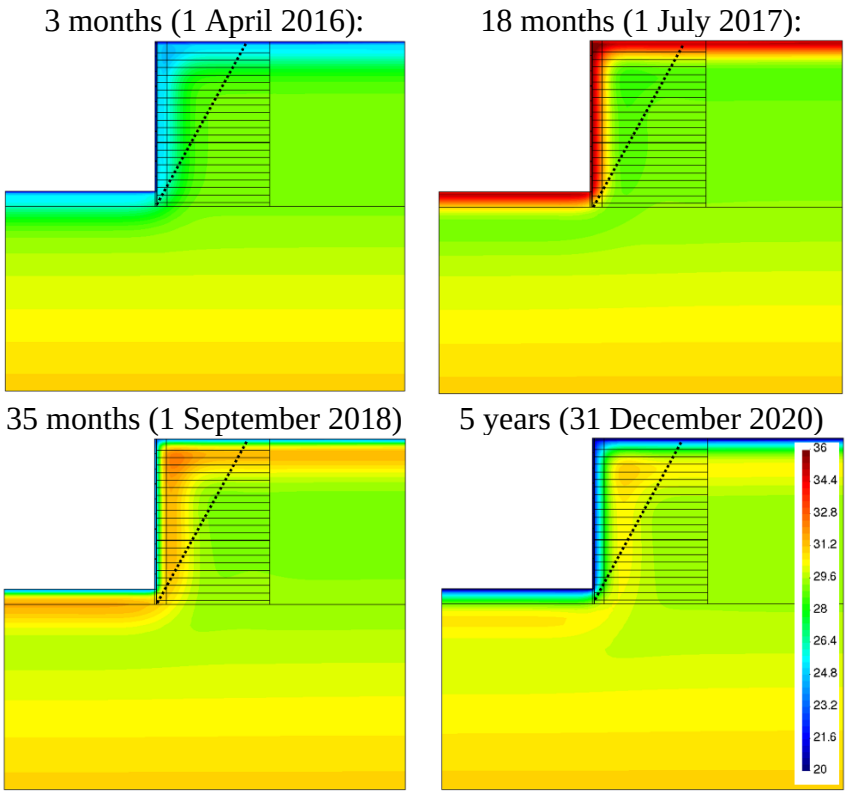

Figure 4-7.TH model 5-year temperature (ºC) results evolution with environmental conditions from Abu Dhabi 2016 to 2020.

Figure 4-9 and Figure 4-10 show T and RH distribution over a 5-year analysis period for Barcelona 2016 to 2020 in-air (atmospheric) conditions. Model results show an important variation of temperature ($\Delta T \approx 10°C$) within the first 2 meters from the domain air boundaries, followed by a 3-meter zone in which variations are visible but less

pronounced (ΔT ≈ 2°C). As depth increases, in-soil T appears to remain unaffected and converges to the imposed lower boundary condition. Regarding RH, a zone of influence of 1 m can be identified at the air boundaries. As initial conditions stabilize, in-soil RH tend to values ranging from 98 to 99%, reaching saturation near the imposed water table. Due to the open joints between panels (2 bearing pads per panel) small propagation zones due to diffusive flow through these openings can be identified.

The dotted line corresponds to the potential failure surface when using extensible reinforcements and thus, the theorical zone of maximum stress the PET straps must endure. Regarding RH, the area in which this boundary is located does not present important variations, save for its ends at the foot and top of the wall, but is exposed to almost constant RH values between 99% to 100%. Temperature wise, the theorical failure line transitions from a zone with relevant temperature variations near surface (ΔT ≈ 10°C) into a more stable temperature ambient (ΔT ≈ 2°C) at the center of the model.

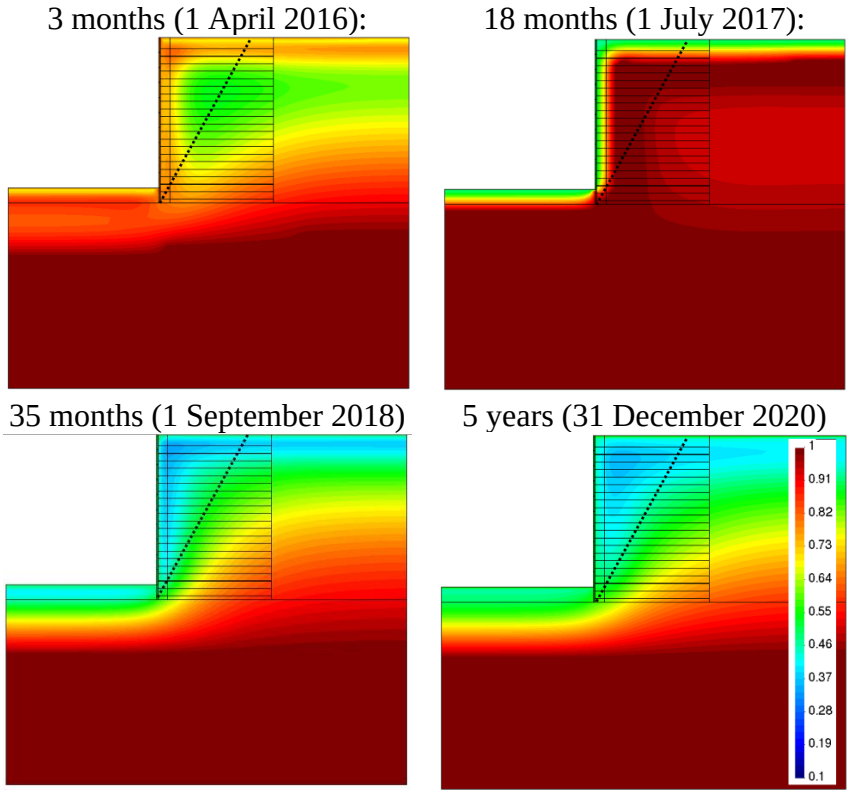

Figure 4-8. TH model 5-year relative humidity (-) results evolution with environmental conditions from Abu Dhabi 2016 to 2020.

Figure 4-11 and Figure 4-12 detail T and RH in-soil distributions after a 5-year analysis period using the 2016 to 2020 Singapore atmospheric records. T profiles show almost constant distributions over time with small variations at surface level due to ambient condition variations and subtle variations within the reinforced and retained backfill (ΔT ≈ 1°C). In a similar manner, RH results show steady distribution throughout the analysis period with overall similar in-depth distributions after 4 meters. Depending on the observed period, near surface values present variations between 70% to 90%. Overall, the maximum tension zone is subjected to average values of T ≈ 28.5°C and RH ≈ 85%.

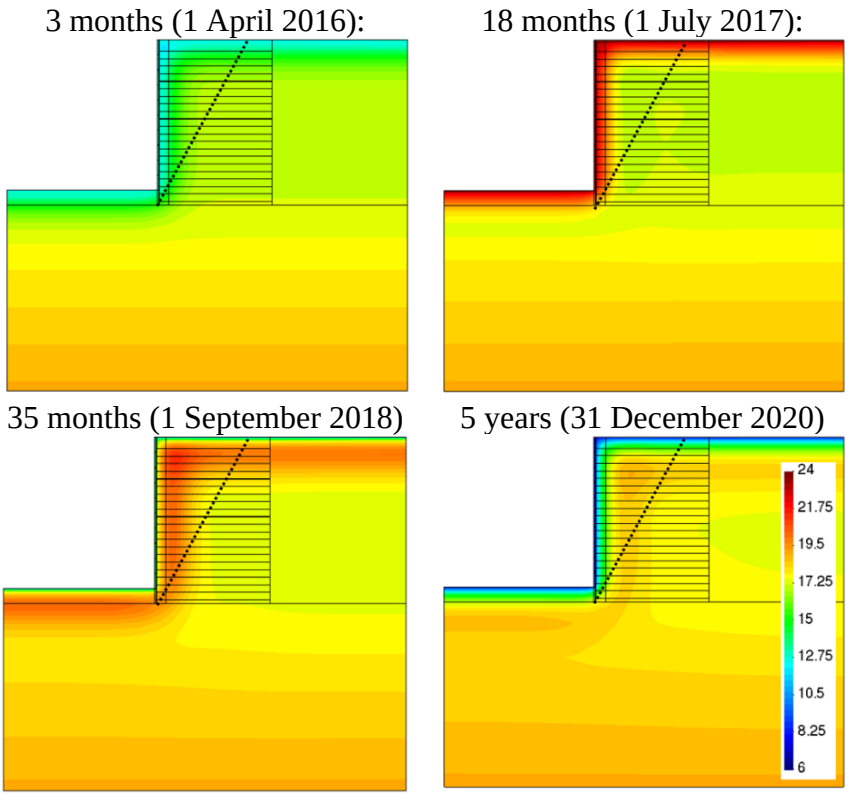

Figure 4-9.TH model 5-year temperature (ºC) results evolution with environmental conditions from Barcelona 2016 to 2020.

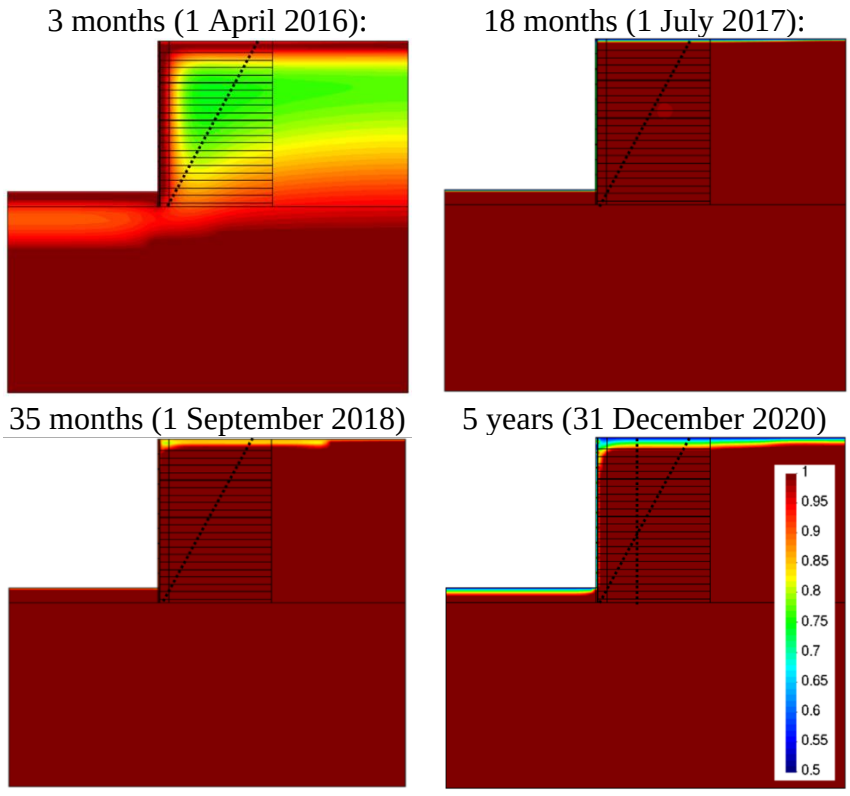

Figure 4-10. TH model 5-year relative humidity (-) results evolution with environmental conditions from Barcelona 2016 to 2020.

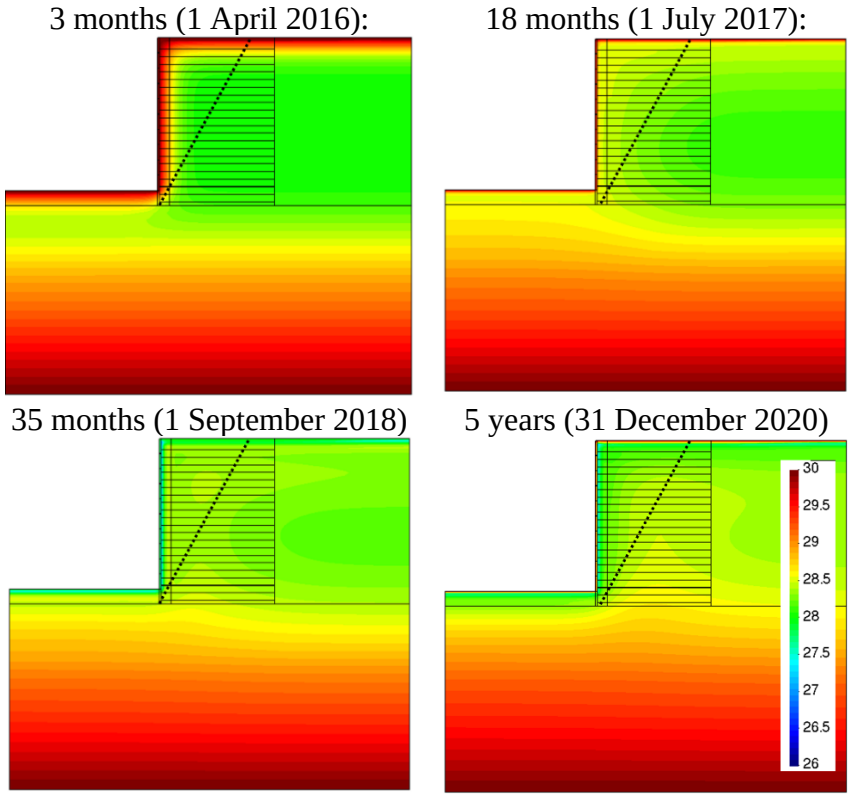

Figure 4-11.TH model 5-year temperature (ºC) results evolution with environmental conditions from Singapore 2016 to 2020.

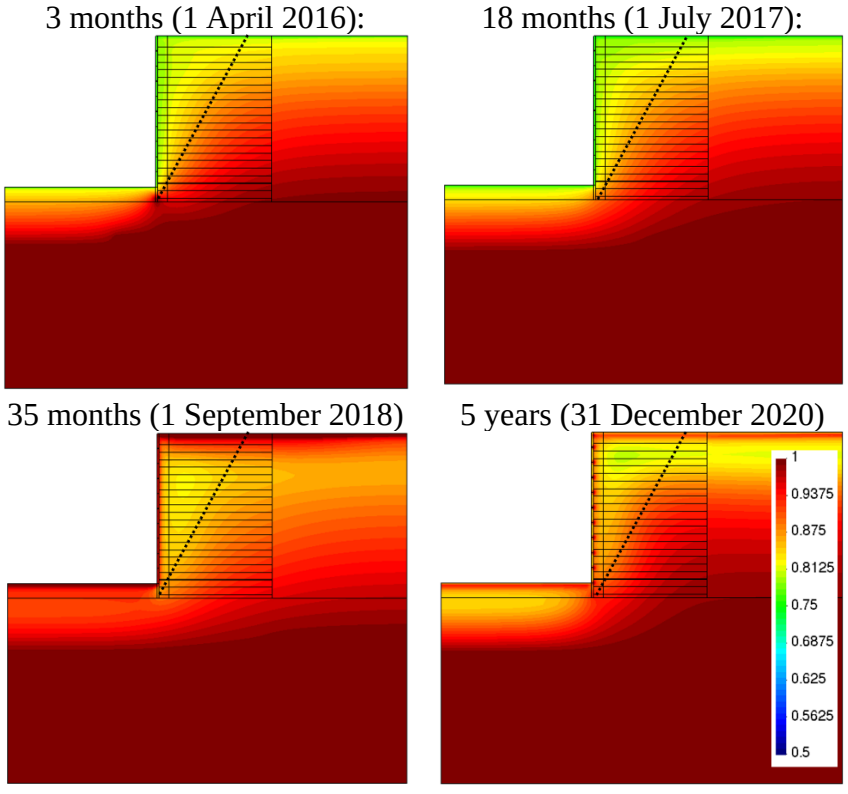

Figure 4-12. TH model 5-year relative humidity (-) results evolution with environmental conditions from Singapore 2016 to 2020.

Figure 4-13 and Figure 4-14 show T and RH distributions of the MSE wall model over a 5-year analysis period for Toronto 2016 to 2020 in-air conditions. In-soil T profiles present variations within the first 3 to 4 meters, particularly in the first meter closest to the boundary condition. As depth increases, in-soil T seems to remain almost constant at approximately 9°C. As with the Barcelona registry case, after an equalization period within the first months, in-soil RH reach a uniform value of 99%. This implies that the PET reinforcements are subjected to a constant almost in-air saturation conditions at roughly 9°C to 10°C.

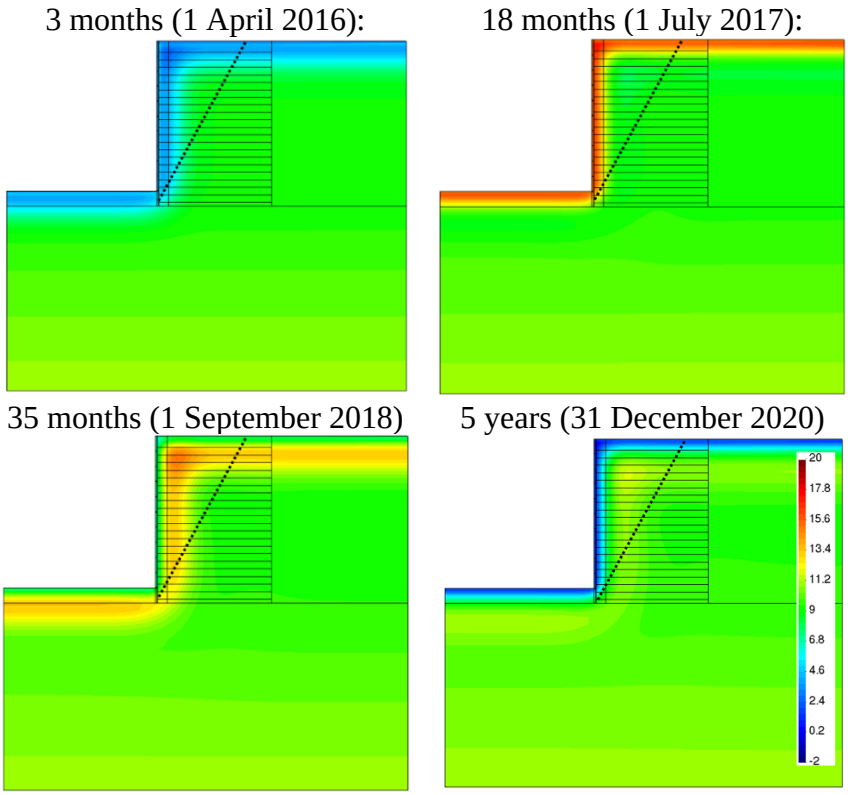

Figure 4-13.TH model 5-year temperature (ºC) results evolution with environmental conditions from Toronto 2016 to 2020.

Figure 4-15 show the in-soil temperature distributions measured in MSE structures for different locations and climates obtained by Segrestin et al. (1988) and Jones (1995). Figure 4-16 details the in-soil temperature iso-surfaces obtained for various time steps using the proposed MSE wall model using 5-year Barcelona registry. As the referenced measurements took place in smaller dimension structures, between 6 and 7 meters tall, for comparison purposes, a detail of the top 5 front facing panels, meaning a dimension of 7.5 x 7.5 m of the full 15 m MSE wall has been selected.

As the model boundary conditions does not correspond to that of Figure 4-15, values are not expected and do not match. Nevertheless, it is of interest to compare in-soil temperature distributions. The modelled T iso-curves follow the boundaries geometry, following an inverted *"L"* shape like distribution in the same way as the measured temperatures. The described distribution presents gradual decreases or increase, depending on the observed season for both, the obtained model results and in-situ measurements.

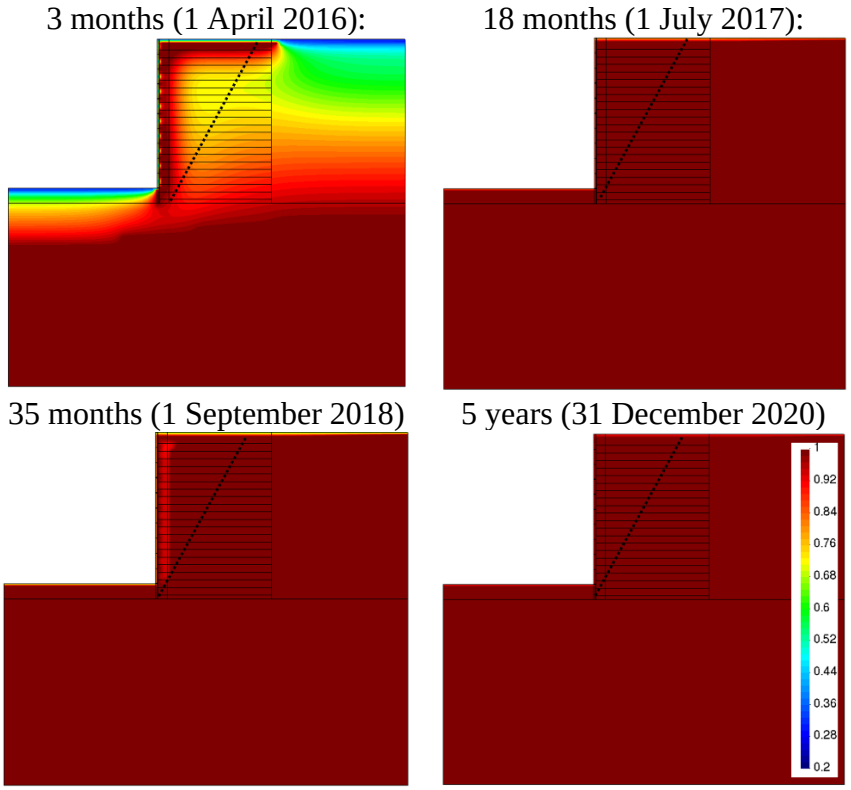

Figure 4-14. TH model 5-year relative humidity (-) results evolution with environmental conditions from Toronto 2016 to 2020.

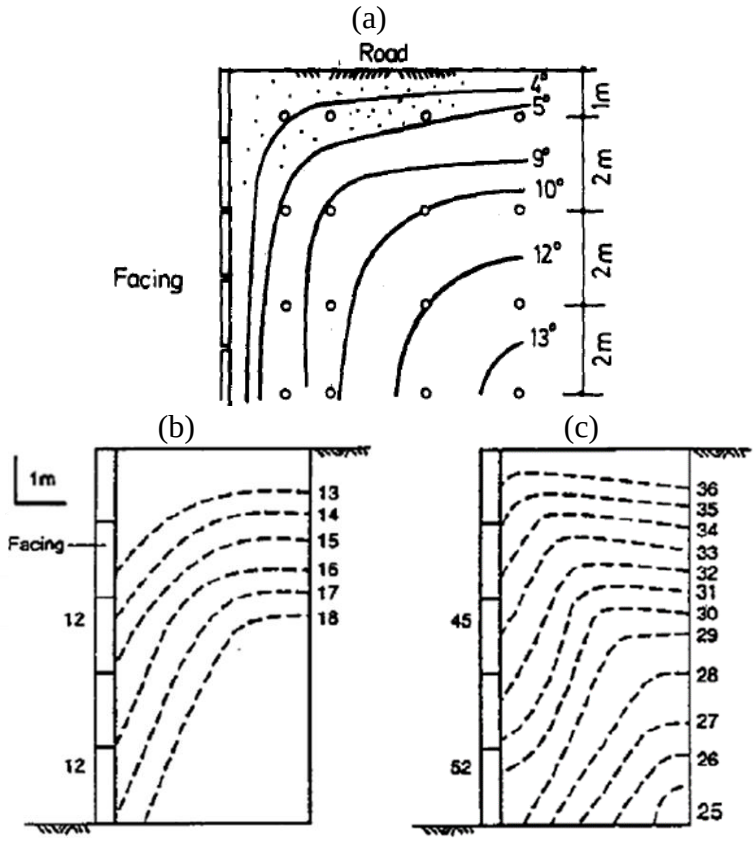

Figure 4-15. In-soil measured temperatures (°C) for a MSE wall structure obtained by (a) Segrestin et al. (1988) in the Frejus tunnel during November and (b) winter and (c) summer measurements by Jones (1995) in Tucson, Arizona.

Figure 4-17 (a) displays the mean in-soil temperature distribution obtained by Kasozi et al. (2015) using a thermal model of a MSE wall of 5.3 m of height located in Tucson, Arizona. Figure 4-17 (b) shows the obtained in-soil T distribution for the proposed MSE wall base case model using Barcelona registry after a 5-year analysis. In order to better compare the obtained results, a section of 6 x 6 m, including the uppermost 4 front facing panels, was selected. Kasozi et al. (2015) presents a thermal 2D model in which results are compared against field data in order to calibrate and validate the model. As mentioned by the authors, results display three distinctive T zone within the reinforced backfill where T variations were negligeable. The model implemented in this study showed similar T distribution with depth, in which three distinct zones can be identified for the observed time step. Since the boundary conditions differ for both cases, only distributions and not values can be compared.

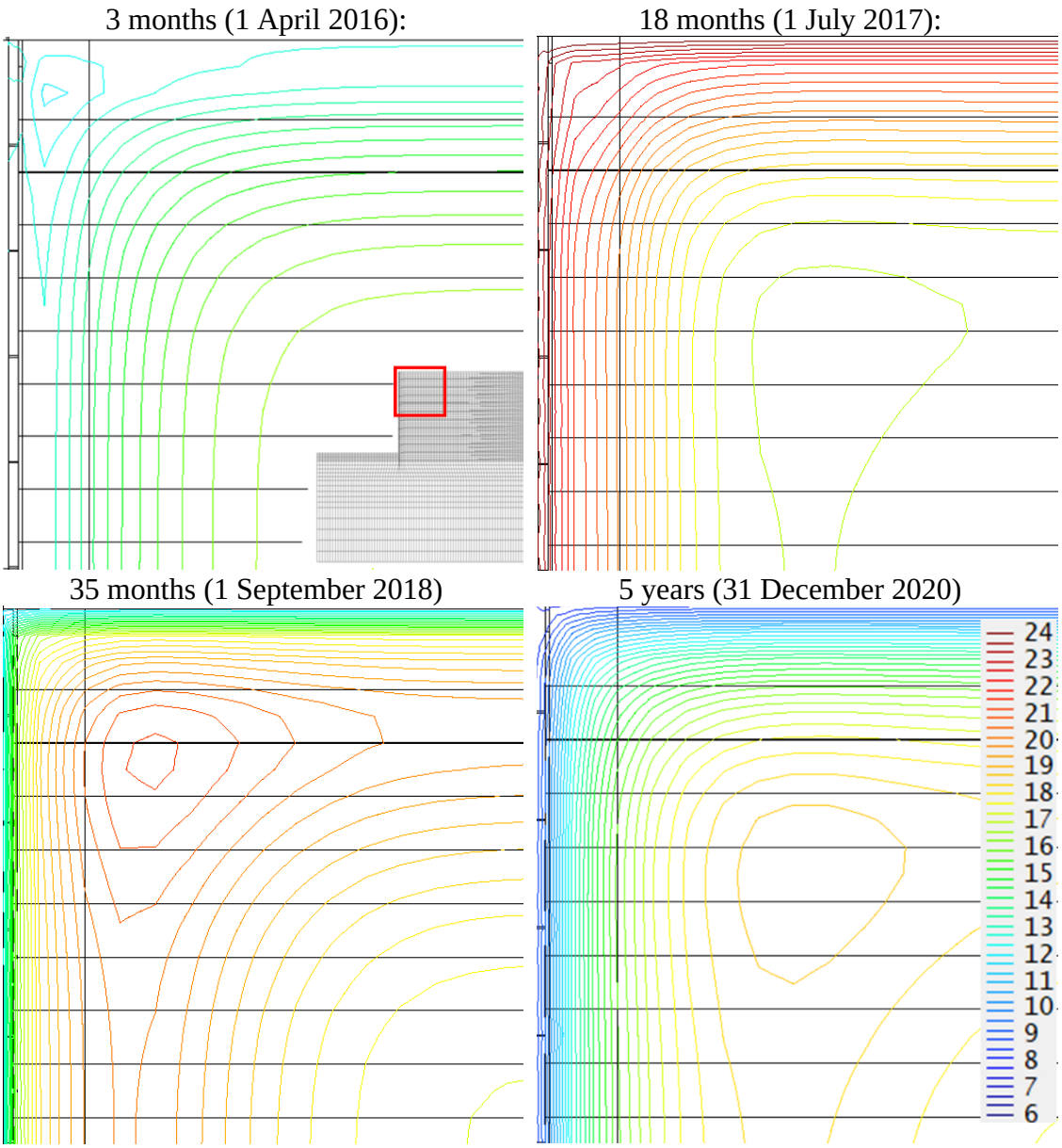

Figure 4-16. In-soil temperature (°C) iso-surfaces model results using Barcelona registry after a 5-year analysis period for various time steps for a 7.5 x 7.5 surface.

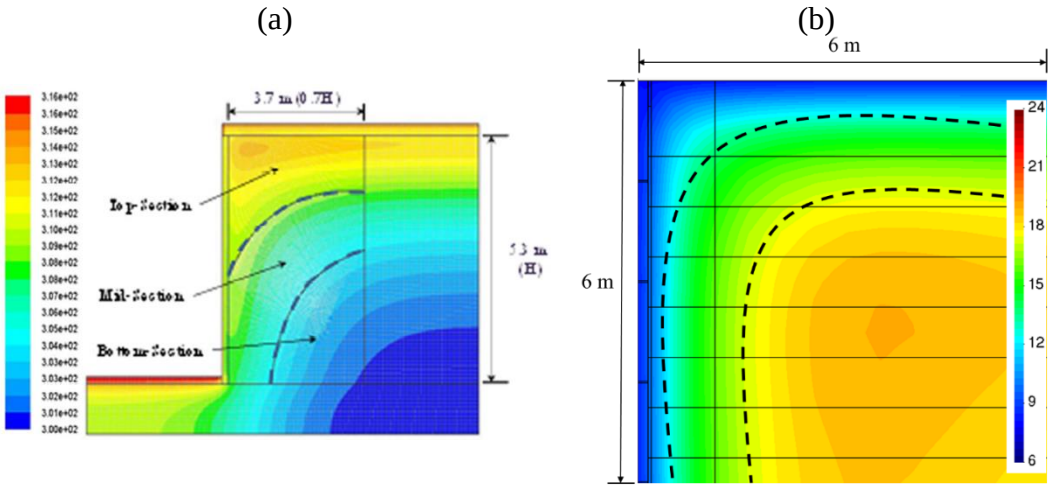

Figure 4-17. Mean in-soil modelled temperature (°C) results of a MSE wall by (a) Kasozi et al. (2015) and (b) in-soil distribution of the study's proposed model superior wall segment with Barcelona registry after 5 years.

Figure 4-18, Figure 4-19, Figure 4-20 and Figure 4-21 depict T and RH evolution over a 5-year analysis period for Abu Dhabi, Barcelona, Singapore and Toronto climate registry, respectively, at points A, B and C.

The case study results for Abu Dhabi climate data (Figure 4-18) present a mean T of 29.5°C, 29.4°C and 29.4°C and RH values of 55%, 59% and 66% at points A, B and C respectively. As depth increases, the influence of ambient temperature changes diminishes, reducing its variations from ±7°C at point A to ±3°C at point B. Points B and C display a similar behaviour regarding T and RH values. As with T, as depth increases, the amplitude of variations in RH values decreases. Overall, relative humidity mean value of 60% is far from air saturation, reaching values over 99% sporadically. As depth increases, the peaks of T occur at a later date with respect to surface values.

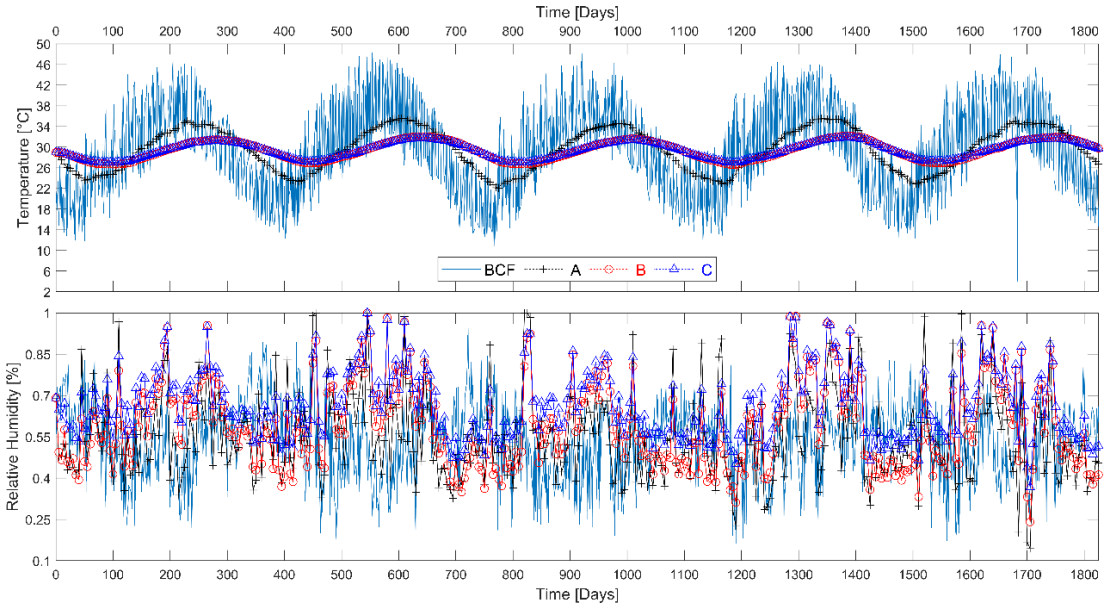

Figure 4-18. Temperature and relative humidity results for points A, B and C after a 5-year analysis period using Abu Dhabi 2016 to 2020 registry

Barcelona case (Figure 4-19) presents a mean T of 17.8°C, 17.6°C and 17.6°C and RH value of 95%, 96% and 97% at points A, B and C, respectively. Even though mean values coincide, both T and RH values present bigger variations at surface level. T values present oscillations of ±5°C at point A while at points B and C variations are within ±2°C. RH values present a more erratic behaviour, oscillating until reaching values of over 98% for a period of approximately 100 days at first and, after 500 days, for the rest of the analysis period for points B and C. Point A presents a similar behaviour with the inclusion of small reductions at certain stages.

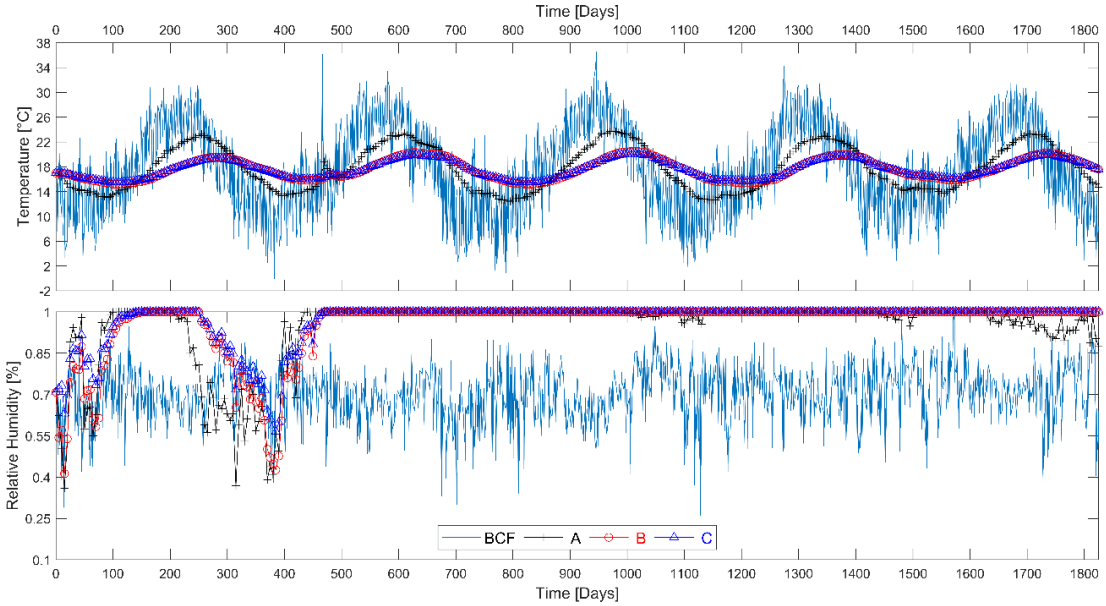

Figure 4-19. Temperature and relative humidity results for points A, B and C after a 5-year analysis period using Barcelona 2016 to 2020 registry

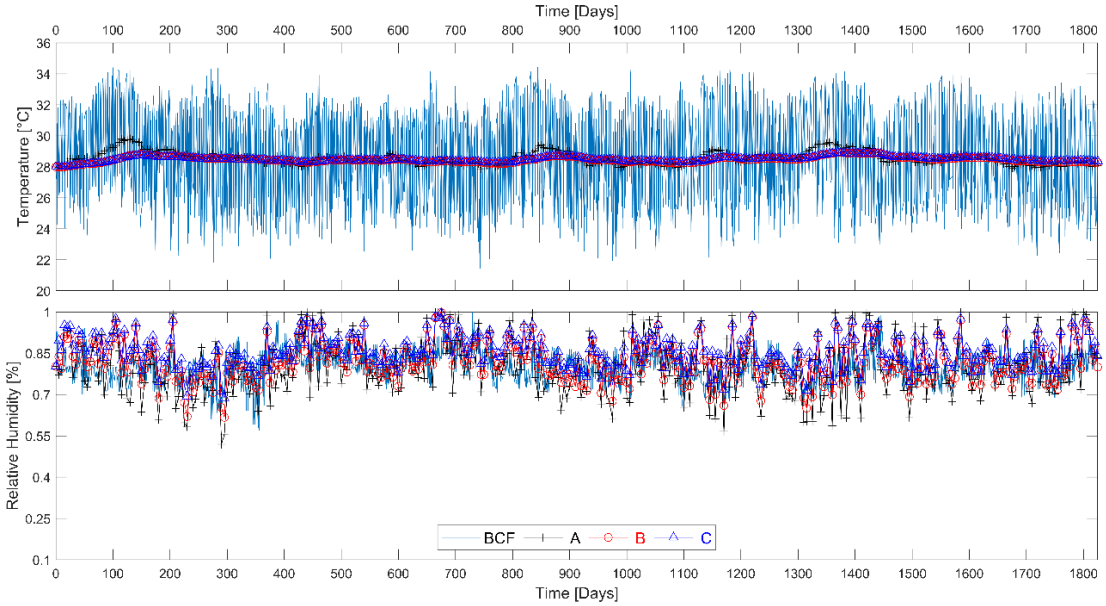

Figure 4-20. Temperature and relative humidity results for points A, B and C after a 5-year analysis period using Singapore 2016 to 2020 registry

Singapore climate data (Figure 4-20) presents lower variations in both T and RH registries. As such, the modelled results present similar variations at surface level and in depth. T mean values for points A, B and C were 28.6°C, 28.5°C and 28.5°C respectively, with variations at point A within ±1°C from the mean results and ±0.5°C for points B and C. Regarding RH, mean values for points A, B and C are 80%, 82% and 85% respectively

For the Toronto ambient data case (Figure 4-21), similar behaviour as to the Barcelona case can observed for both T and RH. Mean values for T and RH are 9.6°C, 9.5°C and 9.5°C and 96%, 97% and 98% for points A, B and C respectively. As the ambient T registry of Toronto presents the major variation, the model results show a difference of ±10°C in point A and approximately ±5°C at points B and C with respect to the mean in-soil T. Near surface (point A) RH values present considerable variations when compared to in-depth values (points B and C). RH values of over 98% can be observed for extended periods of time at all observation points with periodic declines within the first 3 years, followed by almost constant values for the 4th and 5th year.

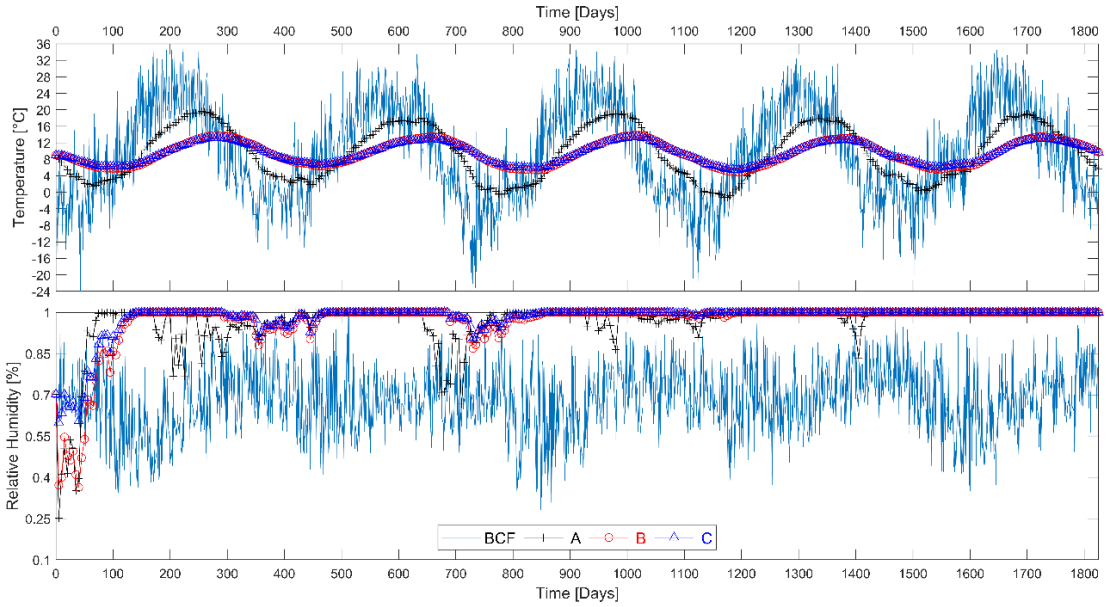

Figure 4-21. Temperature and relative humidity results for points A, B and C after a 5-year analysis period using Toronto 2016 to 2020 registry

When comparing ambient T to in-soil values, there is a delay variation as depth increases. Abu Dhabi and Singapore registries follow similar distributions in both T and RH behaviour when compared to the obtained in-soil values. On the other hand, Barcelona and Toronto cases only present similar results distribution when comparing T data between registry and model. For both of these later cases, once RH values of 99% or more are reached RH seems to stabilize and is scarcely affected by the boundary registry variations, which can be attributed to lower T.

Figure 4-22 shows the variation of T and RH at points A, B and C (locations shown in Figure 2), for Abu Dhabi, Barcelona, Toronto, and Singapore ambient air conditions for year 2 after a 5-year analysis period. As depth increases, the variations in temperature go from approximately ±6°C at 1 meter to a stable ±3°C variation at 14 and 21 meters for all conditions with the exception of Singapore, which remains at a steady 28°C at all

observation points. It can be noted that the effect of ambient temperature delays changes for in-soil T. As depth increases the peaks of temperature distribution curves are present at a later time with respect to surface values. The same latency can be observed in RH variations. Mean model temperatures were 29.7°C, 17.9°C, 28.4°C, and 9.9°C for Abu Dhabi, Barcelona, Singapore, and Toronto, respectively.

Different environmental conditions result in wide in-soil variation of RH, ranging from 39-99% and 32-99% for Barcelona and Abu Dhabi and 65-99% and 66-99% for Singapore and Toronto, respectively. As discussed earlier, laboratory hydrolysis testing was carried out at a constant RH = 100%.

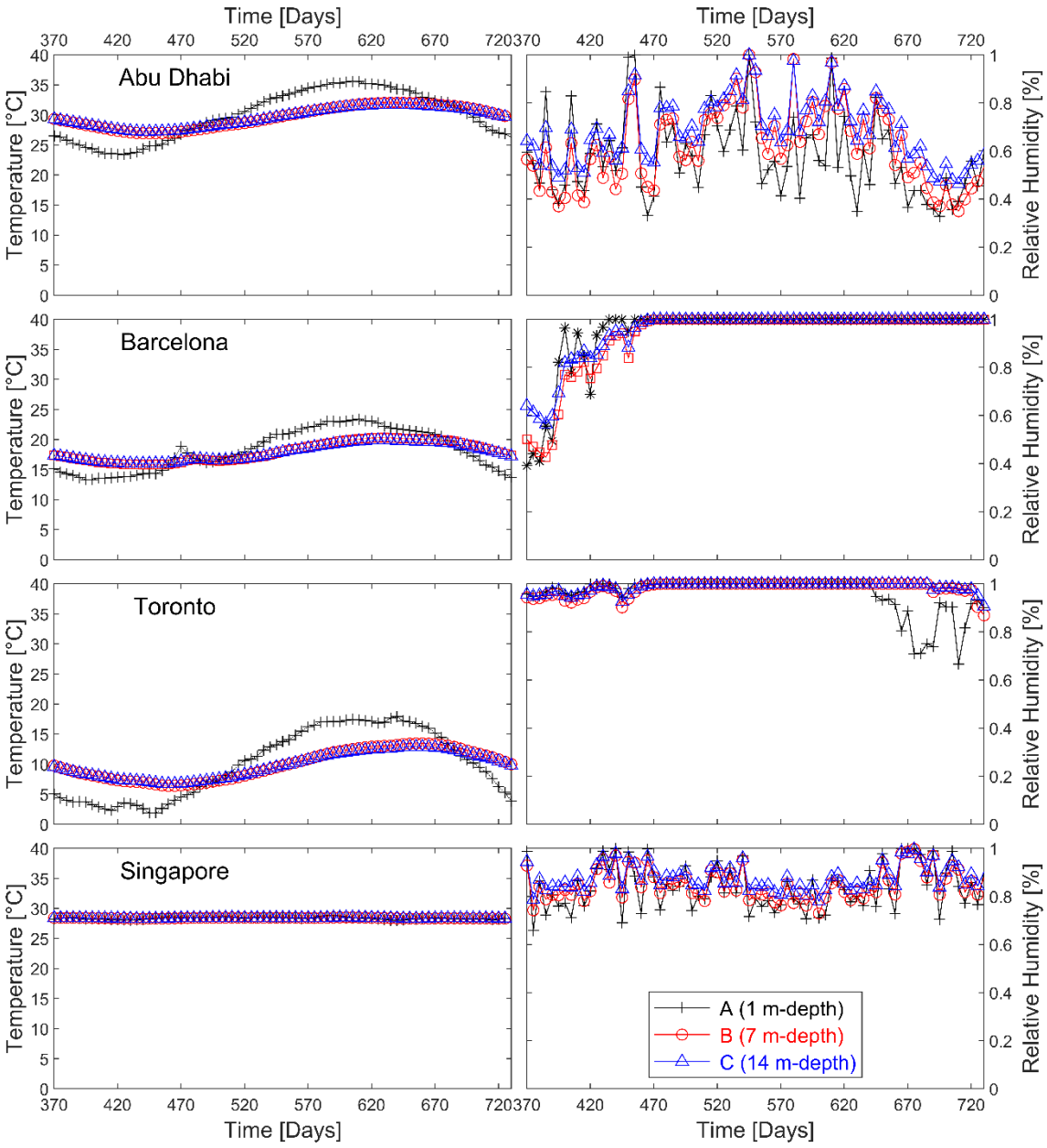

Figure 4-22. Evolution of temperature and relative humidity at points A, B and C for the 4 different locations/climates considered for the second year after a five-year analysis.

The numerical results at lower RH values suggests that a slower rate of chemical degradation of PET strap reinforcement would occur for the simulated conditions in this study for Abu Dhabi and Singapore environmental conditions. Nevertheless, after initial variations of in-soil RH values, results show RH values of over 99% for extended periods of time for year 2 during the 5-year cycle for Barcelona and Toronto. As depth increases, the influence of in-air condition diminishes, as RH tends to constant values as depth increases. Increases of RH within the soil following decreases in temperatures can be observed. Mean RH values for Abu Dhabi, Barcelona, Singapore and Toronto atmospheric conditions were 63%, 94%, 86% and 97%, respectively for the same A-B-C observation points for year 2 over a 5-year analysis.

Figure 4-23 shows the temperature variation of a vertical soil profile at 4 meters from the wall facing (x = 19 m) over a 5-year period using the Barcelona registry. Results show that T changes within the first 3 meters constitute the largest fluctuations matching the prescribed boundary conditions (6°C to 30°C). From 3 to 15 meter-depth, T fluctuations diminish and begin oscillating within ±1.5°C with respect to the annual mean atmospheric temperature (17°C). Below 15 meters, T stabilizes with less than ±1°C variation and approaches a constant value matching the lower boundary condition. Figure 4-24 displays the in-depth profile of accumulated temperature distributions over a 5-year period with the Barcelona registry presented in Figure 4-23. A first 2 meters of considerable temperature variations can be observed, from 30°C to 6°C, which diminishes rapidly to ±2.5°C at 3 meters and ±1.5°C below 5 meters of depth. From 15 meters and below, temperature stabilizes and begins to converge to the lower boundary-imposed temperature.

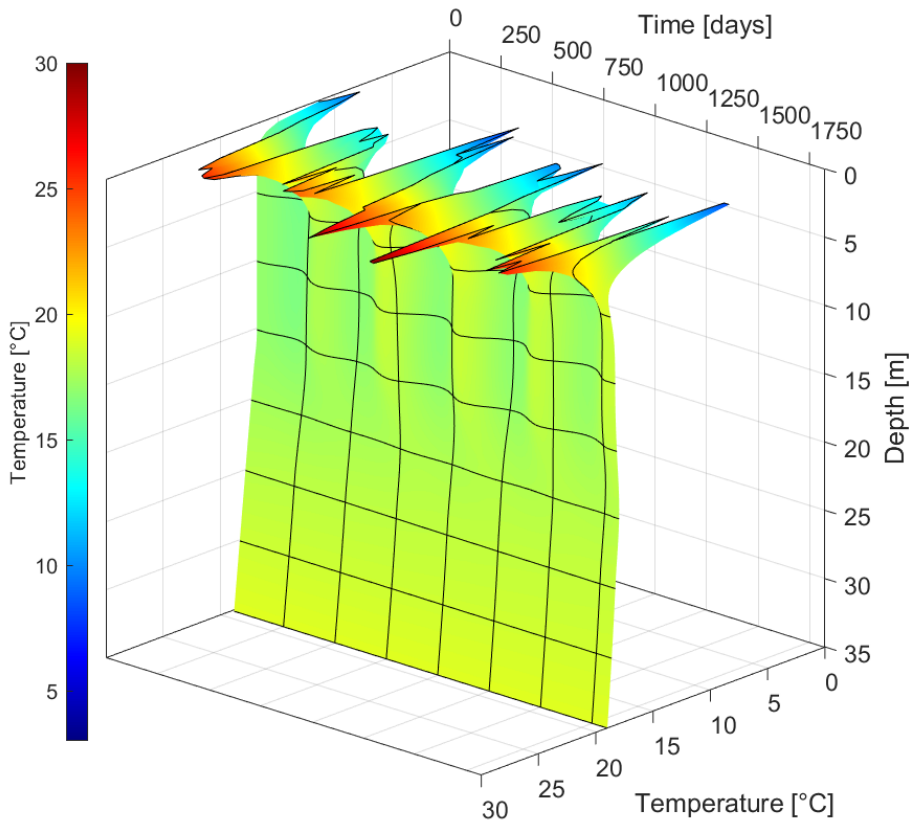

Figure 4-23. In depth temperature distribution over a 5-year analysis with Barcelona climate for sand model.

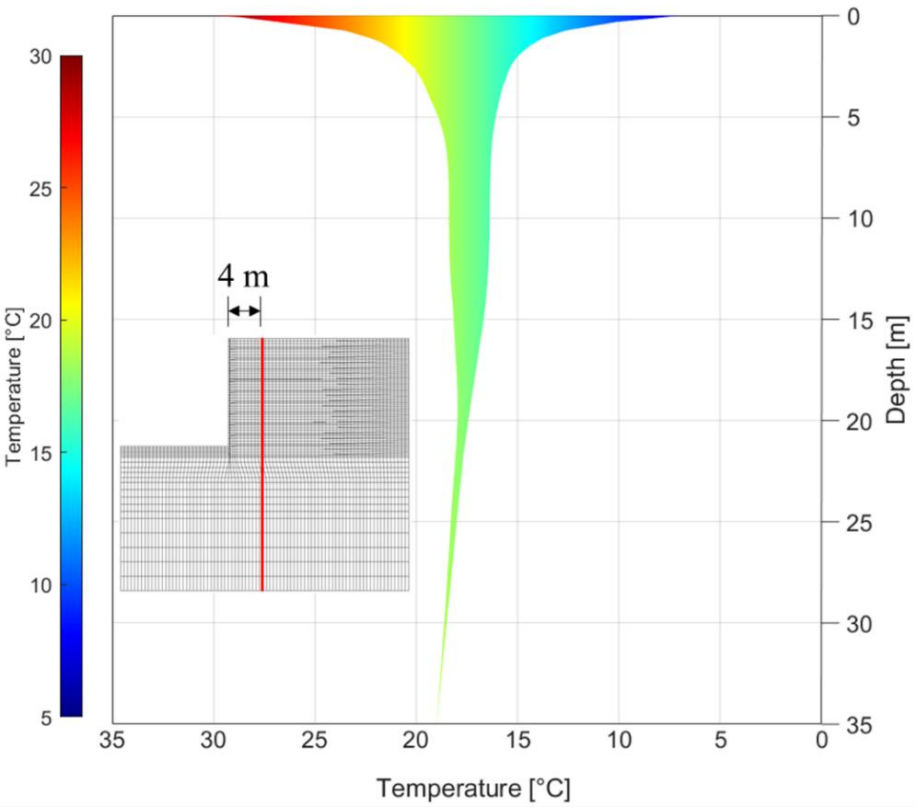

Figure 4-24. In-depth profile of accumulated temperature distributions for a 5-year analysis using Barcelona registry

4.3.2 THM MSE wall base model

As a first approach, a linear elastic reinforcement model with creep (bi-linear elasticity and VE model) was used together with linear elastic concrete and backfill materials for the thermo- hydro-mechanical (THM) model case geometry in Figure 3-2.

Figure 4-25 presents horizontal displacements of the deformed mesh for a 1-year analysis period using Barcelona atmospheric boundary conditions with the bi-linear elastic and VE PET strap model. When comparing linear elastic and VE model results, the maximum displacement increases by about 4% over a 1-year period for the VE model. As shown in Figure 4-4, long term deformations vary with temperature after approximately 5 years. Since the analysis is limited to one year, no significant variations were observed between different boundary condition cases (Desert and Mediterranean).

As described in Figure 2-4, the identification of a maximum stress zone is crucial for internal stability verifications. The proposed model does not include a soil-reinforcement interface at any point in length. Furthermore, PET straps are modelled have one element of thickness, thus, nodes are shared for soil and reinforcement. This results in an inadequate modelling of the PET straps tensile stress due to soil friction. As a consequence, the analytical solution of maximum stress is not reflected on the modelled results.

Figure 4-26 presents the maximum axial strain and maximum applied force at every reinforcement after a 1-year analysis with Barcelona registry. To obtained forces, 2 connections per 2.5 m of depth and 2 PET strap per connections are considered, as well as an average reinforcement width of 89mm. Presented values do not include the first

mesh element of the reinforcement which is linked to the front facing panels, as if no interface section is considered erratic behaviour not corresponding to the PET strap reinforcement but to the concrete facing will be obtained. As a reference value, passive earth pressure considering $K_0 = 0.5$ is displayed. Variations on reinforcement grades are color-labeled. It is to be expected that for the lower most reinforcements forces should decrease as the wall footing provide additional support. This behaviour is not obtained with the proposed model when observing forces but is somewhat observable for axial strain results. Furthermore, maximum forces are present at the free end of the reinforcement, while maximum strains are concentrated near the front facing panels. Obtained strains indicate maximum values within the 0.1% to 0.5%, considerably lower than the 2.5% to 3% values expected near failure (AASHTO 2020). Reinforcement forces values are withing the 0.5-7 kN/m, which correspond to 1-4%, 3-8% and 7-10% of UTS for grades 30, 50 and 70 PET strap reinforcements, depending on the depth. Since the modelled behaviour of PET reinforcements does not indicate to be correctly implemented within the MSE wall model, the presented values must be taken as reference in order of magnitude only.

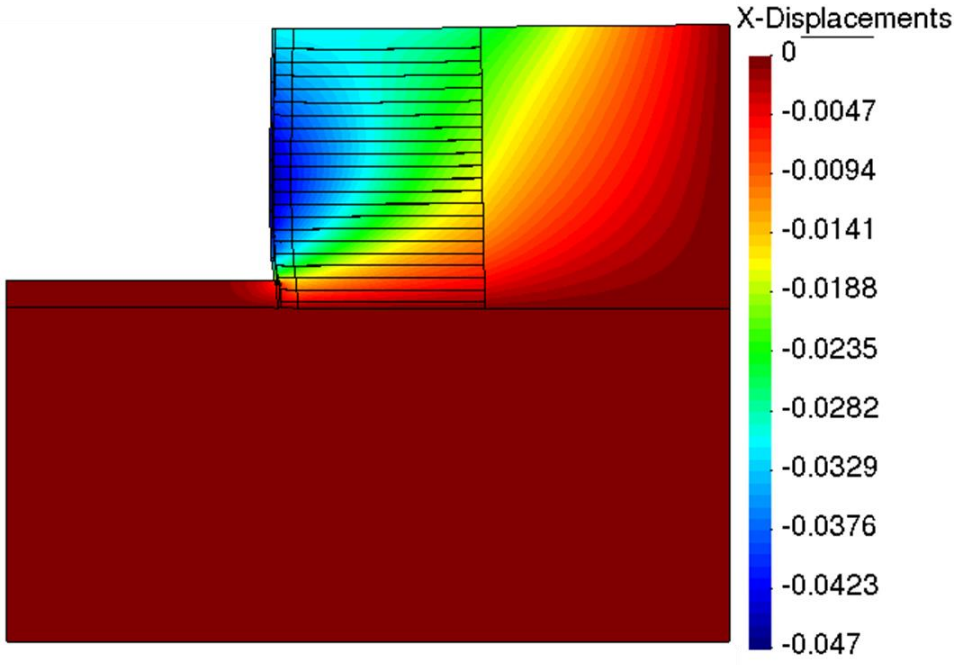

Figure 4-25. Horizontal outward displacements (m) and deformed mesh (amplification factor ×10) after 1 year analysis with an elastic coupled THM model with proposed PET straps reinforcements (Bilinear elasticity and VE) using Barcelona's 2020 atmospheric registry.

Figure 4-27 shows the in-soil distribution of shear strains after a 1-year analysis. Soil shear strains are concentrated withing the base of the structure, above the embedded length. Said location matches the maximum axial strains observed with the reinforcements. Shear strains of up to 2% can be observer along the equivalent interface between soil and facing panels, localized between the second and fourth panels. Based on design specifications, such as AASTHO (2020), which state a maximum strain of 2% for stiff faced walls and 2.5% for flexible faced walls along the failure surface, the proposed MSE wall can be considered stable.

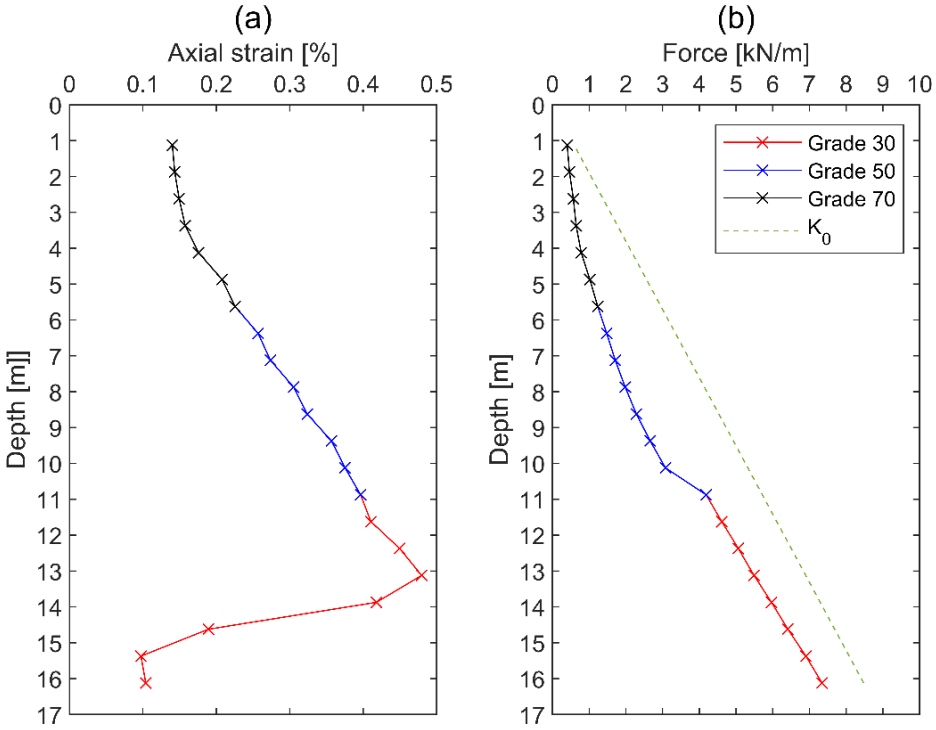

Figure 4-26. Maximum model results for (a) axial strain and (b) applied force over all implemented PET strap reinforcements (Grades 30, 50 and 70)

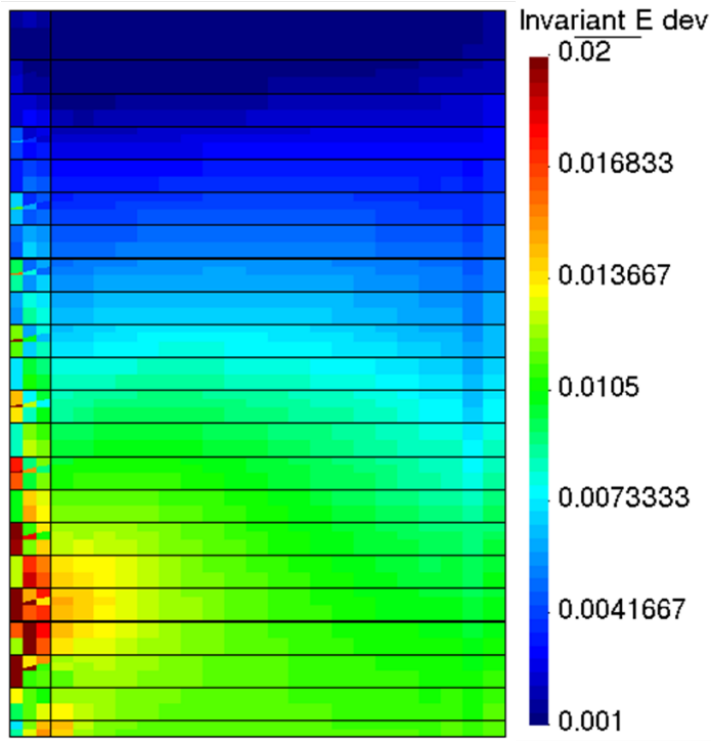

Figure 4-27. Shear deformations of THM MSE wall model using linear elastic soil and proposed PET strap reinforcements (Bilinear elasticity and VE) using Barcelona's 2020 atmospheric registry.

4.3.3 TH MSE wall rainfall model

Rainfall as a boundary condition was only applied on the superior horizontal boundaries and not on the vertical boundary (i.e., the retaining wall structure).

Figure 4-28, Figure 4-29, Figure 4-30 and Figure 4-31 compares the T and RH evolution between the base case and rainfall case of points A, B and C after a 5-year analysis using the Abu Dhabi, Barcelona, Singapore and Toronto atmospheric conditions.

For the Abu Dhabi climate registry case (Figure 4-28), rainfall events are scarce but with high intensities. In-depth temperature values (Points B and C) do not present significant variations due to the lack of water infiltration, as opposed to other study cases. Surface temperature values (Point A), present small variations after rain events but overall follow the same trend as the base case. For this study case, the effect of rainfall is more noticeable in RH distributions variations, as both surface and in-soil values (Points A and B) reach almost air saturation (RH = 99%) for over 150 days. In-depth RH values (Point C) presents small increments of up to 20% after intense rain events manage to infiltrate and not evaporate due to high ambient T and low RH.

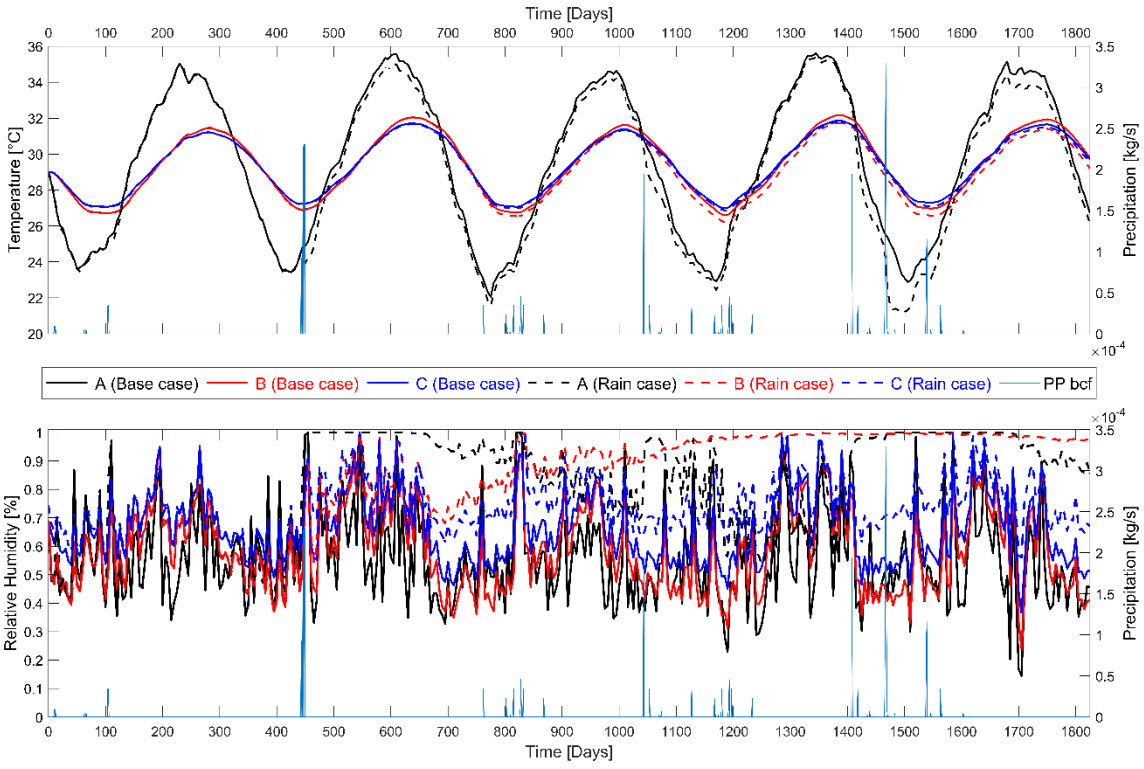

Figure 4-28. Comparison of base case and rainfall case temperature and relative humidity distributions for points A, B and C after a 5-year model period using Abu Dhabi climate registry.

The Barcelona registry boundary condition (Figure 4-29) presents higher intensity and frequency of rain events when compared to Abu Dhabi´s case. Near surface T (point A) mean value decreases 2°C, presenting overall lower maximum and minimum temperatures (i.e., the result T distribution curve is shifted downwards.). Result for points B and C show minor decline in T over the course of the analysis without altering the

resulting distribution shape. For points A and B, RH values increase rapidly to 99% upon the first rain events, maintaining its value within the 99-100% range. Additionally, point A does not present late-stage oscillations as in the base case. Point C presents a similar behaviour as the base case up until day 260, where is does not decrease as much as the base case. After day 415, all three points remain within 99%.

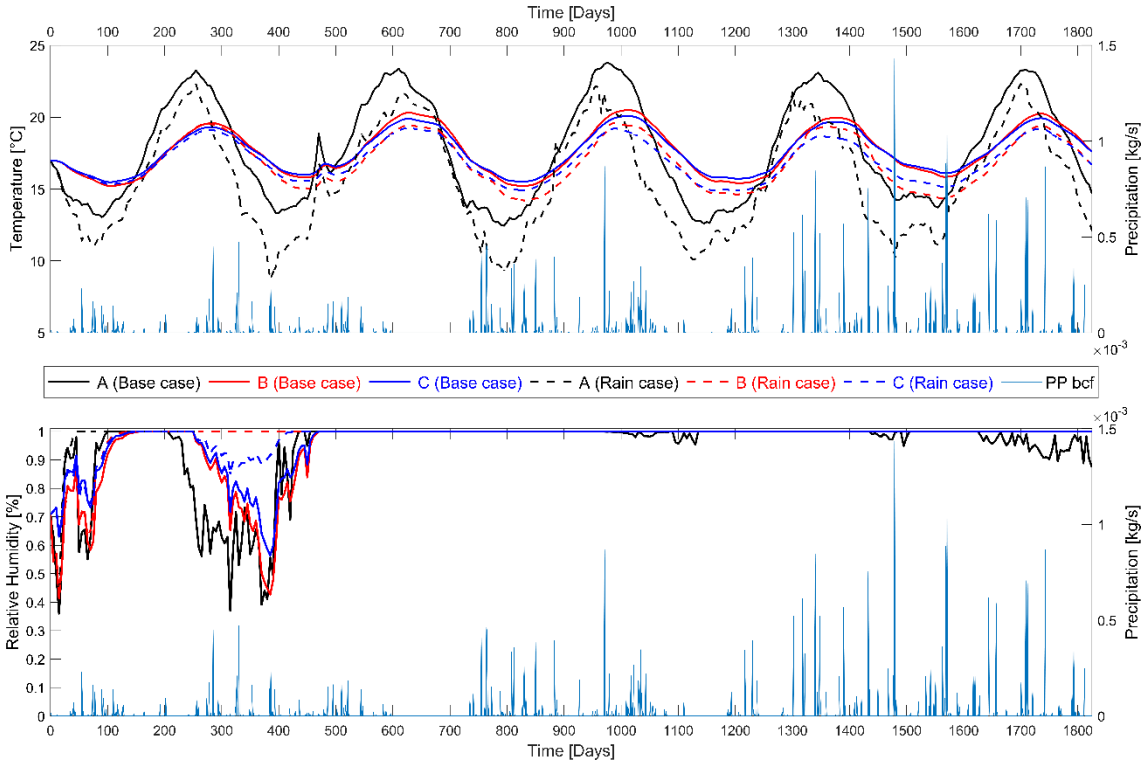

Figure 4-29. Comparison of base case and rainfall case temperature and relative humidity distributions for points A, B and C after a 5-year model period using Barcelona climate registry.

For the Singapore climate registry case (Figure 4-30), rainfall events result in considerable reduction on surface level temperatures. Mean T values are reduced 2°C at point A and 1°C at points B and C. Surface level T values drops coincide with important isolated rainfall events, such as day 280, or continuous rains, such as the 1440-1480-day period. When observing RH distributions, the steady behaviour previously observed is no longer present, as RH increases up to 99% for all of the analysis period after day 20, 90 and 240 for points A, B and C respectively. The delay can be linked with time it takes the flux of water mass to descend through the model.

Regarding the Toronto case (Figure 4-31), incorporating rainfall as a boundary condition reduces the mean in-soil temperature 3°C at point A and less than 1°C at points B and C. Mean relative humidity values are increased 3% at point A and under 1% at points B and C. The effect of rain over in-soil temperature can be observed after events with a higher rain intensity, such as day 1295, 1469 and 1675, where temperature visible decreases. Concerning RH, as soon as the first rain even occurs, values of over 99% are obtained, maintaining variations over 99% throughout the analysis period. Similarly, to the obtained results with Barcelona registry, between days 320 to 420, RH values drop up to 97% in points B and C. Overall, the obtained RH distributions differ from the base case, which sporadically decreases RH values between 80% to 90% depending on the observed

depth. In-soil initial RH is set to match the initial atmospheric value for each boundary condition. As such, the soil is in a dry state. As rain events occur, in-soil moisture content increases and upholds within the soil structure with an overall mean value of 99%.5-year.

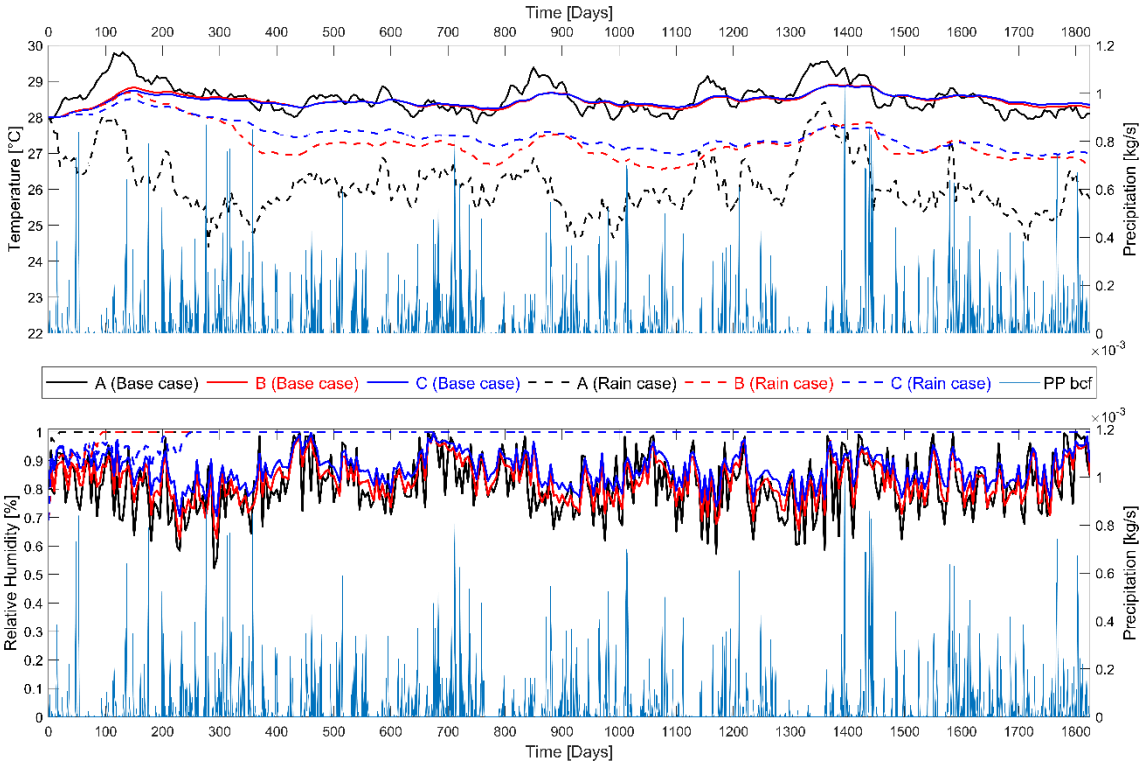

Figure 4-30. Comparison of base case and rainfall case temperature and relative humidity distributions for points A, B and C after a 5-year model period using Singapore climate registry.

Figure 4-32, Figure 4-33, Figure 4-35 and Figure 4-34 presents the base case (left) and rainfall (right) temperature soil profiles of the MSE wall model after a 5-year analysis period using the Abu Dhabi, Barcelona, Toronto and Singapore registry, respectively.

As previously observed in Figure 4-28, in-soil T profile for the Abu Dhabi case (Figure 4-32) does not present significant T variations between the base and rainfall cases. After the 5-year analysis, decreases of approximately 0.5°C can be observed within the active zone behind the retaining structure.

In-soil T distribution for the Barcelona registry case (Figure 4-33) present an overall decrease with the inclusion of rain. When higher ambient T are present at the imposed boundaries, such as after 18 and 35 months, the effect of rainfall is observed at the horizontal boundaries within the first 1 to 3 meters, were T visible decreases ($\Delta T \approx 4°C$). T variations within the theorical rupture zone, shown by the dotted line, are more pronounced at the foot of the structure and at surface level. As the model does not include rain as a boundary condition on the vertical boundary (retaining wall), temperature variations in the vicinity of said boundary are less pronounced.

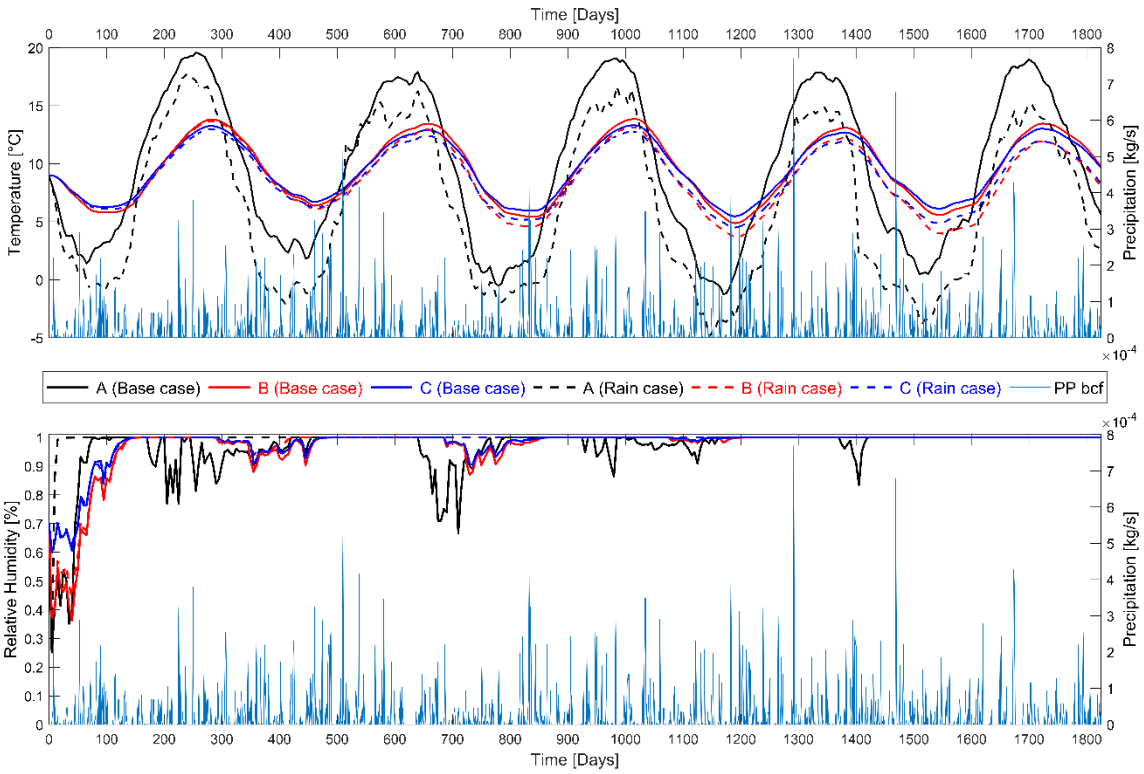

Figure 4-31. Comparison of base case and rainfall case temperature and relative humidity distributions for points A, B and C after a 5-year model period using Toronto climate registry.

For the Toronto ambient condition case (Figure 4-34), in accordance with the results presented in Figure 4-9, the first 2 meters present the most variations as boundary conditions fluctuate. With the incorporation of rain, lower temperatures are observed at surface level for earlier stages (3 and 18 months) and in-depth for later stages (35 and 60 months). Soil back fill temperatures present variations from 1°C up to 8°C depending on the observed depth. Though temperature values decrease, the magnitude of temperature fluctuations do not seem to be affected in the presence of rain- A dotted line represents the theorical line of maximum stress for the extensible reinforcement. Results show that the boundary separating the active and passive zones is located within an area with different ranges of temperature oscillations, depending on the observed depth. The most superficial point, around 2 meters near the boundary on both extremes, presents important T variations of approximately $\Delta T \approx 11°C$. For the in-depth zone, temperature fluctuation is steady throughout the year with $\Delta T \approx 3°C$.

When observing the in-soil T distributions for the Singapore registry case (Figure 4-35), a visible decrease can be identified after the first 3 months at surface level. As the analysis period increases, water fluxes due to rain infiltrate and continue to reduce the in-soil T. A clear progressive descent in T can be observed through the 18-month to 5-year period, affecting the entirety of the retained and reinforced backfill soil. Up to 2°C reduction is observed within the reinforced soil, including the theorical failure zone, detailed by a dotted line. Contrary to the obtained results in the Barcelona and Toronto registries, T reductions take effect throughout all of the retained backfill and not only at the first 3 to 5 meters. This can be attributed to the higher intensity of rains present in the Singapore ambient registry.

Figure 4-32. In-soil temperature distribution after a 5-year analysis period using Abu Dhabi registry for base case (left) and rainfall case (right).

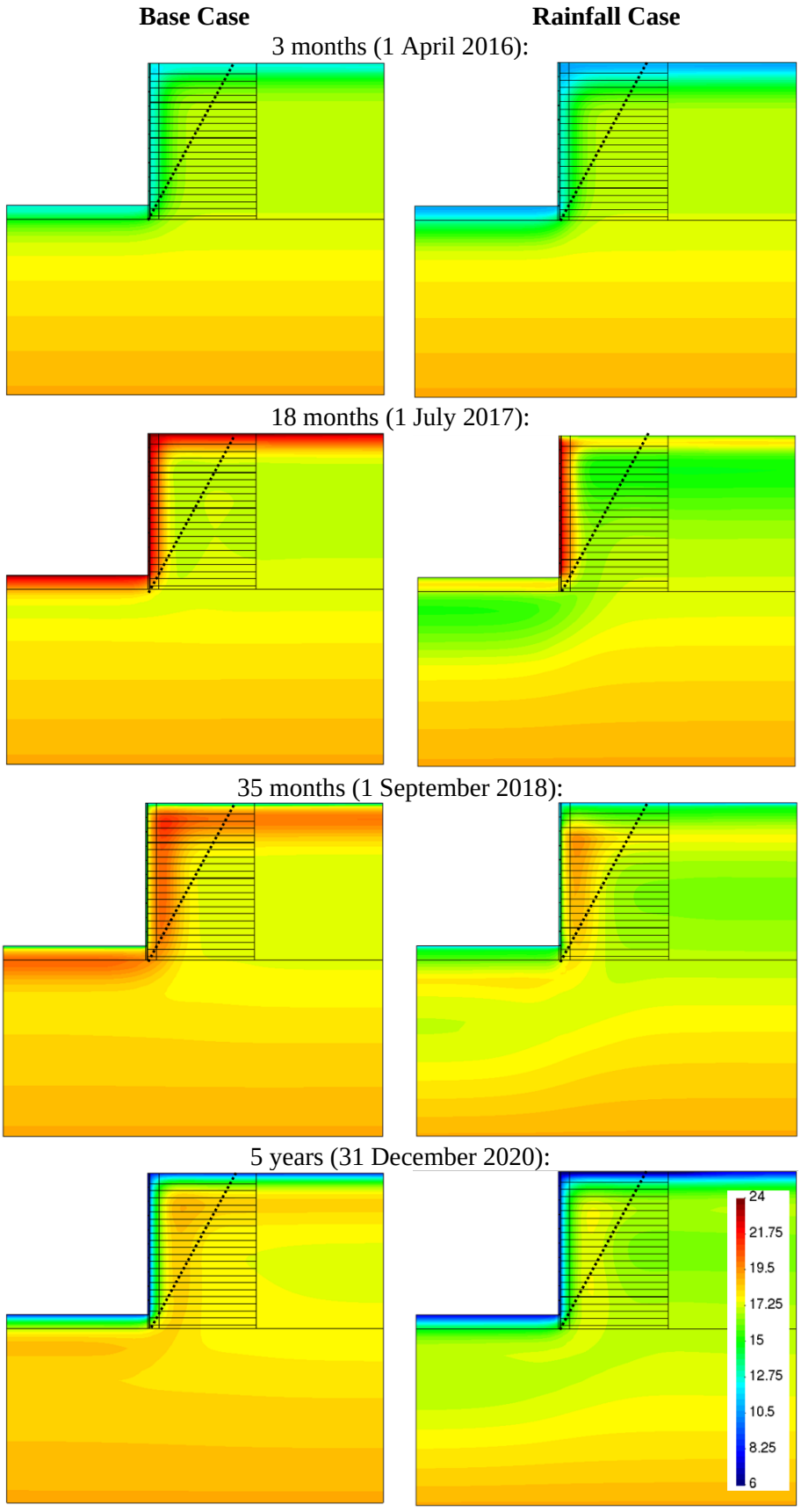

Figure 4-33. In-soil temperature distribution after a 5-year analysis period using Barcelona registry for base case (left) and rainfall case (right).

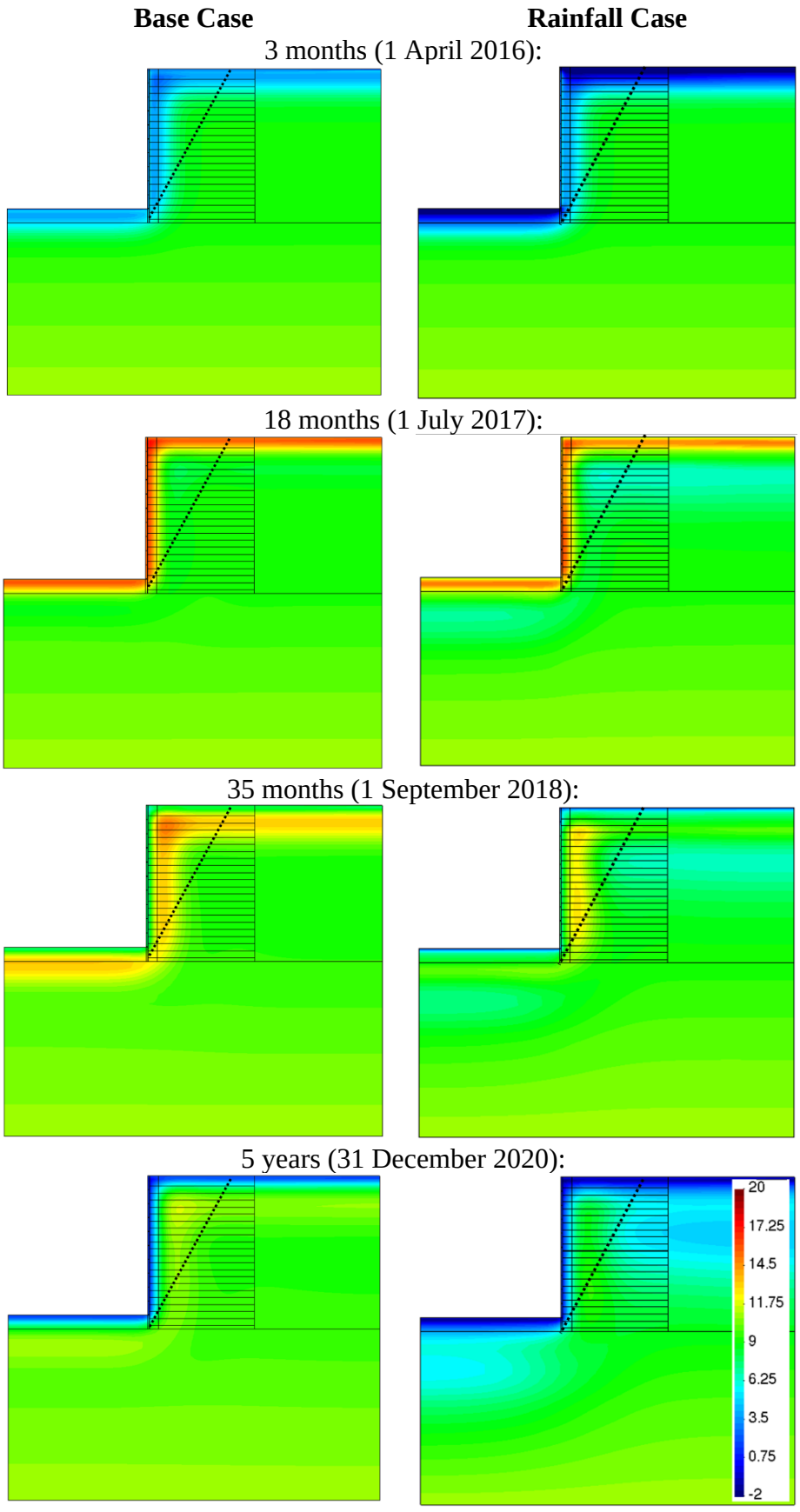

Figure 4-34. In-soil temperature distribution after a 5-year analysis period using Toronto registry for base case (left) and rainfall case (right).

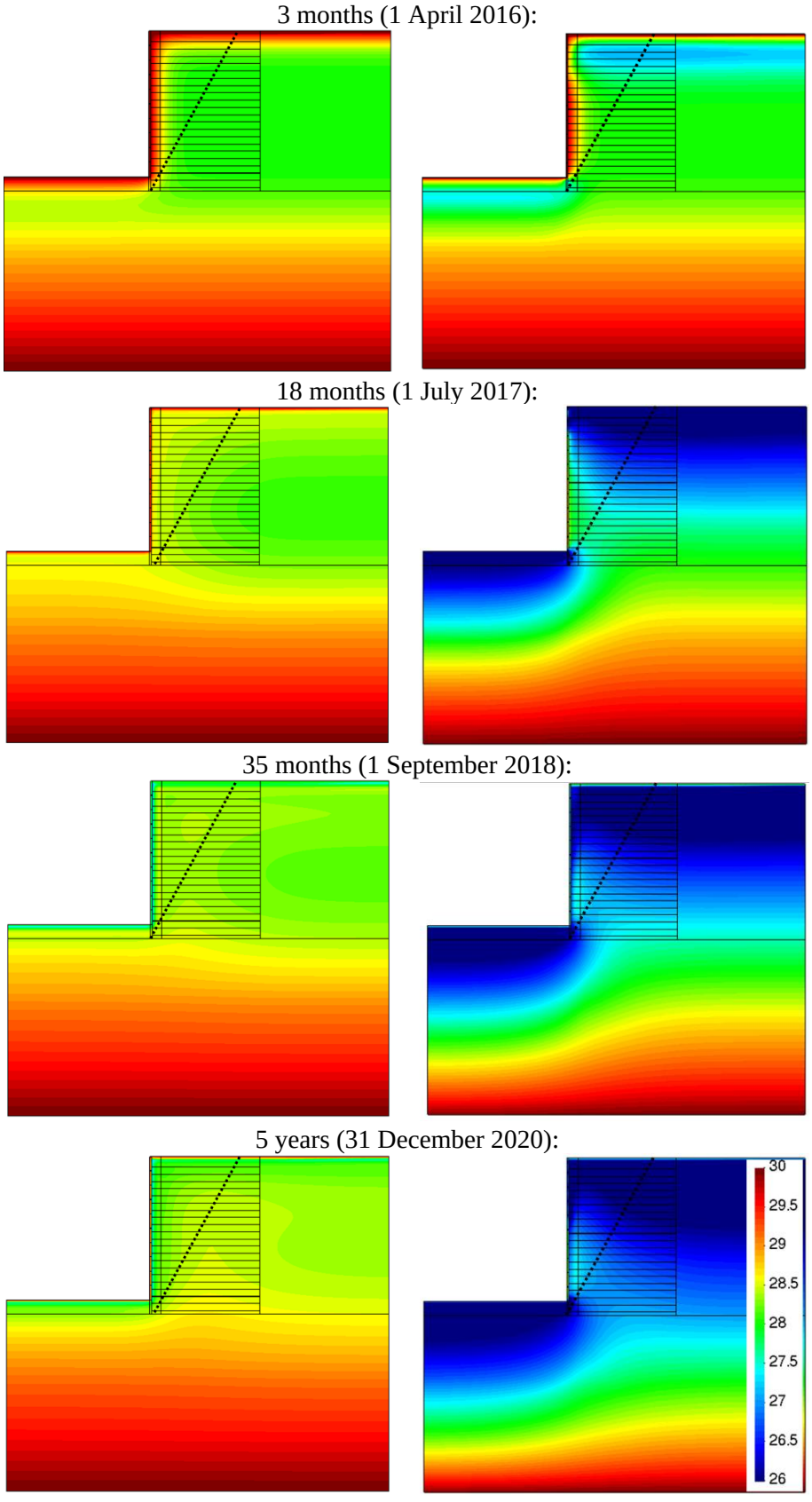

Figure 4-35. In-soil temperature distribution after a 5-year analysis period using Toronto registry for base case (left) and rainfall case (right).

Table 4-2 compares base and rainfall cases the mean T and RH values for points A, B and C after a 5-year analysis period with the four chosen climates. Overall, a reduction of mean in-soil temperature of approximately 1°C can be observed (Points B and C), while surface level values (Point A) present reductions of up to 3°C for Barcelona, Singapore and Toronto cases. RH values increase up to mean values of 97% or more in the mentioned cases. Barcelona, Singapore and Toronto mean RH values increase approximately 3%, 15% and 2% respectively. For the Abu Dhabi registry, T present almost no variations at the three observed depths. RH values increase approximately 25% at points A and B and 8% at point C. The in-depth difference in RH values can be attributed to the lack of higher intensity rain events such as those present in the rest of the climate registries which result in less infiltration, thus less in-depth T and RH variations.

Based on the obtained results and the implemented VE and VP models for PET strap reinforcement, in-soil temperature reductions should imply a lower rate of deformation over a long-term analysis.

Table 4-2. Mean temperature and relative humidity values for all climate conditions with and without the incorporation of rainfall for points A, B and C after a 5-year analysis.

Location	Observation point	Base case		Rainfall case	
		T [°C]	RH [%]	T [°C]	RH [%]
Abu Dhabi	A	29.6	55.6	29.1	81.4
	B	29.4	59.7	29.2	83.8
	C	29.4	67.4	29.3	74.9
Barcelona	A	17.8	94.3	15.7	99.4
	B	17.6	95.6	16.9	98.5
	C	17.6	96.9	17.0	98.2
Singapore	A	28.5	81.1	26.1	99.9
	B	28.5	83.2	27.3	99.4
	C	28.5	86.9	27.5	99.1
Toronto	A	9.6	96.1	6.3	99.7
	B	9.5	96.8	8.7	97.6
	C	9.5	97.9	8.8	98.2

5. CONCLUSIONS

The present study demonstrates the implementation of a hydro-thermal model to evaluate the effects of prolonged ambient conditions on in-soil conditions with different ambient environmental conditions on the backfill soil, and the long-term behaviour of the embedded PET strap reinforcement layers used in MSE walls. Linear elastic models for the MSE wall components were used together with a coupled THM model for the soil as an initial approach.

TH models gave results in accordance with previous studies (e.g., Segrestin and Jailloux 1988, Kazosi et al. 2015) for temperature distributions in-soil as a function of depth. The mean in-soil temperature can be approximated by the annual mean environmental (atmospheric) in-air values when in the absence of rainfall. Over the first 1 to 3 meters, fluctuations of approximately ±10°C were observed, depending on the applied boundary environmental conditions. From 3 to 15 meters, T variations are reduced to ±2°C. At depths greater than 15 meters, T remains constant, converging to the lower boundary-imposed value. Mean annual temperatures used as boundary conditions ranged from 10°C to 29°C.

Regarding RH, air saturation was achieved for extended periods of time (over 1000 days) for Barcelona and Toronto climate registry cases, with a mean value of 96% and 97%, respectively. For desert ambient conditions (Abu Dhabi), air saturation was rarely observed, with a mean RH of 61% at the observation depths. The tropical environment case (Singapore) resulted in almost constant RH values of 84% throughout the analysis period.

When incorporating rainfall as a boundary condition, T reductions were observed as compares to the base case, as such, the mean in-soil temperature could be approximated to 1°C and 3°C lower than the mean ambient temperature at depth and surface levels respectively. Visible reductions in temperature were detected following heavy rain events for all climate conditions save for Abu Dhabi, which can be attributed to the lack of intense rain events. The inclusion of rain increases RH values for all cases. In Barcelona and Canada cases, mean values are increased to 99% and near surface values lack RH oscillations previously observed on the base case. Singapore RH distributions shift completely to an almost constant value of 99%, similar to Barcelona and Singapore. Abu Dhabi presents the least amount of rain events in both frequency and intensity. As a consequence, RH values are increase to almost saturation values for periods of over 100 days at surface level. In-depth values do not present considerable variations. Overall, the mean in soil RH value for the Abu Dhabi case increases to 80%.

The effect of PET strap hydrolysis was measured using fully saturated laboratory specimens. These data are useful to estimate the long-term degradation of the PET straps when in-soil RH periodically reaches full saturation.

Visco-elastic and visco-plastic models were fitted to creep master curves with satisfactory results for different grades of PET straps and a range of UTS loads. The proposed models incorporate temperature dependencies and, as such can prove useful when modelling the effect of in-soil conditions on long-term deformations for these soil reinforcement materials.

When implementing the proposed PET reinforcement model into a fully coupled THM MSE wall linear elastic model, discrepancies in behaviour were observed. Applied forces

over the length of the reinforcement do not present expected values as stresses increase over the elements length and do not reach close-to-null values at the free end. This effect has been attributed to the used mesh geometry as well as the lack of interface elements between reinforcements, soil and facing panels.

Future lines of research include an implementation of plasticity for the reinforced and sustained backfill as well as the foundation soil. A plastic model should allow the correct identification of possible plastic and failure zones within the reinforced backfill assuming reinforcement behaviour is correct. Following this, the implementation of construction phases in order to better model both horizontal stress and strain evolution during and after the building of the structure should be considered.

Additional development of the mesh and geometry qualities of the THM model in order to correctly model the stress and strain allocations with in PET strap reinforcement is proposed. As the implemented model does not include a soil-reinforcement interface at any point in length, results show an inadequate modelling of the PET straps internal tensile stress distribution. This interface elements should include a interaction coefficient related to the pullout resistance based on laboratory and field data for every type of reinforcement element material and geometry. In addition to a soil-reinforcement interface, an equivalent material between reinforcement and front facing panels must be implemented in order to represent stiffer connections.

In order to develop a more robust model, sensitivity analyses for material parameters, including backfill soil, PET reinforcements, foundation soil and retaining wall, numerical parameters and boundary conditions, such as different water table levels are proposed. Based on a parametric analysis, including thermal, hydraulic and mechanical parameters variations, design abacuses could be developed as to better predict the reinforcements and wall behaviour.

Finally, a calibration and validation of the proposed model could be achieved if data of an instrumented MSE walls were to be available, including in-soil temperature, relative humidity and facing displacement records.

Further investigation is encourage as generating additional information on the effect of ambient conditions of MSE wall behaviour, could be used to improved partial factor selection at a design phase, optimizing the available material strength regarding PET strap reinforcements.

REFERENCES

AASHTO, 2020. LRFD Bridge Design Specifications (9th edition). American Association of State Highway and Transportation Officials (AASHTO), Washington, DC, USA.

ASTM D4595-17. 2017. Standard Test Method for Tensile Properties of Geotextiles by the Wide-Width Strap Method, ASTM International, West Conshohocken, PA, USA.

ASTM D5262-97. 1997. Standard Test Method for Evaluating the Unconfined Tension Creep Behavior of Geosynthetics. ASTM International, West Conshohocken, PA, USA.

ASTM D6992-03. 2003. Standard Test Method for Accelerated Tensile Creep and Creep-Rupture of Geosynthetic Materials Based on Time-Temperature Superposition Using the Stepped Isothermal Method. ASTM International, West Conshohocken, PA, USA.

Bathurst, R.J. 1992. Case study of a monitored propped panel wall. In Proceedings of the International Symposium on Geosynthetic-Reinforced Soil Retaining Walls, Denver Colorado, pp. 159-166, August 1991 (published by A.A. Balkema).

Bathurst, R.J., and Naftchali, F.M. 2021. Geosynthetic reinforcement stiffness for analytical and numerical modelling of reinforced soil structures. Geotextiles and Geomembranes, 49, 921-940.

Berg, R.R., Christopher, B.R., and Samtani, N.C., 2009. Design and construction of mechanically stabilized earth walls and reinforced soil slopes, Volume I (FHWA NHI-10-024) and Volume II (FHWA NHI-10-025), National Highway Institute, Federal Highway Administration. U.S. Department of Transportation, Washington, DC, USA.

Chamberlain, B. & Cooper, G. 2009. Paraweb straps for reinforced soil retaining walls and bridge abutments, Linear Composites Ltd. Roads and Bridges Certificate No 09/R146, Product Sheet 1. British Board of Agrément (BBA), Garston, Watford, UK.

CODE_BRIGHT User's Guide. 2021. Department of Civil and Environmental Engineering, Universitat Politècnica de Catalunya·BarcelonaTech (UPC) and International Center for Numerical Methods in Engineering (CIMNE). https://deca.upc.edu/en/projects/code_bright

Damians, I. P., Bathurst, R. J., Olivella, S., Lloret, A. and Josa, A. 2021. 3D modelling of strip reinforced MSE walls. Acta Geotechnica, 16 (3), 711-730.

Damians, I.P., Bathurst, R.J., Adroguer, E.G., Josa, A. and Lloret, A. 2018. Sustainability assessment of earth retaining wall structures. Environmental Geotechnics 5 (4), 187-203.

Damians, I.P., Bathurst, R.J., Adroguer, E.G., Josa, A. and Lloret, A. 2016. Environmental assessment of earth retaining wall structures. Environmental Geotechnics, hppt://dx.doi.org/10.1680/jenge. 15.00040.

Damians, I. P. 2016. Mechanical Performance and sustainability assessment of reinforced soil walls. Doctoral thesis. Department of Civil Engineering and Environmental Engineering, Universitat Politecnica de Catalunya, Barcelona, Spain.

Damians, I. P., Yu, Y., Lloret, A., Bathurst, R. J., & Josa, A. 2015. Equivalent interface properties to model soil-facing interactions with zero-thickness and continuum element methodologies. In From Fundamentals to Applications in Geotechnics (pp. 1065-1072). IOS Press.

Dixon, N., Fowmes, G., and Frost, M. 2017. Global challenges, geosynthetic solutions and counting carbon. Geosynthetics International, 24(5), 451-464.

EN 12447-02. 2001 Geotextiles and geotextile-related products – Screening test method for determining the resistance to hydrolysis in water. CEN/TC 189, European Standard.

GECO 2021. GECO Industrial Co., Ltd. Gyeonggi-do, Republic of Korea. http://gecoind.com/en/product/fasten.php

Gelhar, L.W., Welty, C., and Rehfeldt, K.R. 1992. A critical review of data on field-scale dispersion in aquifers. Water Resources Research, 28(7), 1955-1974.

Greenwood, J.H., Schroeder, H.F., and Voskamp, W.; 2012. Durability of Geosynthetics (Publication 243). CUR Committee C 187. Building and Infrastructure. ISBN 978-90-376-0533-4.

ISO (2006a) ISO 14040: Environmental management – life cycle assessment – principles and framework. ISO, Geneva, Switzerland.

ISO (2006b) ISO 14040: Environmental management – life cycle assessment – requirements and guidelines. ISO, Geneva, Switzerland

ISO 10319-15. 2015. Geosynthetics - Wide-width tensile test. ISO, Geneva, Switzerland.

ISO/TR 20432:2007. Guidelines for the determination of the long- term strength of geosynthetics for soil reinforcement. ISO, Geneva, Switzerland.

Jailloux, J.M., Nait-Ali, K.L., and Freitag, N. 2008. Exhaustive long-term study on hydrolysis of high-tenacity polyester–10-year results. In Proceedings of the 4th European Geosynthetics Conference, Edinburgh, UK, 6p.(CD-ROM–Paper 212).

Jones C.J.F.P. (1995). The development and use of polymeric reinforcements in reinforced soil. Proceedings of the symposium: The Practice of Soil Reinforcing in Europe, ed. T.S. Ingold, Thomas Telford, UK.

Kasozi, A.M., Siddharthan, R.V., and Mahamud, R. 2015. Temperature distribution in mechanically stabilized earth wall soil backfills for design under elevated temperature conditions. Journal of Thermal Science and Engineering Applications, 7(2).

Murray, R.T., and Farrar, D.M. 1988. Temperature distributions in reinforced soil retaining walls. Geotex and Geomem 7(1-2), 33-50.

Naughton, P.J., and Kempton, G.T. 2006. Life-time assessment of polyester based geosynthetics. In Proceedings of the 8th International Conference on Geosynthetics, Yokohama, Japan.

Olivella S, Gens A, Carrera J, Alonso E. 1996 Numerical formulation for a simulator (CODE_BRIGHT) for the coupled analysis of saline media. Engineering Computations 13(7), 87-112.

Segrestin, P., and Jailloux, J.M. 1988. Temperature in soils and its effect on the ageing of synthetic materials. Geotex and Geomem, 7, 51-69.

Vahedifard, F., Tehrani, F.S., Galavi, V., Ragno, E., and AghaKouchak, A. 2017. Resilience of MSE walls with marginal backfill under a changing climate: Quantitative assessment for extreme precipitation events. J of Geotech and Geoenviron Engineering, 143(9), 04017056.

You-Kyum, K., Gyeong-Yun, S. 2018. Reliability assessment of polymeric straps (FASTEN FS) for soil reinforcement. H411-18-00067. GECO Industrial Co., Ltd. FITI Testing and Research Institute, Chungbuk, Korea.

WeatherOnline Ltd. Meteorological Services, viewed on March 2021, https://www.weatheronline.co.uk/

ANNEXES

Annex A. Used ambient in-air temperature, relative humidity and precipitation registries from years 2016 to 2020.

1. Abu Dhabi:

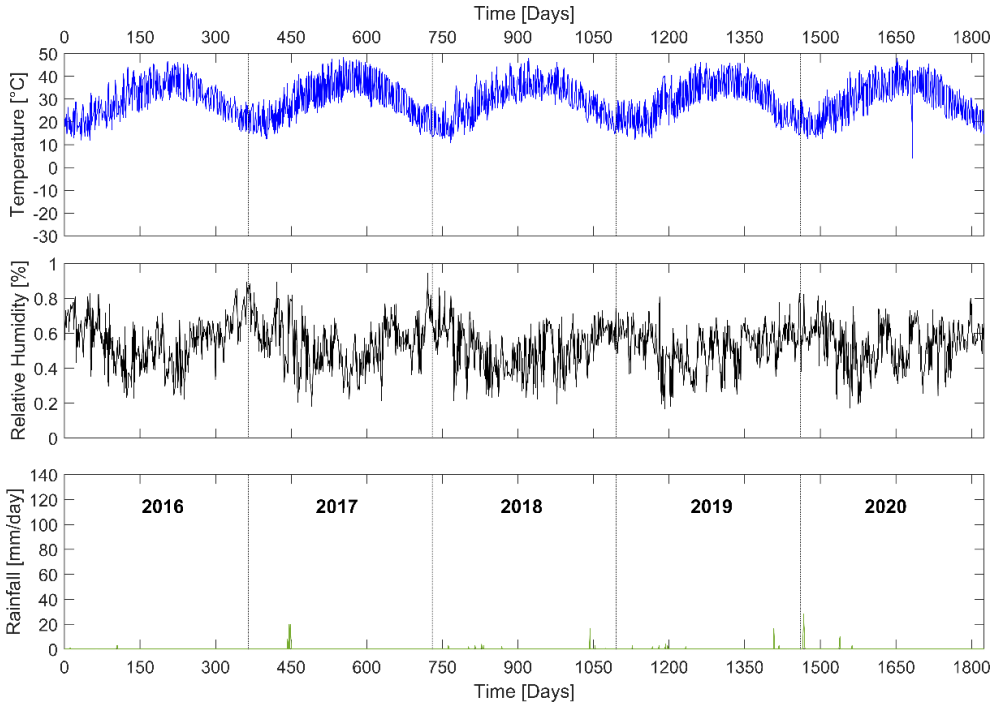

2. Barcelona:

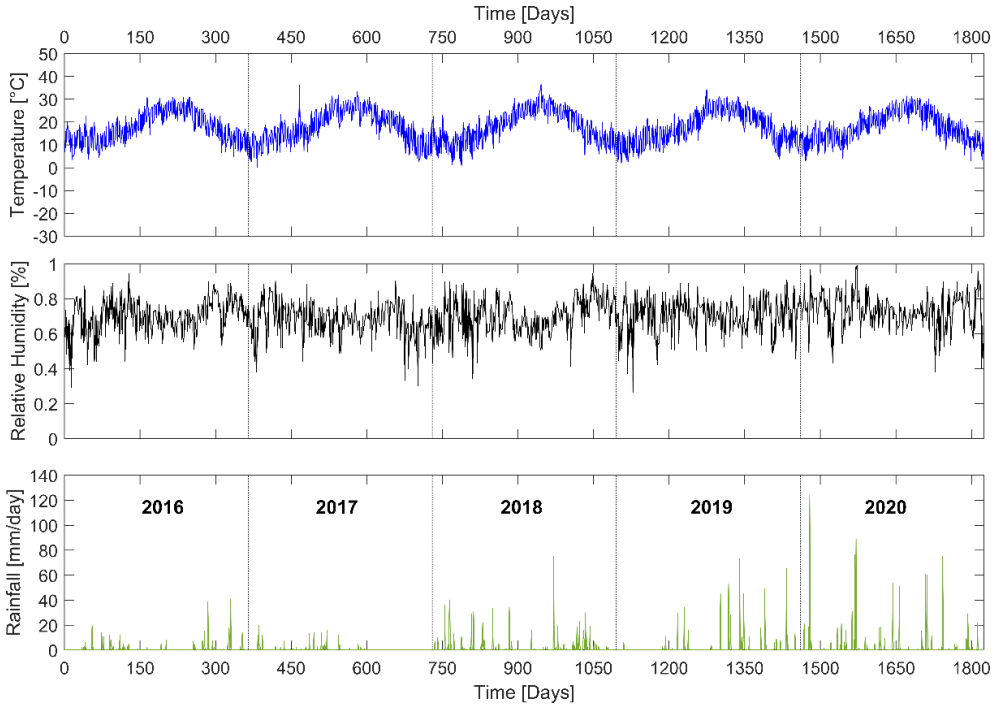

3. Singapore:

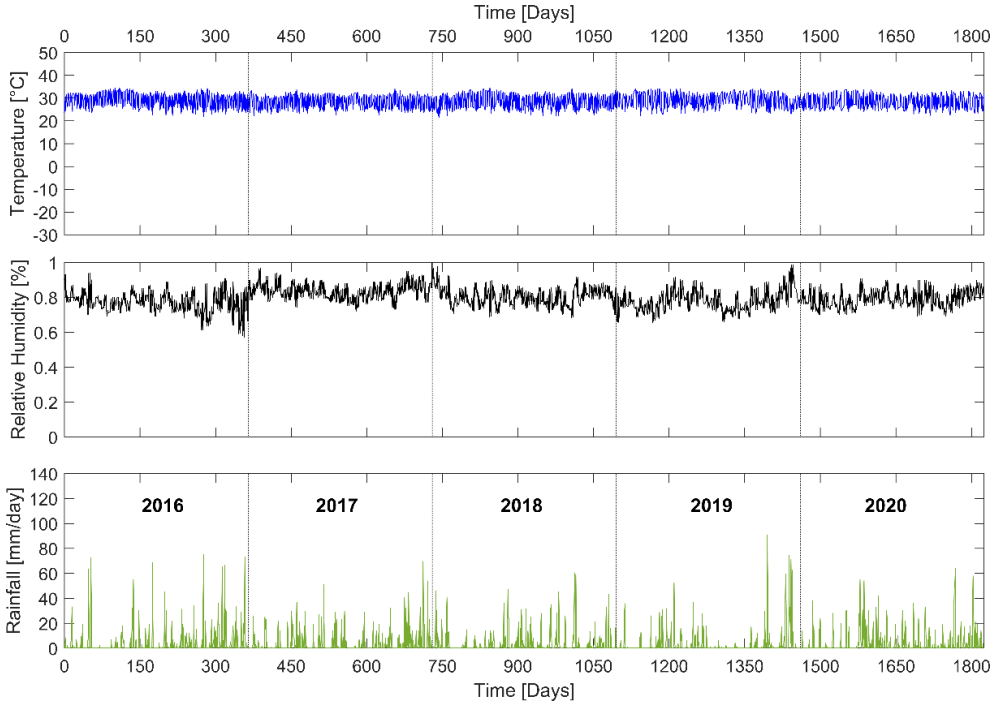

4. Toronto:

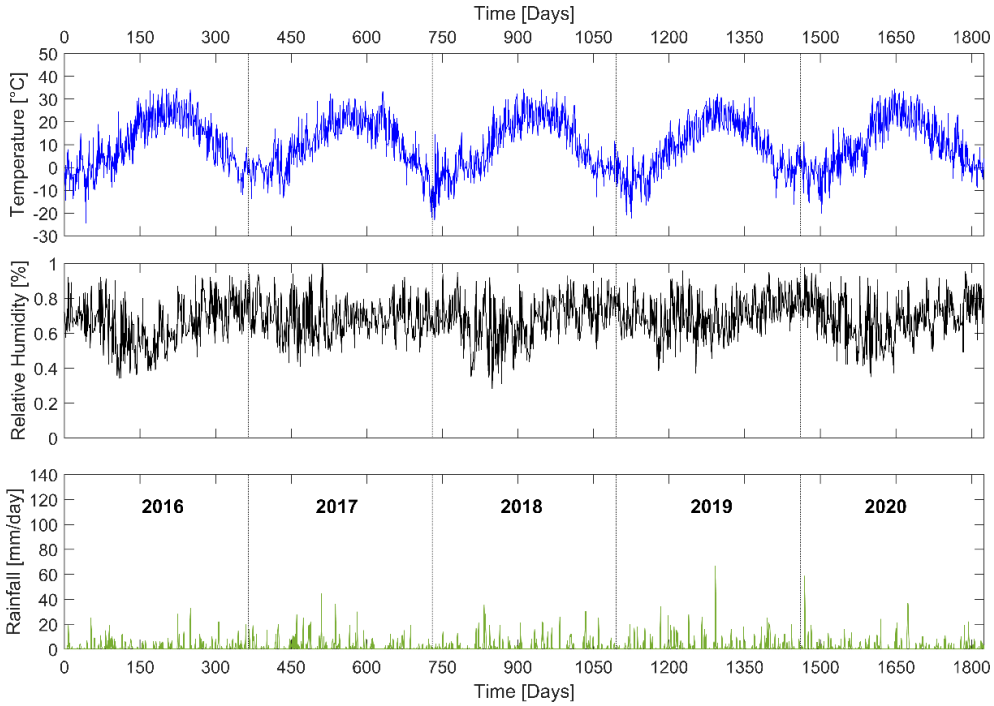

Annex B. Creep Master Curve for FASTEN FS30kN

1. 66% of UTS, FASTEN FS30kN:

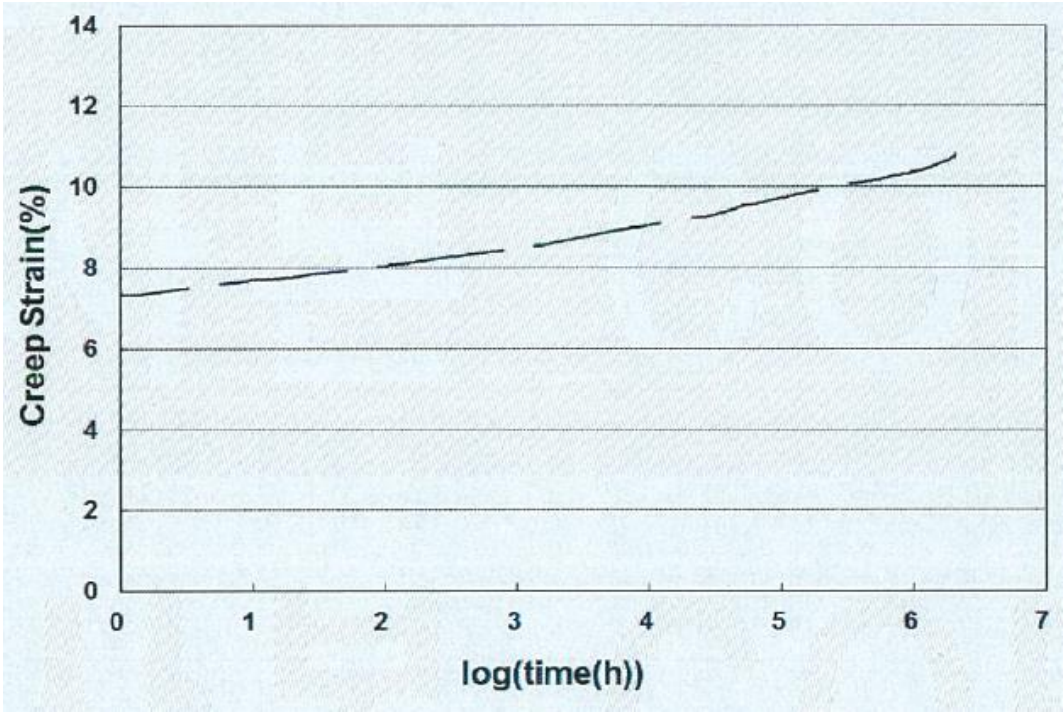

2. 70 of UTS, FASTEN FS30kN:

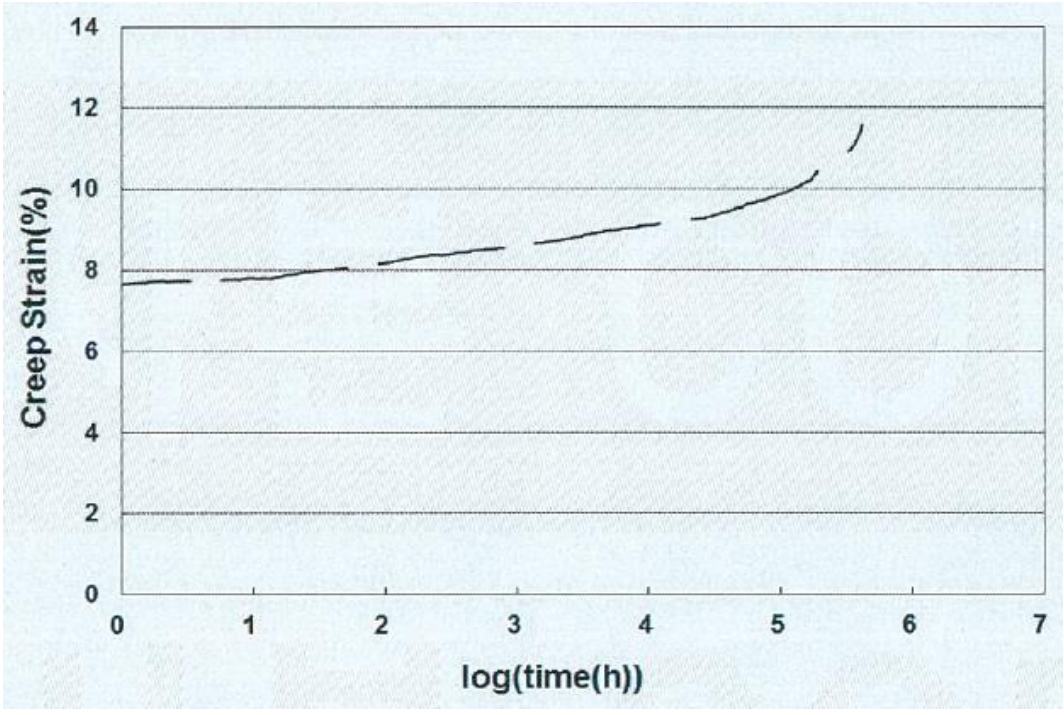

3. 74 of UTS, FASTEN FS30kN:

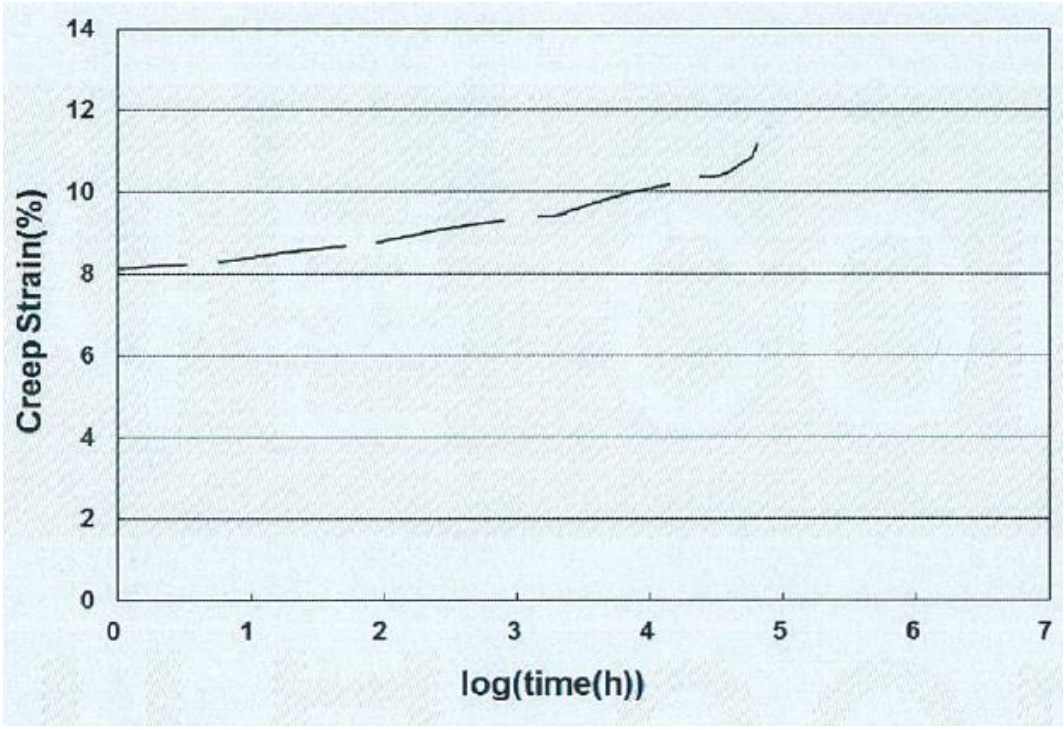

4. 80 of UTS, FASTEN FS30kN:

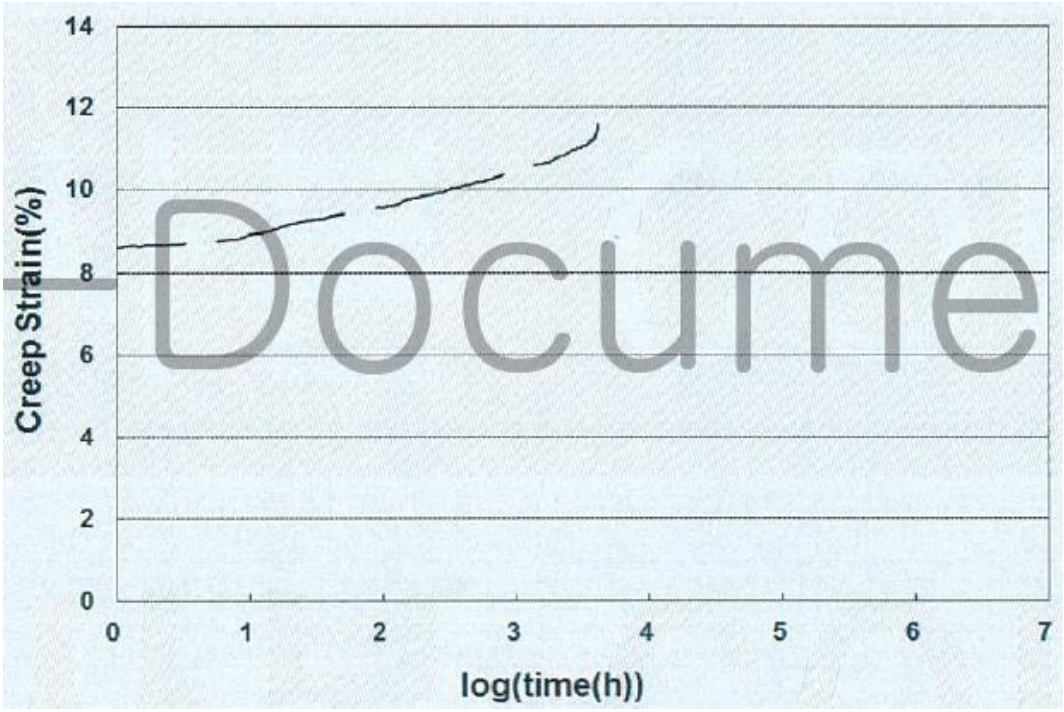

Annex C. Creep Master Curve for FASTEN FS50kN

1. 68% of UTS, FASTEN FS50kN:

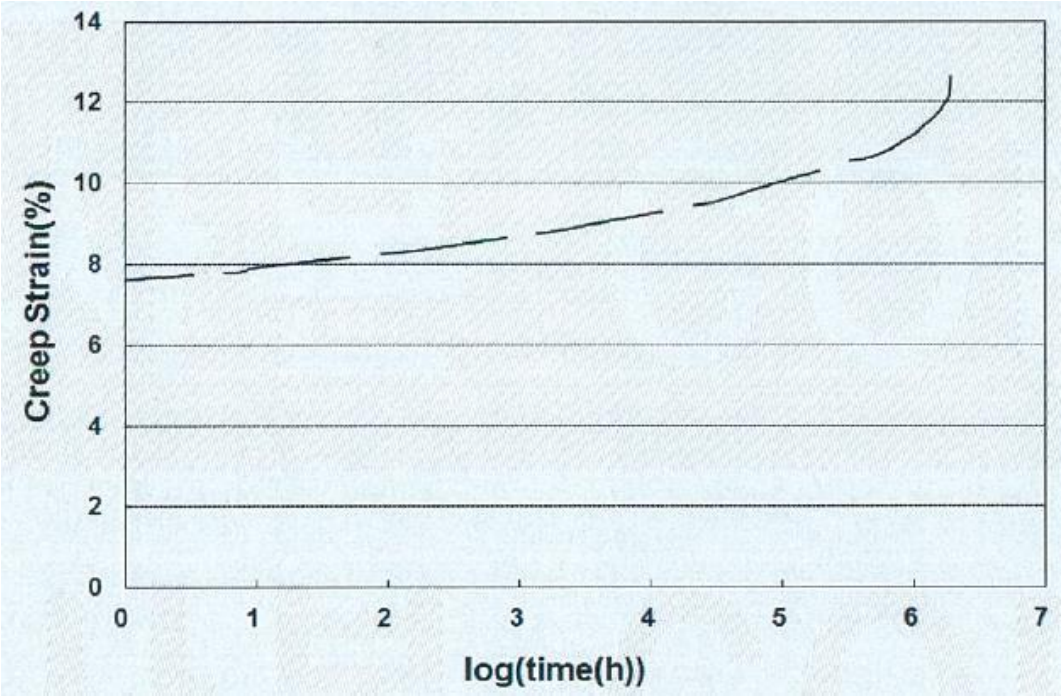

2. 70% of UTS, FASTEN FS50kN:

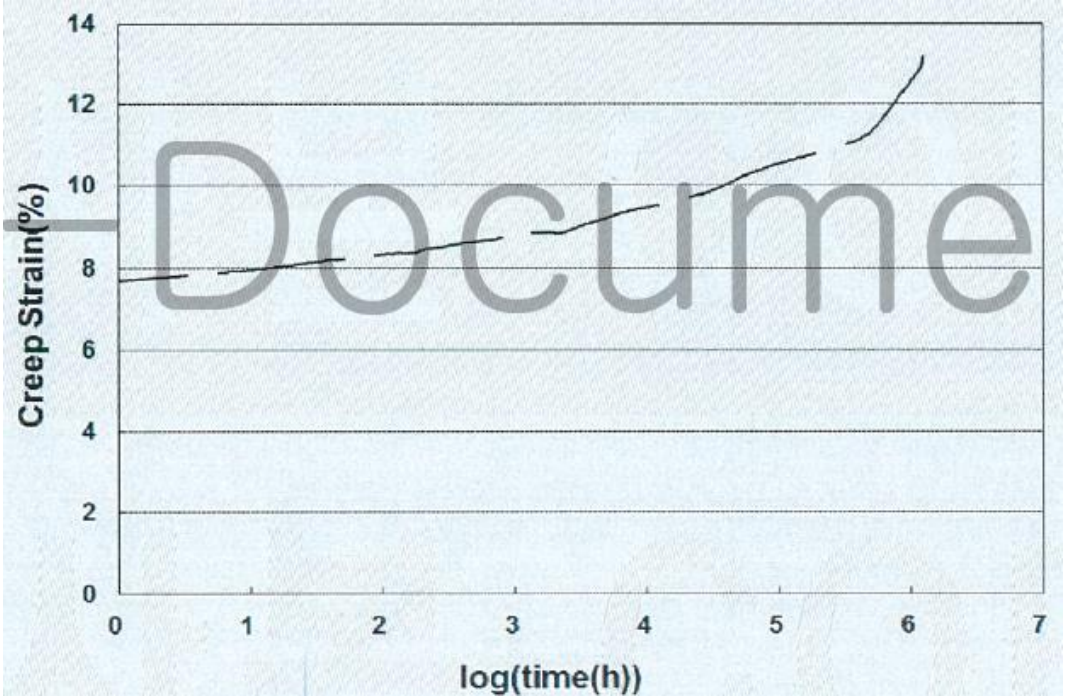

3. 74% of UTS, FASTEN FS50kN:

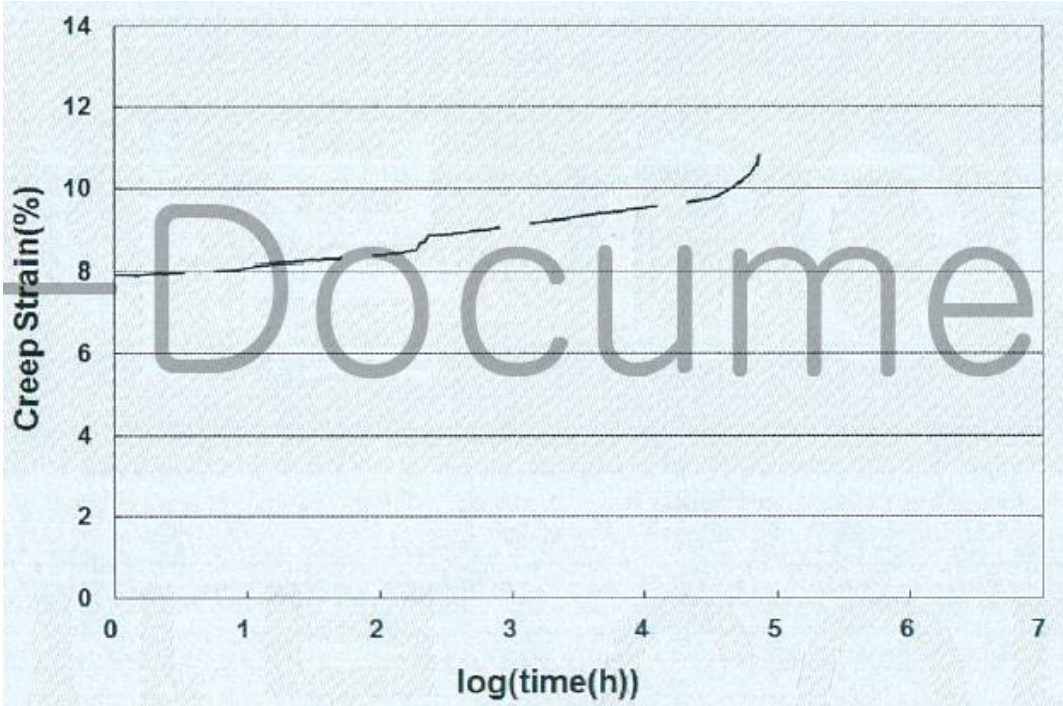

4. 80% of UTS, FASTEN FS50kN:

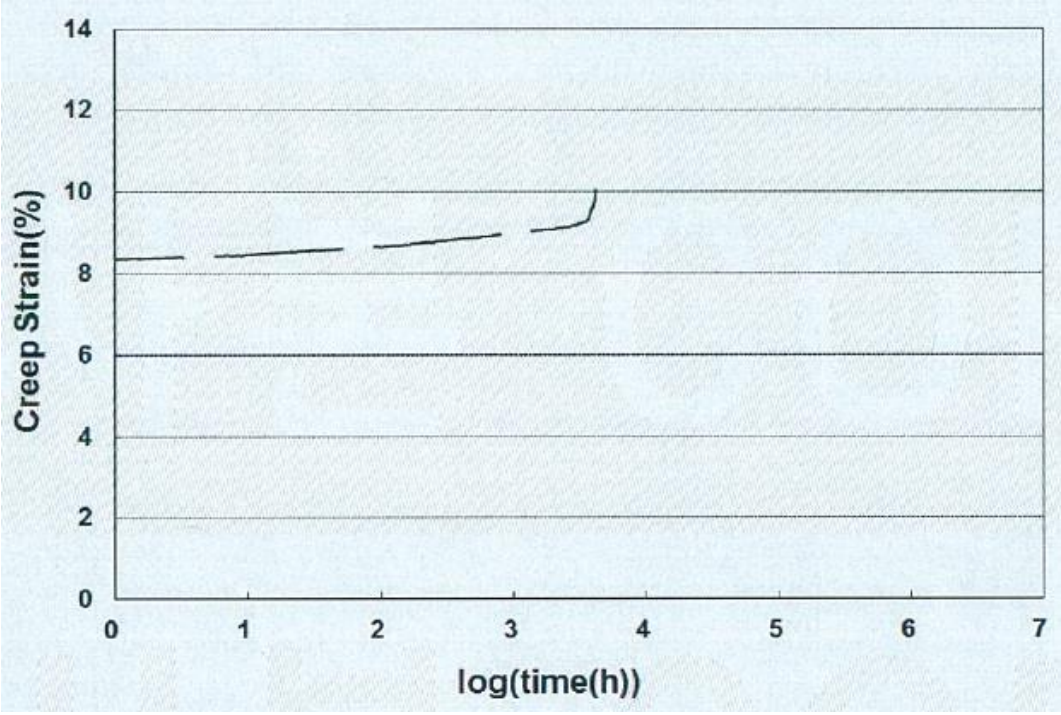

Annex D. Creep Master Curve for FASTEN FS70kN

1. 66% of UTS, FASTEN FS70kN:

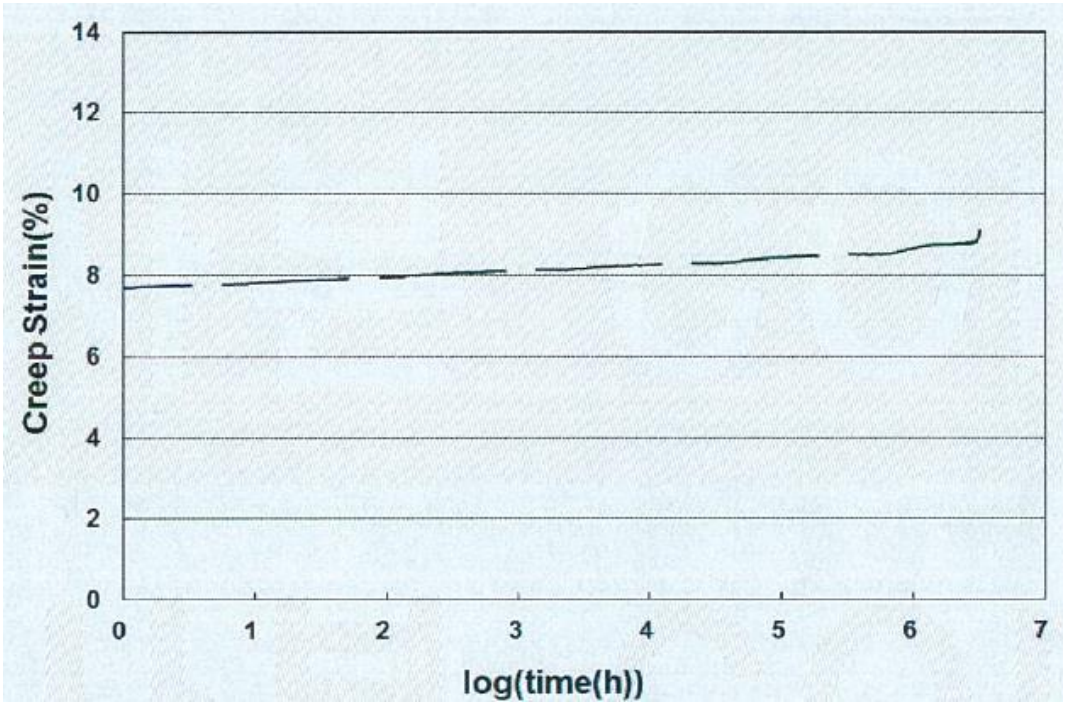

2. 70% of UTS, FASTEN FS70kN:

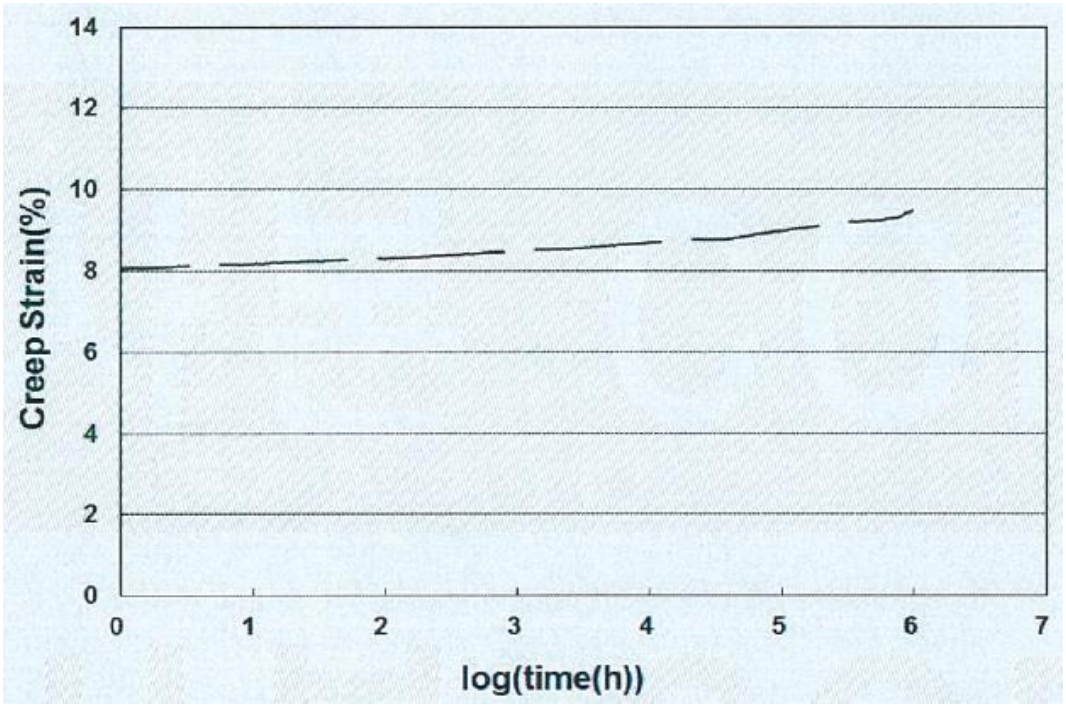

3. 74% of UTS, FASTEN FS70kN:

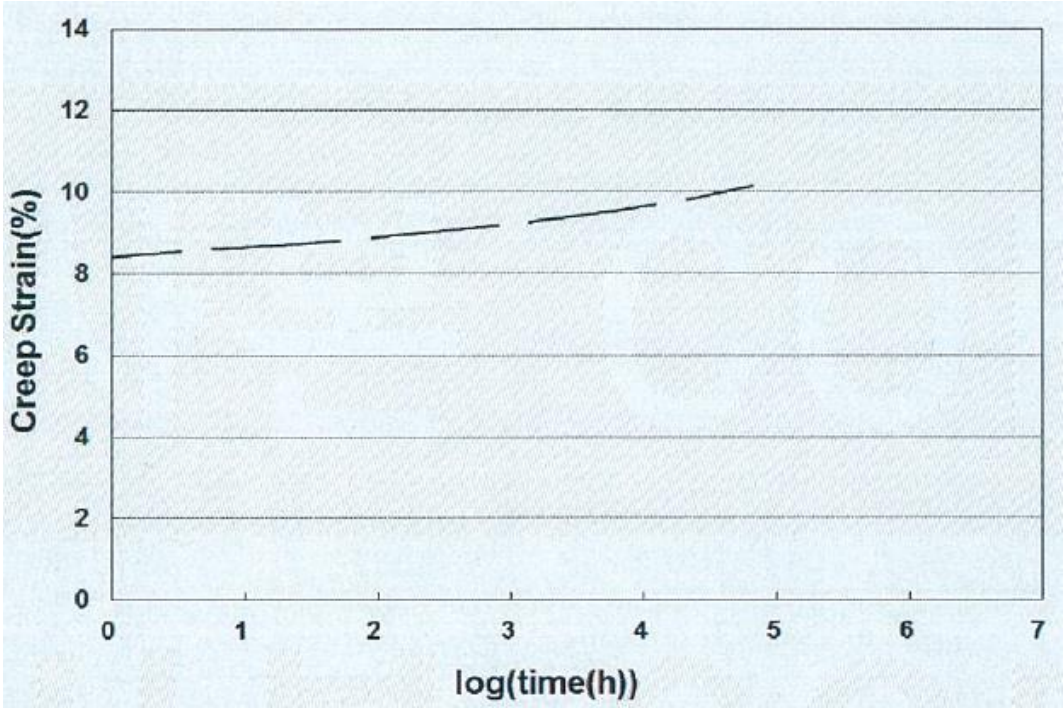

4. 80% of UTS, FASTEN FS70kN: